Institut für Geowissenschaften, Universität Potsdam

MIOCENE CLIMATE AS RECORDED ON SLOPE CARBONATES: EXAMPLES FROM MALTA (CENTRAL MEDITERRANEAN) AND NORTHEASTERN AUSTRALIA (MARION PLATEAU, ODP LEG 194)

Dissertation

Zur Erlangerung des akademischen Grades
Doktor der Naturwissenschaften
(Dr. rer. nat.)
in der Wissenschaftsdiziplin Geologie

Eingereicht and der
Mathematisch-Naturwissenschaftlichen Fakultät
Der Universität Potsdam

Von
Cédric Michaël John
Geboren am 10.09.1974 in Genf, Schweiz

Potsdam, im August 2003

ABSTRACT

This study investigated the slope carbonates of two Miocene carbonate systems: the Maltese Islands (in the Central Mediterranean) and the Marion Plateau (Northeastern Australia, drilled during ODP Leg 194). The aim of the study was to trace the impact of the Miocene cooling steps (events Mi1-Mi6) in these carbonate systems, especially the Mi3 event, which took place around 13.6 Ma and deeply impacted the marine oxygen isotope record. This event also profoundly impacted oceanographic and climatic patterns, eventually leading to the establishment of the modern ice-house world. In particular, East Antarctica became ice covered at that period. The rational behind the present study was to investigate the impact that this event had on shallow water systems in order to complement the deep-sea record and hence acquire a more global perspective on Miocene climate change.

The Maltese Islands were investigated for trends in bulk-rock carbon and oxygen isotopes, as well as bulk-rock mineralogy, clay minerals analysis and organic geochemisty. Results showed that the mid Miocene cooling event deeply impacted sedimentation at that location by changing sedimentation from carbonate to clay-rich sediments. Moreover, it was discovered that each phase of Antarctic glaciation, not just the major mid Miocene event, resulted in higher terrigenous input on Malta. Mass accumulation rates revealed that this was linked to increased runoff during periods when Antarctica was glaciated, and thus that the carbonate sediments were "diluted" by clay-rich sediments. The model subsequently developed to explain this implies feedback from Antarctic glaciations creating cold, dense air masses that push the ITCZ Northward, thus increasing precipitation on the North African subcontinent. Increased precipitation (or stronger African monsoon) accelerated continental weathering and runoff, thus bringing more terrigenous sediment to the paleo-location of the slope sediments of Malta. Spectral analysis of carbonate content and organic matter geochemical analysis furthermore suggest that the clay-rich intervals are similar to sapropelic deposits.

On the Marion Plateau, trends in oxygen and carbon isotopes were obtained by measuring *Cibicidoides* spp foraminifers. Moreover, carbonate content was reconstructed using a chemical method (coulometer). Results show that the mid Miocene cooling step profoundly affected this system: a major drop in accumulation rates of carbonates occurs precisely at 13.8 Ma, around the time of the East Antarctic ice sheet formation. Moreover, sedimentation changes occurred at that time, carbonate fragments coming from neritic environments becoming less abundant, planktonic foraminifer content increasing and quartz and reworked glauconite being deposited. Conversely, a surprising result is that the major N12-N14 sea-level fall occurring around 11.5 Ma did not impact the accumulation of carbonates on the slope. This was unexpected since carbonate platform are very sensitive to sea-level changes. The model developed to explain that mass accumulation rates of carbonates diminished around 13.6 Ma (Mi3 Event) instead of 11.5 Ma (N12-N14 event), suggests that oceanic currents were controlling slope carbonate deposition on the Marion Plateau prior to the mid-Miocene, and that the mid Miocene event considerably increase their strength, hence reducing the amount of carbonate being deposited on slope sites. Moreover, by combining results from deep-sea oxygen isotopes with sea-level estimates based on coastal onlaps made during Leg 194, we constrain the amplitude of the N12-N14 sea-level fall to 90 meters. When integrating isotopic results from this study, this amplitude is lowered to 70 meters.

A general conclusion of this work is that the mid Miocene climatic shift did impact carbonate systems, at least at the two locations studied. However, the nature of this response was highly dependant on the regional settings, in particular the presence of land mass (Malta) and the absence of a barrier to shelter from the effects of open ocean (Marion Plateau).

ZUSAMMENFASSUNG

Im Rahmen dieser Doktorarbeit wurden die Hangkarbonate von zwei miozänen heterozoischen Karbonatsystemen näher untersucht: die Malta Inselgruppe (zentrales Mittelmeer) und das Marion Plateau (Nordost Australien, ODP Leg 194). Die Auswirkungen der mittelmiozänen Abkühlung (Mi3), die auf 13.6 Ma datiert wird und starken Einfluß auf die Sauerstoffisotopenkurve hatte, in den oben genannten Flachwassersystemen stellten das Ziel dieser Arbeit dar. Dieses Abkühlungsereignis beeinflußte außerdem sehr stark die ozeanographischen und klimatischen Muster, die im weiteren Verlauf zum modernen Eishausklima führten. So steht insbesondere die Vereisung von Ostantarktika mit diesem Ereignis in Verbindung. Diese Arbeit untersucht den Einfluß dieses Ereignisses auf Flachwassersysteme, um vorliegende Untersuchungen in Tiefwassersystemen zu ergänzen und so zum globalen Verständnis des miozänen Klimawechsels beizutragen.

Die Profile auf der Maltainselgruppe wurden mit Hilfe von Kohlenstoff- und Sauerstoffisotopen Auswertungen im Gesamtgestein, Gesamtgesteinmineralogie, Tonmineralanalyse und organischer Geochemie untersucht. Durch einen Wechsel von karbonatischeren zu tonigeren Sedimenten beeinflußte das mittelmiozäne Abkühlungsereignis die Sedimentation in diesem Gebiet sehr stark. Weiterhin wurde beobachtet, daß jede Phase der antarktischen Vereisung, nicht nur das mittelmiozäne Hauptereignis, zu einem erhöhten terrigenen Eintrag in den Hangsedimenten der Maltainselgruppe führte. Akkumulationsraten zeigen, daß dieser erhöhte terrigene Eintrag mit den einzelnen Vereisungsperioden zusammenhängt und die karbonatischen Sedimente durch tonreiche Sedimente "verunreinigt" wurden. Das daraufhin entwickelte Modell erklärt diesen erhöhten terrigenen Eintrag mit einer nordwärtigen Verlagerung der innertropischen Konvergenzzone durch die Bildung von kalten, dichten Luftmassen, die zu verstärkten Niederschlägen in Nordafrika führten. Diese verstärkten Niederschläge (oder verstärkter afrikanischer Monsun) beeinflußten die kontinentale Verwitterung und den Eintrag, mit der Folge, daß verstärkt terrigene Sedimente im Bereich der Hangsedimente der Maltainselgruppe abgelagert wurden. Die tonreichen Intervalle weisen Ähnlichkeiten zu sapropelischen Ablagerungen auf, was mit Hilfe der Spektralanalyse des Karbonatgehalts und der geochemischen Analyse des organischen Materials gezeigt wurde.

Auf dem Marion Plateau wurden die Sauerstoff- und Kohlenstoffisotopenkurven anhand von Foraminiferen der Gattung *Cibicidoides* spp. rekonstruiert. Der Karbonatgehalt wurde mit Hilfe einer chemischen Methode (Coulometer) ermittelt. Genauso wie die Sedimente der Maltainselgruppe beeinflußte das mittelmiozäne Abkühlungsereignis (Mi3) auch die Sedimente auf dem Marion Plateau. So kam es bei 13,8 Ma, in etwa zur Zeit der Vereisung von Ostantarktika, zu einem Abfall der Karbonatakkumulationsraten. Weiterhin traten Änderungen in der Zusammensetzung der Sedimente auf, so nehmen neritische Karbonatfragmente ab, der planktische Foraminiferengehalt nimmt zu und es wurden verstärkt Quarz und Glaukonit abgelagert. Ein überraschendes Ergebnis ist die Tatsache, daß der große N12-N14 Meeresspiegelabfall um 11,5 Ma die Akkumulationsraten der Karbonate auf dem Hang nicht beeinflußte. Dieses Ergebnis ist umso erstaunlicher, da Karbonatplattformen normalerweise sehr sensitiv auf Meeresspiegeländerungen reagieren. Der Grund, warum sich die Karbonatakkumulationsraten schon um 13,6 Ma (Mi3)

und nicht erst um 11,5 Ma (N12-N14) verringerten, liegt in der Tatsache, daß die ozeanischen Strömungen die Karbonatsedimentation auf dem Hang des Marion Plateau schon im Miozän kontrollierten. Das mittelmiozäne Ereignis (Mi3) erhöhte die Stärke diese Strömungen und als eine Ursache wurde die Karbonatakkumulation auf den Hängen reduziert. Die Amplitude des N12-N14 Meeresspiegelabfalls liegt bei 90 m unter der Berücksichtigung der Sauerstoffisotopendaten aus der Tiefsee und Berechnungen des Meeresspiegels anhand des "coastal onlaps", die während Leg 194 gemacht wurden. Die Isotopendaten dieser Arbeit weisen hingegen auf einen verringerten Meeresspiegelabfall von 70 m hin.

Als allgemeine Schlußfolgerung kann gesagt werden, daß der mittelmiozäne Klimaumschwung die Karbonatsysteme zumindest an den beiden untersuchten Lokalitäten beeinflußt hat. Allerdings waren die Auswirkungen sehr von den unterschiedlichen lokalen Gegebenheiten abhängig. Insbesondere wirkten sich die Anwesenheit einer Landmasse (Malta) und die Abwesenheit einer Barriere vor den Einflüssen des offenen Ozeans (Marion Plateau) stark auf die Ablagerung der Karbonate aus.

Table Of Content

- CHAPTER 1 –

General Introduction

1.0 Background on Miocene Climate Change

The Cenozoic is characterized by important global climatic changes. After the warm and equable climate of the Eocene, Earth entered into a long-term cooling mode that eventually led to Quaternary glaciations and to our modern world (See fig.1, modified from Zachos et al., 2001). The Miocene is a critical phase in this long-term cooling trend since one of the largest cooling "steps" occurred during this period. The East Antarctic ice sheet was permanently established in the mid Miocene (see Fig.1), and this triggered one of the largest Cenozoic sea-level fall (N12-N14 event, 11.5-12.5 Ma, Isern, Anselmetti and Blum 2002). Miocene-Oligocene climatic events are furthermore characterized by large perturbations in the average oceanic stable isotopic ratios of both carbon and oxygen. Major changes in carbon and oxygen isotopes as well as in marine $^{87}Sr/^{86}Sr$, as recorded in deep-sea sediments, show the following features:

Carbon isotopes- Major variations in mean ocean $\delta^{13}C$, involving redistribution between carbon reservoirs (Kennett, 1985; Miller and Fairbanks, 1985; Vincent and Berger, 1985). The mean $^{13}C/^{12}C$ ratio is generally controlled by the proportions of carbon deposited as organic versus inorganic carbon (calcium carbonate) in the ocean. Assuming that the rate of delivery to the ocean of terrestrial organic carbon, depleted in $\delta^{13}C$, has not varied greatly during the Cenozoic, a higher mean $^{13}C/^{12}C$ ratio reflects an increase in organic carbon storage (e.g., Vincent and Berger, 1985).

Two major maxima in mean ocean $\delta^{13}C$ occur during the late Oligocene-Miocene: the first near the Oliogocene-Miocene boundary, around 24 Ma (Zachos et al., 1997; Zachos et al., 2001), and the second during the late Early to Middle Miocene from 17 to 13.5 Ma, termed the Monterey Carbon Isotope Excursion (Vincent and Berger, 1985). The Monterey $\delta^{13}C$ maximum has been attributed to the storage of large volumes of organic carbon in the Monterey Formation of California, circum-North Pacific and the southeastern shelf of North America, and is postulated as a major contributor to global cooling through drawdown of atmospheric CO_2 and a series of positive feedback mechanisms (Vincent and Berger, 1985).

Oxygen isotopes- Twelve significant $\delta^{18}O$ increases (0.5 ‰ to more than 1.0‰) in latest Oligocene to early Late Miocene benthic foraminiferal records have been identified by Miller et al. (1991b) and Wright et al. (1992), classified as Oi and Mi zones, and interpreted as large but transient Antarctic glaciations. The most prominent $\delta^{18}O$ feature is an abrupt increase at 14.6 Ma. The middle Miocene $\delta^{18}O$ increase has been interpreted to primarily record the intensification of continental glaciation in Antarctica (Shackleton and Kennett, 1975; Savin and Woodruff, 1990) or an increase in deep-water cooling, unaccompanied by Antarctic ice growth (Matthews and Poore, 1980; Prentice and Matthews, 1988). Planktic-benthic foraminiferal $\delta^{18}O$ covariance at low-latitudes associated with major oxygen isotope events (Miller et al., 1991b; Wright et al., 1992) suggests that Antarctic ice sheets waxed and

waned throughout the Early and Middle Miocene. More recently, Zachos et al. (1997) have shown a strong 40 ka periodicity in an equatorial oxygen isotope record, consistent with a high-latitude orbital control on ice volume and temperature.
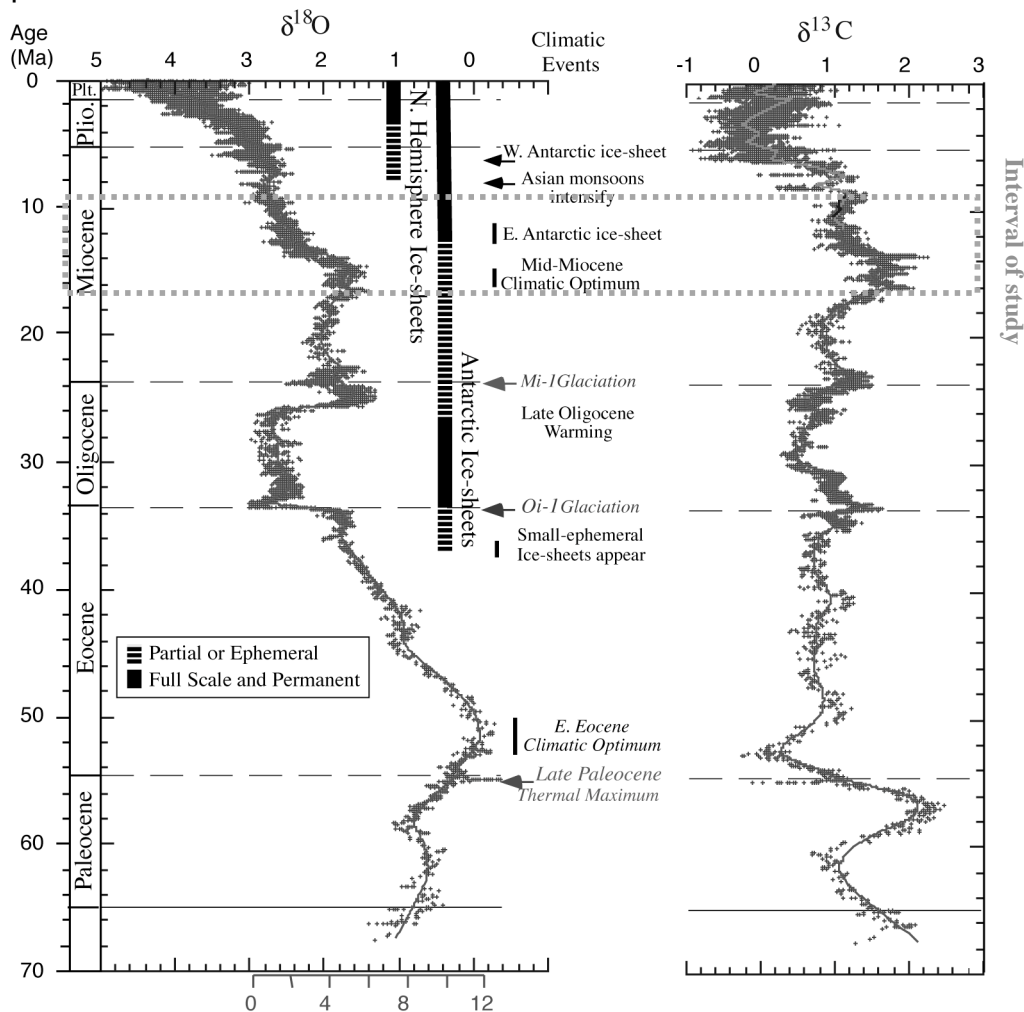
Figure 1: *Oxygen and carbon evolution from the Paleocene to Recent. Note the major mid Miocene cooling step (from Zachos et al. 2001).The dashed box represent the time frame of this study.*

Strontium isotopes- The $^{87}Sr/^{86}Sr$ ratio in sea-water is believed to be uniform at any given time, because the strontium residence time is much longer than ocean mixing times. This ratio has increased and decreased throughout geologic history, and has shown the greatest Cenozoic rate of change during the early Miocene (DePaolo and Finger, 1991; Hodell and Woodruff, 1994). As the $^{87}Sr/^{86}Sr$ ratio at any given time is a function of the amount of the high $^{87}Sr/^{86}Sr$ terrigenous detrital flux relative to the low $^{87}Sr/^{86}Sr$ oceanic crustal input, enhanced ^{87}Sr fluxes are interpreted to reflect tectonic changes (e.g., increased uplift) or other mechanisms for increasing continental erosion (Molnar and England, 1990). The global increase in weathering and/or carbon burial related to the uplift of the Himalayan mountain chains has been suggested as one of the major players controlling the long-term climate cooling of the Cenozoic (Molnar and England, 1990; Raymo and Ruddiman, 1992; Raymo, 1994; Derry and France-Lanord, 1996). In addition, the stark variations in the $^{87}Sr/^{86}Sr$ ratio during the Miocene can

be used to date and correlate carbonate rocks where other techniques would provide lower resolution (e.g. Mutti et al., 1997).

As previously stated, models established to link the isotopic trends to Miocene climate included thermal isolation of Antarctica after the opening of the Drake Passage and the establishment of the Circum Antarctic Current (Kennett, 1985; Flower and Kennett, 1993), the "Monterey Hypothesis" where increased upwelling currents triggered productivity events (Vincent and Berger, 1985) and finally increased siliciclastic weathering linked to the uplift of the Himalayan Plateau which would lower pCO_2 and change marine strontium isotopic ratios (Raymo et al., 1988; Raymo, 1994; Derry and France-Lanord, 1996; France-Lanord and Derry, 1997). However, none of the models established on deep-sea record can fully account for the trends observed. In particular, they lack a convincing negative feedback to explain the stabilization of the oxygen isotopes curve after the major mid-Miocene rapid cooling step.

To complement the deep-sea record, shallow marine environments where numerous complex geochemical and biological reactions occur have to be investigated. Feedbacks between continental nutrient supply rates, rates of marginal seas productivity and atmospheric pCO_2 are potentially critical parameters that have a strong impact over Earth's climate (Föllmi, 1995). Moreover, shelf environments are major reservoir of organic and carbonate carbon: the accumulation rate of one versus the other might impact oceanic carbon composition and atmospheric pCO_2 (Weissert and Mohr, 1996; Weissert et al., 1998). Hence, to reach a better understanding of the mechanisms of Miocene climate changes, it is essential to integrate the evolution of shallow-water systems –where the response of continents is better preserved- with the deep-sea record. The present study can be considered as a first step towards a more extensive utilization of the shallow-water record.

1.1 Aims and Locations of this Study

This study attempts to identify the coupling and feedback between carbonate systems, continents and stratigraphic evolution of carbonate margins. The nature of the scientific questions behind this work, namely integrating paleoceanographical changes with continental weathering and climatic history, required a multi-proxy approach as well as working on an archive providing insight on both continental and marine processes. Carbonate systems were selected as ideal shallow-water archive for several reasons. First, isotopic composition of the shell of carbonate organisms contains geochemical information on environmental parameters such as water-temperature and productivity. Then, carbonate systems can be more easily dated than siliciclastic sequences, and also allow for more precise water depths estimates. Finally, the production of carbonate is sensitive to changes in nutrient supply, salinity and water temperature (Hallock, 1987; James, 1997; Hallock, 2001; Mutti and Hallock, In press). This work is based primarily on heterozoan carbonates ("cool water" carbonates, characterized by the absence of green algae and hermatypic corals) as opposed to tropical photozoan carbonates ("Reef" carbonates composed of light dependant biota, James, 1997). Heterozoan carbonates are advantageous to the objectives of this study for two reasons: **a)** the Miocene is a time of more widespread heterozoan facies with respect to today, even at low latitudes and **b)** heterozoan carbonates can persist across a broader spectrum of

environmental changes and would thus record them in a more complex way than as an "on/off" switch. Though potentially harder to interpret, this response would provide more information on the coupling between shallow-water seas and continents. The specific questions that we want to address here are **(1)** did heterozoan carbonate systems react to the mid Miocene climate change? **(2)** if yes, what was the nature of this response? and **(3)** was it similar for every heterozoan systems around the world?
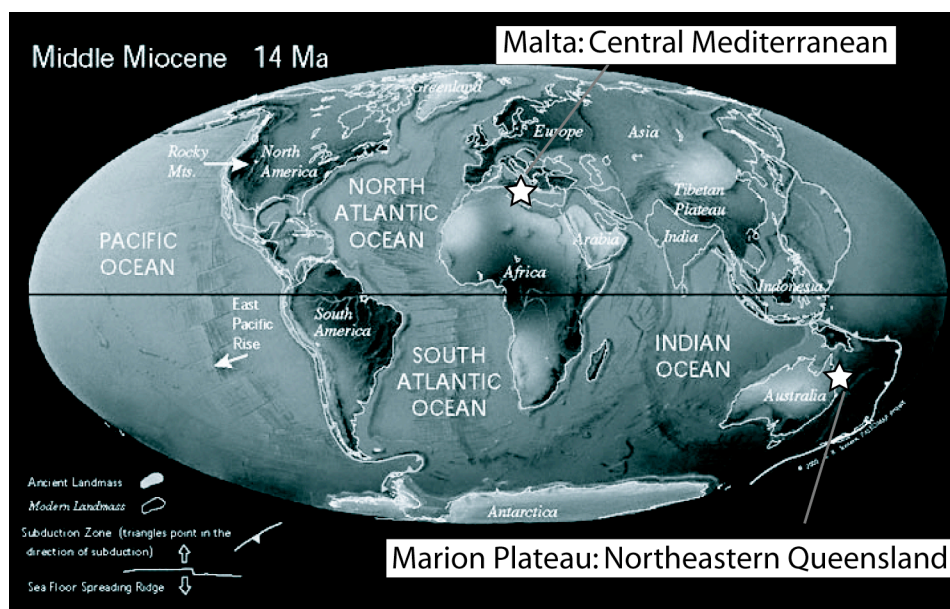
Figure 2: Paleo-location of the two carbonate systems studied in this thesis (white stars). Paleomap can be downloaded at www.scotese.com.

To answer this, we selected two locations for investigation (see Fig.2): the slope carbonates of the Maltese Islands (African margin, central Mediterranean) and the slope carbonates of the Marion Plateau (Northeastern Queensland, Australia, ODP Leg 194). The Maltese Islands and Marion Plateau carbonate systems are both heterozoan systems, i.e. contain non-tropical carbonates dominated by bryozoans, mollusks and foraminifers. However, beyond these compositional similarities, marked differences in the paleoceanographical settings between the two systems exist. During the Miocene, Malta was attached to the Ragusa platform on the North African margin, and thus surrounded by a large land mass. The Marion Plateau carbonate platforms on the other hand were formed on an ocean-facing plateau. Located on the Australian coast and thus in the southern hemisphere, they were also closer to Antarctica, the continent driving global changes at that time. The combination of the similarity in nature of Malta and the Marion Plateau, and yet difference in settings allow for interesting comparisons of the response of heterozoan carbonate to climate change in different situations.

We concentrated our efforts on slope carbonates since they offer several advantages over shallower platform carbonates: they are less prone to extensive early marine cementation, they have higher sedimentation rates and therefore can be sampled at higher time-resolution, and finally they contain a mix of detrital and in-situ sediments thus providing critical information on continental weathering rates, export of terrigenous sediment and in-situ carbonate production. In this study, we have investigates bulk and

12

element-specific stable isotopes of the oxygen, carbon, nitrogen and strontium, as well as mineralogical evolution (clay minerals and bulk-rock analysis) and elemental analysis (organic and inorganic carbon content, nitrogen content and organic carbon to nitrogen molar ratios).

1.2 Organisation of the Thesis

Results of this study were divided into four papers. Each paper is presented here as a chapter. Chapter 2 and 3 deal with results from Malta, whereas chapters 4 and 5 deal with results from the Marion Plateau (Leg 194). The specific division of the thesis is the following:

Chapter 1: *"General introduction".* The present chapter, describing some background on Miocene climate, reasons and location for this study and organization of the thesis.

Chapter 2: "*Mixed carbonate-siliciclastic record on the North African margin (Malta) - coupling of weathering processes and mid Miocene climate*". This chapter establishes the link between global climate and accumulation of carbonate on the slope of the Maltese system. Clay mineral analysis are also shown to support an interpretation of increased rainfall around 16.5 Ma, and a model explaining these links is proposed. This paper was published in 2003 in the *GSA Bulletin* (v.115, p.217-229) and the authors are John, C.M., Mutti, M. and Adatte, T. Contribution from C.John: field work, sample preparation, carbonate analysis, data interpretation, writing first draft of the manuscript and integrating subsequent comments from the co-authors.

Chapter 3: "*History of the African monsoon inferred by Middle Miocene sapropels-like deposits in the Mediterranean".* This chapter presents some geochemical results obtained on the Maltese section and stresses the similarities between the Maltese sediments and Pleistocene sapropels. The occurrence of sapropelic deposits as early as the mid Miocene is significant because it is an indication that the African monsoon was strengthen already at that period. The model introduced in chapter 2 is consequently extended to account for feedbacks from the African monsoon. This paper is in preparation and the authors are John, C.M., Mutti, M., Laskar, J. Contribution from C.John: field work, sample preparation, carbonate analysis, data interpretation, orbital tuning, writing first draft of the manuscript and integrating subsequent comments from the co-authors.

Chapter 4:*" Relative control of paleoceanography and eustasy over slope sedimentation in a subtropical heterozoan carbonate system (Marion Plateau, ODP leg 194) ".* This chapter presents oxygen, carbon and strontium isotopes results from the Marion Plateau. These geochemical data are used to obtain an integrated chemostratigraphic framework and to establish new age models. Results from the age model revealed the timing of an as yet inferred condensed interval. Mass accumulation rates of carbonate combined with sedimentological observations reveal significant changes in accumulation over the investigated time interval. This trend is interpreted as a control of current patters over slope carbonate deposition. This paper is in preparation and the authors are John, C.M. and Mutti, M. Contribution from C.John: participation on Leg 194 and sampling, sample preparation, sieving of samples and picking of foraminifers, carbonate analysis, data interpretation, writing first draft of the manuscript and integrating subsequent comments from the co-author.

Chapter 5: "*$\delta^{18}O$ and Marion Plateau backstripping: combining two approaches to constrain late Middle Miocene eustatic amplitude".* Using the

oxygen isotopes presented in chapter 4 and combining them with the latest sea-level fall magnitude estimates based on stratigraphic relationships (coastal onlap) from Leg194, this chapter tries to constrain the amplitude of the N12-N14 sea-level fall. The framework of Leg 194 offers the unique opportunity to undertake this integrated approach for several reasons: the tectonic setting of the plateau is well constrained, the goal of the Leg was to estimate the magnitude of the fall using coastal onlap, and finally the relative abundance of foraminifers on the slope sites allows for reconstruction of oxygen isotope evolution. This paper is under review and the authors are John, C.M., Karner, G.D. and Mutti, M. Contribution from C.John: participation on Leg 194 and sampling, sample preparation, sieving of samples and picking of foraminifers, data interpretation, writing first draft of the manuscript and integrating subsequent comments from the co-authors.

Chapter 6: *"General conclusions, acknowledgments and reference cited".* This final short chapter presents some conclusions on the results of chapters 3 to 5, and discusses whether and how the two carbonate systems studied reacted to mid Miocene global changes. It also contains the acknowledgements and cited references for the entire thesis.

- CHAPTER 2 –

Mixed Carbonate-Siliciclastic Record On The North African Margin (Malta) - Coupling Of Weathering Processes And Mid Miocene Climate

2.0 ABSTRACT

We investigated rock outcrops spanning the mid Miocene global climate-cooling step on the Maltese Islands in order to reconstruct continental weathering rates and terrigenous fluxes, as well as exploring the coupling with regional climate and carbonate accumulation. Oligocene and Early Miocene sedimentation at this location was dominated by transitional platform to slope carbonates, but progressively switched to a clay-rich carbonate slope system in the Middle Miocene. Around 13 Ma, an abrupt change toward clay-dominated marls occurred, and marl deposition persisted until the Tortonian (~12 Ma) when a shallow-water carbonate ramp was re-established. Clay mineralogy and bulk-rock oxygen isotopes analysis suggest that the deposition of the Blue Clay formation was mainly caused by changes in global climate and in the rate of continental weathering.

A significant negative correlation (R^2=0.65) exists between the carbonate content and the $\delta^{18}O$ record. This, combined with the variation of mass accumulation rate of terrigenous material, suggests that shorter-term periods of globally cooler climate ("Mi" events) were associated with higher rates of accumulation in continental derived material. Since Malta was during the Miocene part of the North African Margin, we propose that the observed trends were due to a regional increase in rainfall during cooler periods, which consequently increased continental weathering and runoff. We furthermore suggest that this pattern was linked to the perturbation of atmospheric front due to an increased thermal gradient during the Miocene. Thus, regional increase in rainfall might have been linked to the northward migration of the ITCZ.

2.1 INTRODUCTION

The Cenozoic is a time interval characterized by significant changes in climate. The Middle Miocene in particular is characterized by stepwise cooling and represents a critical period for understanding the establishment of the modern climatic system. After this time, the East Antarctic Ice sheet was permanently established (Kennett, 1985; Zachos et al., 2001) causing a eustatic sea level drop of around 100 meters (Isern, Anselmetti, Blum et al. 2001). Ocean circulation patterns became similar to modern, and the planet entered into a cooling mode (Kennett, 1985; Flower and Kennett, 1994).

Glacio-eustatic and carbon cycle changes associated with this transition can be traced using variations in both oxygen and carbon isotopes. Cenozoic long-term $\delta^{18}O$ deep-sea record reveals high-latitude cooling and increasing ice-volume since the early Eocene (Miller et al. 1987; Zachos et al 2001). Until the early Middle Miocene, ice volume remained low with the exception of several, brief periods of more extensive glaciations (Mi-events). This episod was followed by a step-wise but intense restablishment/growth of

a major ice-sheet on Antarctica and deep water cooling, as indicated by successive $\delta^{18}O$ shifts beginning at 14.5 Ma (Mi-events Mi3a, 3b,4, Miller et al., 1987).

Mechanisms causing the mid-Miocene climatic cooling are still a matter of debate. Although it is generally accepted that these climatic changes are triggered when critical tresholds levels of one or more parameters of the climate system were breached (Kennett 1977; Crowley and North 1988; Zachos et al. 1993), there is no consensus regarding the responsible parameters themselves. Discussion centers around two major controls: (1) alteration of ocean circulation driven by widening or closing of oceanic passages (Kennett 1977; Woodruff and Savin 1989; Wright et al 1992) and (2) pCO_2 variability involving CO_2 sequestering and consequent cooling either via increased organic carbon burial (Vincent and Berger, 1985; France-lanord and Derry, 1997) or via increased rates of silicate chemical weathering (Raymo et al., 1988; Molnar and England, 1990; Raymo, 1991; Raymo and Ruddiman, 1992; Raymo, 1994). These two main controls are often discussed separately, but are not necessarily mutually exclusive (see discussion in Zachos et al. 2001). Positive shift in marine $\delta^{13}C$ up to 1.5 ‰ (Monterey excusion, ~17.5-13 Ma) coeval with the deposition of the organic-rich Monterey Formation, followed by a positive shift in foraminiferal $\delta^{18}O$ suggest a possible sequence of increased rates of organic carbon burial, CO_2 removal and consequent global cooling (Monterey Hypothesis, Vincent and Berger 1985). The Monterey excursion includes several higher frequency (~400 kyr) peaks (carbon maxima, CM, Woodruff and Savin, 1991), which correlate with increased benthic foraminifera $\delta^{18}O$ values and increased carbonate preservation, implying coupling between organic carbon burial, lower pCO_2, and bottom water cooling (Woodruff and Savin 1991).

No model to date can fully account for the observed trends in climate during the Cenozoic. The Monterey Hypothesis of (Vincent and Berger, 1985) has been recently challenged because the mass accumulation rate of organic matter in the Monterey Formation is low and phosphorus accumulation (thought to be a limiting factor in organic matter accumulation) is high even after the major mid-Miocene cooling step (Isaacs, 2001; John et al., 2002). Geochemical budget of strontium for the Miocene (Goddéris and François, 1996) has questioned the siliciclastic weathering hypothesis, and even the notion of a large drop in pCO₂ at the mid-Miocene climate shift is currently being argued over (Pagani et al, 1999).

Thus, understanding the coupling of changes in weathering with the carbon cycle is more than ever of direct relevance to the study of these large climatic changes. The goal of the present paper is to explore the relationship and possible feedback between carbonate accumulation, continental weathering and runoff, and tie these to climate change in the Miocene. The Maltese sedimentary record is ideal to study these relationships since it consists of a mixed siliciclastic-carbonate system, offering the opportunity to establish a detailed oxygen and carbon isotope record based on carbonates, and combine it with a clay mineral record. Most clay minerals inherited from the continents are end-products of the siliciclastic weathering chain. This means that study of clay assemblages offers the opportunity to investigate the intensity of continental weathering as well as the climatic condition under which these clays were formed.

The specific objectives of the study are to: (1) investigate temporal trends in the nature and abundance of clay species in order to track changes in weathering products, (2) using mass accumulation rates of continental derived materials, to reconstruct changes in continental runoff, and (3) develop a local chemostratigraphic framework of carbon and oxygen isotopes, to link the observation made in steps 1 and 2 with global climatic events.

2.2 GEOGRAPHIC AND LITHOSTRATIGRAPHIC SETTING
The Maltese islands are located in the central Mediterranean and are composed of the islands of Malta, Gozo and Comino (Fig. 1).
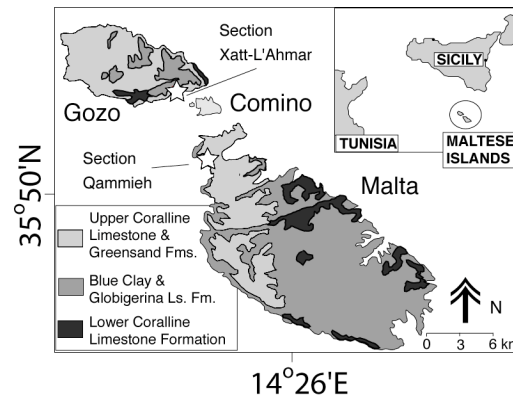
Figure 1: General map of the Maltese Islands showing the location of Malta, Gozo and Comino. Stars show the location of the two outcrops (Xatt-L'Ahmar and Qammieh) used to build the composite section discussed in this paper. Modified after Felix (1973).

The Maltese Islands and Sicily were part of the Malta-Ragusa platform in the Oligo-Miocene, and as such attached to the North African margin, probably representing a basin ward extension of the Tunisian carbonate shelf (Dercourt et al., 1992). The lithologic sequence of the Maltese Islands is classically divided into 5 units (Felix, 1973).

The lowermost unit is the Lower Coralline Limestone Formation, which consists of massive biogenic limestone beds of shallow marine origin. This shallow carbonate ramp phase is Oligocene in age. Deeper water slope carbonates of the Globigerina Limestone Formation begin depositing in the Chattian and span the Early Miocene to late Middle Miocene.
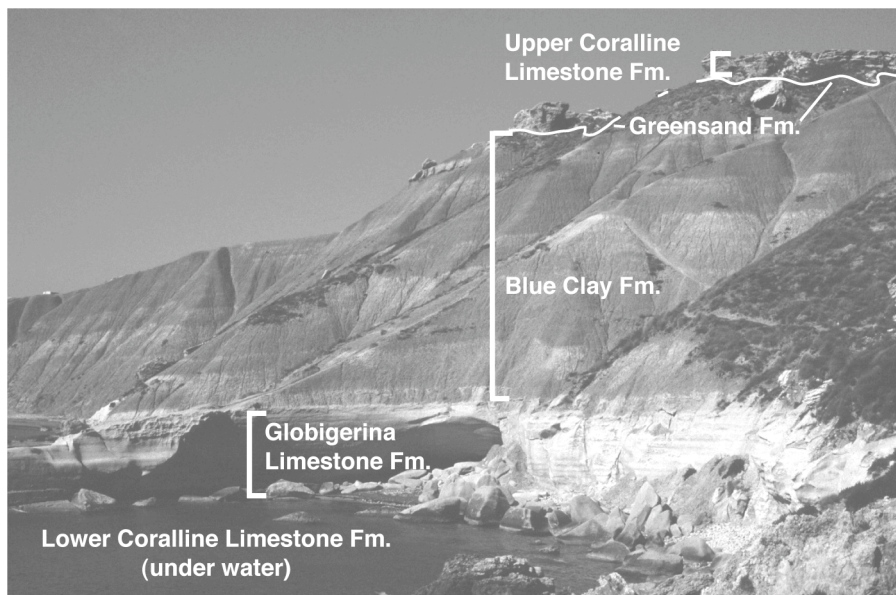
Figure 2: Outcrop picture of the various lithologic units of the Maltese Islands. The Lower Coralline Limestone Formation is under water and thus not visible. The Greensand Formation forms a very thin interval marked by a white line on the figure. Fm: Formation.

They consist mainly of loosely aggregated planktonic foraminifers, whereas larger skeletal fragments, such as echinoids or mollusks, are rare. Three main phases of phosphate precipitation/condensation (Pedley and Bennett, 1985), termed Phosphatic Layer 1, 2 and 3 in this paper, are recognized (Fig. 3). These beds can be as thick as 1 meter and are synchronous throughout Malta (Jacobs, 1996; Jacobs et al., 1996). Phosphatic Layers 1 and 2 are sea-floor cemented layers with pebble sized phosphatic particles that are trapped in a mixed calcitic-phosphatic grey matrix. The surface of these layers is brown-coated by phosphate and iron oxides, and boring by organisms is extensive. These features are typical of hardgrounds. Phosphatic Layer 3 on the other hand consists of gravel-sized, rounded phosphatic particles loosely distributed in a foraminifer matrix.

A marly unit of alternating light to dark layers, called the Blue Clay Formation and spanning the Serravalian (CN4 to CN6, Kienel et al., 1995) abruptly follows the Globigerina Limestone. Carbonate content in the Blue Clay is relatively low (~20%) and the water depth at which these deposits were formed is estimated on the basis of benthic foraminifers to be ~150-200 meters (Jacobs et al., 1996), or even ~500 m (Foresi et al., 2001). Planktonic and benthic foraminifers form the bulk of the skeletal components within this unit. An earlier investigation of clay mineralogy of the Globigerina Limestone and Blue Clay formations (Visser, 1991) identified a higher kaolinite and chlorite content in the Blue Clay formation. The Blue Clay Formation is unconformably overlain by the Greensand Formation and the Upper Coralline Limestone Formation, both Late Miocene in age. The Greensand Formation consists of a glauconitic sand bed ranging from 0-10 meters in thickness, while the Upper Coralline Limestone Formation testifies of the re-establishment of shallow water carbonate ramp conditions.

18
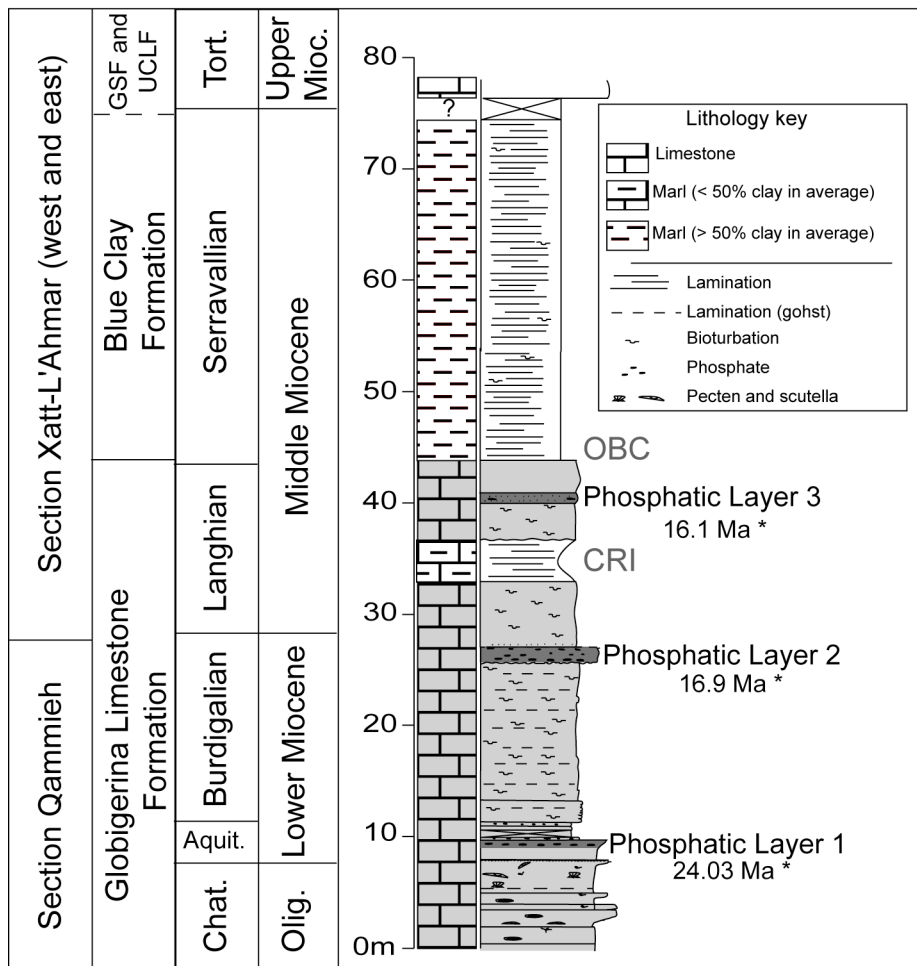
Figure 3: Composite section spanning the Globigerina and Blue Clay formations. Section below and including Phosphatic Layer 2 was collected on Malta. Portion above Phosphatic Layer 2 was collected on Gozo (see Fig. 1). Dates with stars are strontium isotope ages from Jacobs et al. (1996). "OBC" is the Onset of the Blue Clay, "CRI" is a Clay Rich Interval within the Globigerina Limestone. GSF: Greensand Formation, UCLF: Upper Coralline Limestone Formation.

2.3 COMPOSITE SECTION AND SAMPLING

The Globigerina Limestone Formation (Early Miocene to late Middle Miocene) and Blue Clay Formation (late Middle Miocene to early Late Miocene) were investigated since they comprise the time interval of interest to this study. Measuring and sampling were carried out in two locations (Fig. 1) in order to obtain the most complete and expanded composite section possible (Fig. 3). Section Qammieh on the island of Malta was selected for the Globigerina Limestone Formation below Phosphatic Layer 2 and was sampled with a resolution of 1 sample / 50 cm. Above Phosphatic Layer 2, section Xatt-L'Ahmar on the island of Gozo was selected due to the accessibility and good outcrop condition of the Blue Clay Formation. Sampling resolution for this interval was 1 sample / 10 cm.

The three phosphatic layers (Phosphatic Layer 1, 2 and 3, respectively), a clay-rich interval visible within the Globigerina Limestone Formation ("CRI" for "Clay Rich Interval"), and the Onset of the Blue Clay deposition ("OBC") are represented in the composite section (Fig. 3).

19

2.4 ANALYTICAL METHODS

Powders for Coulomat and stable isotopes analysis were obtained by hand grinding samples using an agate mortar. Carbonate content was measured for 492 samples (Table DR1). The powders were dried overnight in an oven set at 60 °C. Between 40 and 60 mg of sample material were analyzed using a Coulometer 5020 from UIC Inc. attached to a CM TIC Auto sampler from Orbis bv. Results were converted to calcite values by multiplying the TIC (Total Inorganic Carbon) results by the appropriate factor (8.33). Reproducibility based on triplicates from samples was ± 2 wt% carbonate.

Stable isotopes ($\delta^{13}C$ and $\delta^{18}O$) were measured for 490 samples on bulk carbonate at the University of Southern California (USC) using a V.G Isotech Prism, Isotope Ratio Mass Spectrometer (Table DR1).   About 0.1 mg of sample was loaded into stainless steel metal boats and analyzed on a V.G Automated Carousel Carbonate Device. An in-house pure carbonate standard calibrated against Vienna PDB was used for calibration. Analytical error based on standard for carbona and oxygen isotopes was ±0.2‰.

XRD analyses of the whole rock were carried out for 68 samples at the Geological Institute of the University of Neuchâtel, Switzerland (Table DR2). The samples were prepared following procedures described in Kübler (1987) and Adatte et al. (1996). Whole rock composition was determined by XRD (SCINTAG XRD 2000 Diffractometer) based on methods described by Ferrero (1965, 1966), Klug and Alexander (1974) and Kübler (1983). Clay minerals analyses were done on the same sample set as for bulk-rock analysis. Clay minerals were separated and quantified in two different fractions: fine silt (2-16µm, Table DR3) and clay-sized (<2µm, Table DR4). Analytical procedure was based on methods developed by Kübler (1987). A complete description of the methods used for XRD analysis in available in the appendix.

2.5 RESULTS
2.5.1 Bulk-rock mineralogy

Minerals identified include calcite and phyllosilicates, with accessory minerals such as quartz, ankerite, Carbonate apatite, K-felspar and plagioclase. The mineralogy is dominated by the presence of calcite and phyllosilicates. Carbonate apatite and plagioclases are not continuously present and never exceed 2%. Carbonate apatite only occurs in significant amounts in the Phosphatic Layers. Hence, these two minerals will not be further discussed. Major trends observed in these curves are (Fig. 4):
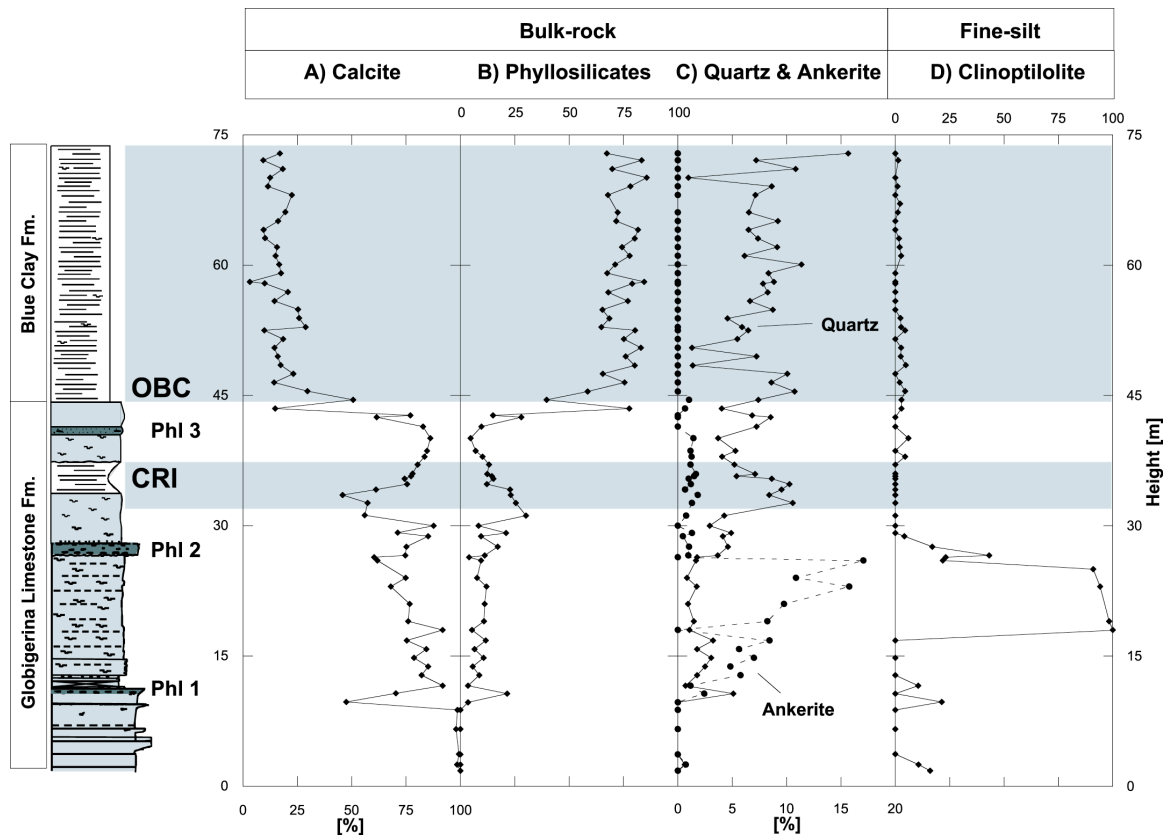
Figure 4: Bulk-rock mineralogical analysis for calcite (A), phyllosilicates (B) and quartz (C). Values are in %. Clinoptilolite (D) is quantified in the 2-16 μm fraction, not bulk-rock. A lithology key can be found on FIGURE 3. Phl: Phosphatic Layer. Bulk-rock data are available in TABLE DR2, fine-silt data in TABLE DR3.

Ankerite: Ankerite was mainly distinguished from dolomite by the position of its 100% intensity peak (30.74 ° 2θ versus 30.94 ° 2θ for the dolomite). No dolomite was found. Ankerite is mainly present in one interval situated between Phosphatic Layer 1 and Phosphatic Layer 2. The maximum in ankerite content is reached below Phosphatic Layer 2 (~15 %).

Calcite: Calcite content is high between Phosphatic Layer 1 and Phosphatic Layer 2 (~70-80 %). A decrease in calcite content (down to ~50%) starts after Phosphatic Layer 2. This episode, occurring within the Globigerina Limestone, is termed here "Clay Rich Interval" (CRI). Between the CRI and Phosphatic Layer 3, calcite content rapidly increases up to ~ 80%. However, at the onset of the Blue Clay Formation ("OBC") a dramatic drop (from 80 to ~29%) in calcite content takes place. Calcite content remains low throughout deposition of the Blue Clay Formation.

Phyllosilicates: phyllosilicates content curve is a mirror image of the carbonate curve. Its minimum occurs below Phosphatic Layer 1 (~0%) and it has its maximum for the Globigerina Limestone in the CRI (~ 25%). At the OBC, phyllosilicate content jumps to 75% (a threefold increase as compared to its CRI maxima). The phyllosilicates curve clearly shows that phyllosilicates constitute the bulk of the terrigenous material in the Blue Clay formation.

Quartz: Quartz content follows the phyllosilicates trend from the base of the section up to the OBC. At the OBC however, quartz content stays around levels close to its CRI values (~10%).

21

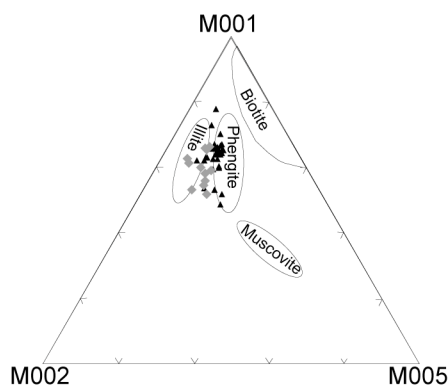***Figure 5:*** Triangular plot of the M001, M002 AND M005 peaks used to distinguish from different micas species (after Rey and Kübler, 1983). Results show that the mica from the Maltese islands is of the illite-phengite type.

2.5.2 Fine silt and clay-sized fractions

Minerals identified in both the fine silt (2-16 μm) and clay-sized (<2 μm) fractions are clay minerals such as mica, smectite, palygorskite, chlorite, kaolinite, and accessory minerals such as zeolite (clinoptilolite), quartz, k-felspar and plagioclases. The mica is of the illite-phengite type (Fig. 5) and is therefore here referred to as "illite". The clay mineral curves (Fig. 6) represent quantification (in relative %) of a given clay mineral in the clay-sized fraction. The abundance and type of minerals found in both the clay-sized and fine-silt fractions are similar (with the exception of an interval of abundant clinoptilolite content occurring only in the fine-silt fraction, Fig 4D), and thus only the clay-sized fraction curves are systematically shown. Trends observed in these curves (Fig. 4D and Fig. 6) include:

Clinoptilolite: the zeolite shown on Fig. 4D was quantified in the fine-silt (2-16 μm) oriented fraction, not the bulk rock. Although zeolite is a relatively minor component, a distinct peak (~100%) occurs between 15 and 30 meters, slightly before the CRI. This zeolite is of the heulandites-clinoptilolite series (Fig. DR1 A), and is simply referred to here as "clinoptilolite".

Smectite, palygorskite and illite: These three clay minerals have their maximum at the base of the section (~80% for smectite, ~20% for palygorskite and ~30% for illite) and reach a minimum in the CRI (~20% smectite, ~5% palygorskite and ~15% for illite).

Kaolinite: Kaolinite content increases from the base of the section (between 0% and 50%) towards the CRI where it accounts for 75% of the clay fraction. This ratio then stays relatively stable until the upper part of the Blue Clay Formation.

Chlorite: Chlorite content has a maxima during the CRI (~35% compared to < 5% prior to this event). Chlorite abundance then drops and reaches a relatively constant level of ~10% during Blue Clay deposition.

22
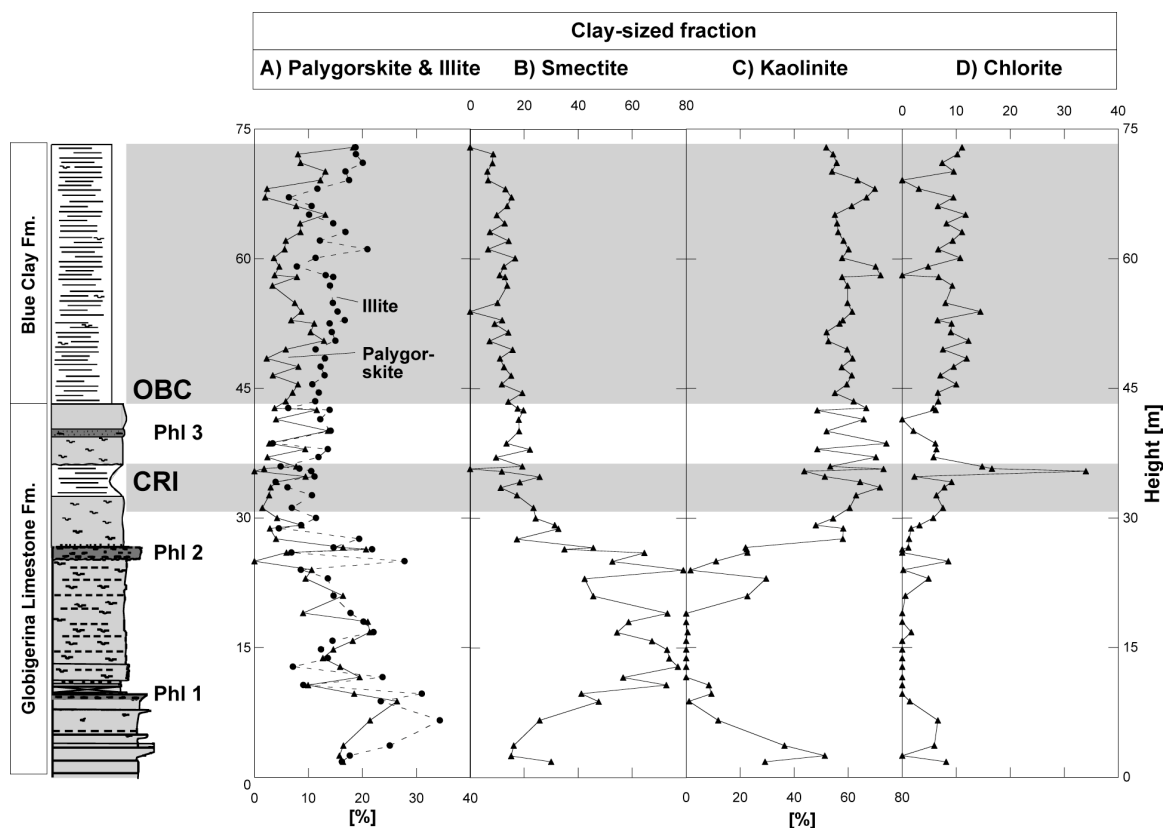
Figure 6*:* Relative abundance (%) in the clay fraction (*<2μm*) of clay minerals. A) Palygorskite, B) smectite, C) kaolinite, D) chlorite. A lithology key can be found on FIGURE 3. Phl: Phosphatic Layer. Clay-sized xrd data is available in TABLE DR4.

2.5.3 Carbonate content

The general trend of the carbonate content record measured by coulometric method (Fig. 7A) is the same as observed in XRD data although at a much higher resolution, with high values at the base of the section (~80wt%), a carbonate minima in the CRI (~45wt%), followed by higher values and then a carbonate crash at the OBC (~20 wt%). Because the coulometric method dissolves all carbonate minerals, between between Phosphatic Layer 1 and Phosphatic Layer 2, an interval where ankerite has been identified by XRD data, calcite content is slightly higher than content deduced from XRD. The higher resolution of the coulometric calcite curve (Fig. 7A) relative to the XRD calcite curve allows for interpretation of more precise shorter-term oscillations. Thus, at least 6 high carbonate content peaks occur during the Blue Clay deposition with values higher than the background (background ~20%, peaks ranging from ~40 wt% to 60 wt%). These peaks in carbonate content occur apparently cyclically, and appear to be compatible with an eccentricity forcing characterized by a marked 100 k.y. period (John, work in progress).

23
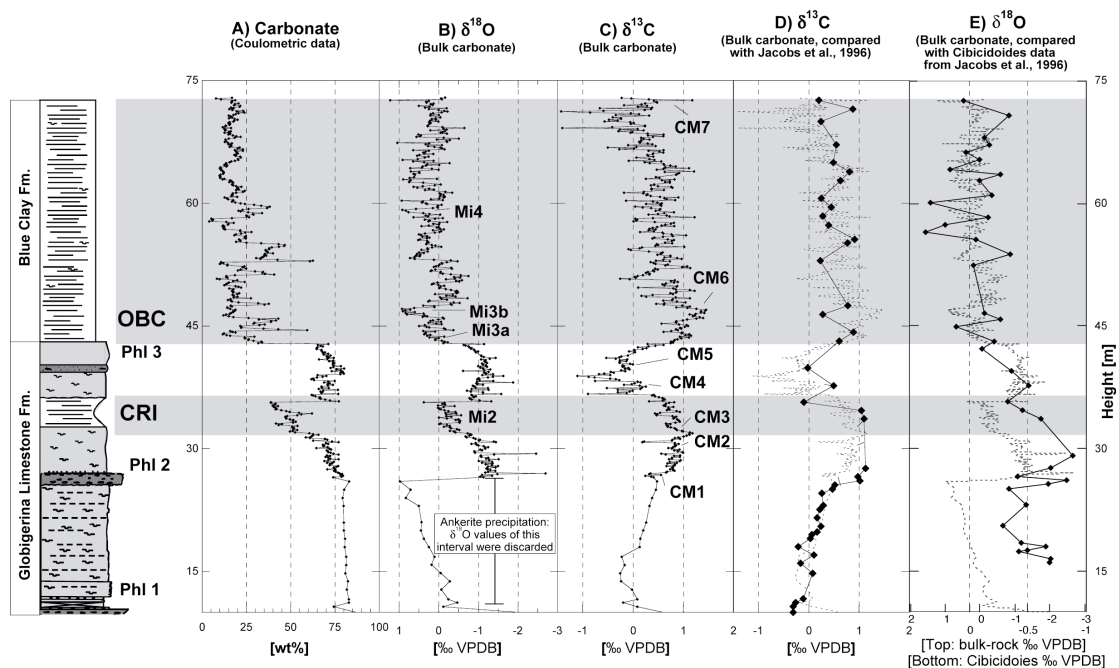
Figure 7: Geochemical results. A) Carbonate content in wt% measured with a coulometric method, B) Bulk carbonate $\delta^{18}O$ [‰ VPDB] values and interpretation of the Mi events 2, 3a and b, and 4, C) Bulk carbonate $\delta^{13}C$ [‰ VPDB] values and interpretation of the CM events 1through 7, D) Bulk carbonate $\delta^{13}C$ [‰ VPDB] values of this study (dashed line) compared with $\delta^{13}C$ [‰ VPDB] bulk carbonate data from the Qammieh section obtained by Jacobs et al., (1996, solid line). E) Bulk carbonate $\delta^{18}O$ [‰ VPDB] values of this study (dashed line) compared with $\delta^{18}O$ [‰ VPDB] Cibicidoides data from the Qammieh section measured by Jacobs et al., (1996, solid line). The heights of the samples from Jacobs et al. (1996) were modified according to our own section. A good fit exists between the high-resolution dataset of this study and the dataset from Jacobs et al. (1996). A lithology key can be found on FIGURE 3. Carbonate content, $\delta^{18}O$ and $\delta^{13}C$ values from this study are available in TABLE DR1.

2.5.4 Isotope stratigraphy

Even though bulk analyses reflect a mixing of carbonates from different sources, it has been shown that under certain circumstances, the isotopic composition of deep-sea sediments derived from bulk analyses resembles closely the record derived from single foraminifera analyses (Shackleton and Hall, 1984; Shackleton et al., 1993). In the case of the present study of shelf carbonates, the isotopic composition of bulk-rock samples measured reflects mainly a planktonic foraminifera and calcareous nannoplankton signal, with very minor input from benthic foraminifera. Thus, the bulk $\delta^{13}C$ signal in the Maltese sections has been shown to reflect values measured on *Globigerinoides bulloides,* with an offset of up to ~2 ‰ towards lower values (Jacobs et al, 1996, see Figure 7 "D"). Moreover, trends identified by the same authors in oxygen isotopes measured on epi-benthic foraminifers of the genus Cibicidoides are similar then trends identified in the bulk-rock (Figure 7, "E"). For these reasons, we rule out the control of either differential diagenesis or sediment composition over trends in stable isotopes recorded on the bulk-rock. The trends of both carbon and oxygen isotopes are interpreted here as reflecting changes in the isotopic composition of sea-water.

All the samples, including those in the Globigerina Limestone, are uncemented but hardened by mechanical compaction. A visual check of sieved samples showed that foraminifers were dominating the carbonate

24

fraction and that they were generally well preserved. Alteration by meteoric water can be ruled out based on $\delta^{18}O$ and $\delta^{13}C$ data which show marine values throughout the Lower Coralline Limestone Formation and its transition to the Globigerina Limestone (Knoerich and Mutti, in review). On the basis of this information, we can reasonably exclude diagenetic alteration effect on measured values. The only exception regards the interval between Phosphatic Layer 1 and Phosphatic Layer 2 where post-depositional ankerite precipitation (up to 15% dolomite) has occurred. As a consequence, oxygen isotope values are slightly more positive than in the rest of the section, and are discarded from further discussion.

From Phosphatic Layer 2 to the top of the section, we identified four major increases in $\delta^{18}O$ (Fig. 7C, Table 1) that were correlated to the globally recognized "Mi" isotopic zones (Miller et al., 1991a; Miller et al., 1991b; Miller et al., 1996b).

$\delta^{13}C$ values were measured and maxima were identified and correlated to global events ("CM" events of Woodruff and Savin, 1991, see also Wright and Miller, 1992). Features identified with certainty (Table 1) include the onset of the Monterey Excursion (OME), as well as the CM3 and CM6 events which are distinct (see also Jacobs et al, 1996). Events CM1, CM2, CM4 and CM5 are somewhat less conspicuous but can be inferred by the position of the two main peaks in $\delta^{13}C$ and the Mi Events, thus refining the age model. A final peak in $\delta^{13}C$ occurs at the end of the Blue Clay Formation. Although it is poorly documented in this sedimentary sequence, previous studies (Jacobs et al., 1996) suggest that it could represents the onset of the CM7 event. High-resolution $\delta^{13}C$ data obtained in this study show an almost perfect fit with low-resolution data obtained by Jacobs et al (1996, Fig. 7D).

Ages obtained by comparing CM and Mi events match well. Thus, by combining chemostratigraphy with strontium datum obtained on phosphatic layers (Jacobs et al., 1996) an age model comprising 14 datum levels is obtained (Table 1).

Sample	Height [m]	Isotopes	Δ Value	Peak Value	Name of Event	Age assigned (Ma)	Sed. rate [m/m.y.]
Q13	9.9	*Strontium*	-	-	*Phosphatic Layer 1*	*24.03*	
Q22	18	Carbon	-	-0.2	OME	18	1
Q30	26	*Strontium*	-	-	*Phosphatic Layer 2*	*17*	9
M0630	31.8	Carbon	0.7	0.5	CM1	16.4	10
M0750	33	Oxygen	1.5	1.5	Mi2	16.1	4
M0800	33.5	Carbon	0.7	0.9	CM2	15.8	2
M0910	34.6	Carbon	0.5	1.2	CM3	15.5	3
M1020	37.5	Carbon	1.2	0.3	CM4	15.1	7
M1470	40.2	Carbon	1.1	0.0	CM5	14.6	5
M1820	43.7	Carbon	2.0	1.5	CM6	14.2	9
M1850	44	Oxygen	1.7	1.8	Mi3a	14.1	2
M2130	46.8	Oxygen	1.2	1.1	Mi3b	13.6	6
X0770	59.8	Oxygen	1.1	1.6	Mi4	12.6	13
X2080	72.9	Carbon	2.6	0.3	CM7 ?	11.5	12

Table 1: *Global events recorded on the Maltese shelf and used for dating. Column 1 yields the sample name, column 2 sample height (meters) in the composite section, column 3 the type of isotopes recording the event. Strontium data are from Jacobs et al. (1996), carbon and oxygen data are from this study. Column 4 gives the difference between the base and the summit of the peak, and column 5 the absolute value of the peak maxima (for oxygen and carbon isotopes only). Column 6 yields the name of the event recorded, column 7 its assigned age and column 8 the sedimentation rate (in m/m.y.) between this sample and the one before in the table. OME is the Onset of the Monterey formation, "CM" events are $\delta^{13}C$ isotopic events described by Woodruff and Savin (1991), and "Mi" events are $\delta^{18}O$ events described by Miller et al. (1991). Events recorded on oxygen isotopes are shaded for easy reading of the table.*

The age model obtained in this study integrates well with ages obtained in nearby sections (Foresi et al., 2001) or on similar deposits in Sicily (Spezzaferri et al., 2001).

2.6 DISCUSSION
2.6.1 Origin and significance of clay minerals

Clay minerals and their relative abundance in marine sediments may record information on climate, eustasy, diagenesis, or deposit reworking (Dixon & Weed, 1977; Chamley, 1989). In order to be able to interpret clay mineral associations we have to distinguish the relative role of detritism and authigenesis.

Authigenesis of clay minerals can take place either syn-sedimentary, or post-sedimentation through fluid flow and burial diagenesis. The thickness of the Neogene deposits does not exceed 100 m on the Maltese Islands, indicating that primary clay mineral composition was preserved since burial diagenetic transformations generally occur at sediment depths exceeding 2 km (Chamley, 1998). Other diagenetic pathways nevertheless exist for authigenic clay minerals formation. It has been for instance demonstrated that clay minerals, such as kaolinite, can commonly crystallize in permeable sandstone (Weaver, 1989). However, the sections presented in this study consist mainly of marls and limestone, in particular during the Blue Clay interval where the maxima in kaolinite content has been observed. Smectite too can be locally formed in the marine realm from early diagenesis, halmolysis (Karpoff *et al.*, 1989) or hydrothermal weathering of volcanic rocks

(Chamley, 1998). Smectite and zeolite may also be derived from alteration of ash layers. Finally, palygorskite and sepiolite are fibrous clay minerals that can be formed *in situ* as a result of hydrothermal processes as well as low temperature alteration of Mg-bearing rocks (Kastner, 1981; Karpoff *et al.*, 1989, and references therein).

Most of the mechanisms explaining the authigenesis of palygorskite, sepiolite and smectite occur in hydrothermal environments such as mid-ocean ridges (e.g. Karpoff et al, 1989). However, the section studied here is located on a carbonate margin and no evidence of such processes could be found.

The second, more common, source of clay minerals is detritism. Clays represent the end product of continental weathering, and are ultimately transported into marine basins. The climatic conditions as well as the very nature of the rock being weathered has a profound influence on the type of clay being formed. However, many studies –including this one- cannot determine with certainty the type of bedrock being weathered since the exact source area remains unknown. Nevertheless, clay minerals can still be useful as climate proxy, especially when used in parallel with oxygen stable isotopes.

Illite, chlorite, together with quartz and feldspars constitute typical terrigenous species (Chamley, 1998). These minerals prevail generally in areas of steep relief where active mechanical erosion limits soil formation, particularly during periods of enhanced tectonic activity, or in cold and/or desert regions where low temperatures and low rainfall reduce chemical weathering (Millot, 1970; Chamley, 1998). The illite identified in this study has a high crystallinity (illite crystallinity index of Kübler, 1987), a sure sign of its detrital origin. Smectite for its part is better formed, when detrital, in soils developed under a warm to temperate climate characterized by alternating humid and dry seasons (Chamley, 1998). Moreover, it has been shown that maximum amounts of smectite frequently coincide with long-term or short-term high sea levels through reworking processes (Deconinck 1992). Palygorskite and to a lesser extent sepiolite are continental products frequently found in lacustrine environment and calcrete soils in arid to semi-arid climatic zones. Nevertheless, palygorskite preferentially forms in perimarine environments where continental alkaline waters are concentrated by evaporation. This latter process is accelerated in warmer temperature zones (Millot, 1970; Singer, 1979; Callen, 1984; Robert & Chamley, 1991). Since each of the mechanisms for palygorskite formation requires warm and arid climatic conditions, its occurrence is considered as an indicator of continental aridity (Chamley, 1989; Adatte *et al.*, 2002). Finally, kaolinite is typically formed in tropical soils and is characteristic of warm-humid climate zones. Areas of kaolinite formation are well-drained with high precipitation, accelerated leaching of the bedrock (Robert and Chamley, 1991) and minimum temperature of 15°C (Gaucher, 1981). Increased kaolinite content may also result from increased erosion, which could be caused by sea level falls (Robert & Kennett, 1994) or by reworking of older sediments and soils during transgressive periods (Chamley, 1998; Thiry, 2000, and references therein).

Clinoptilolite, the zeolite series identified in this study, is abundant in calcareous and clayey rocks of Miocene and Cretaceous age (Kastner and Stonecipher, 1978). This mineral requires Si enrichments in order to be

formed, and thus two main mechanisms exist to explain its presence in non-siliciclastic sediments: input of volcanic material (either basaltic or rhyolitic), or high opal-CT content due to high primary productivity. This second mechanism accounts for 40-60% of the clinoptilolite occurrences (Kastner and Stonecipher, 1978). However, the section between Phosphatic Layer 1 to Phosphatic Layer 2 does not exhibit any of the features common in high productivity environments: no opal remains are present, the sedimentation rate is low, and the sediment is well bioturbated pointing to oxygenated bottom-water conditions. Thus, a volcanic precursor for the clinoptilolite observed in the Maltese section seems likely.

2.6.2 Clay minerals and continental weathering pattern

Between Phosphatic Layer 1 and Phosphatic Layer 2 a paragenesis comprising ankerite, palygorskite, clinoptilolite and smectite exists. This could point to early diagenetic precipitation of clays in this interval, especially since it has the lowest sedimentation rate of the section and is bound by two hardgrounds. However, several facts suggest that a potential diagenetic overprint of the clay signal is unlikely or only limited. First, Pletsh (2001) has shown that in order to grow palygorskite in situ a detrital precursor was needed. Thus, even if the signal could be amplified by diagenesis, detrital palygorskite is still needed. Moreover, kaolinite disappears altogether (0%) in this interval whereas this clay specie is well preserved during diagenetic processes (Chamley, 1989). The complete absence of kaolinite thus points to climatic processes rather than diagenetic transformation. Finally, this Miocene trend of decreasing smectite and increasing kaolinite content has been traced by Visser (1991) in sections located throughout the Central Mediterranean as well as in Atlantic cores from Northwestern Africa. Such a consistent regional trend, found in sections and cores located in two different oceanic basins (Mediterranean and Atlantic), can be more easily explained by a regional change in climate than a similar diagenetic history.

Thus, in agreement with Visser (1991), we interpret the trend from Phosphatic Layer 1 to the CRI (Fig. 6), which shows a net decrease of palygorskite and smectite with a major increase in kaolinite (from near 0% to ~80%, occurring mainly after Phosphatic Layer 2) as a change in regional climate from warm arid to warm humid. A humid climate in the early Late Miocene is also supported by recent palynofacies studies of the Tunisian shelf (Gaaloul et al., 2001). This climatic change subsequently affected weathering patterns in the source area of the clays, in this case the North African margin. The increase of smectite observed between Phosphatic Layer 1 and Phosphatic Layer 2 might not only indicate a climatic change from arid to more seasonal conditions and/or volcanic material weathering, but may also reflect increasing water depth throughout the early Middle Miocene. However, no significant correlation exists between abundance of kaolinite and sea level fluctuations for the Miocene sedimentary sequence of Malta (see also Visser, 1991).

If the OBC and subsequent Blue Clay formation are not differentiated from the Globigerina Limestone formation by significant changes in clay mineral assemblages, some differences in terms of continental weathering between these two formations exist. Thus, quartz and chlorite contents, two minerals resulting from mechanical weathering, have their maximum in the

CRI, while total phyllosilicates content measured in the bulk-rock fraction (reflecting mainly kaolinite content) is dominant after the OBC (threefold increase as compared to their CRI values, Fig. 4 and 5). This probably indicates that the increase in clay and quartz content at the CRI is linked to the reworking of terrigenous material deposited during a relatively more arid period when mechanical weathering was prominent. On the other hand, clays that accumulated after the OBC were mainly derived from weathering under intense hydrolysis. Furthermore, before the OBC (Fig. 8, black triangles) quartz and clays have a positive correlation whereas in the Blue Clay Formation (Fig. 8, gray dots) no correlation is statistically present.
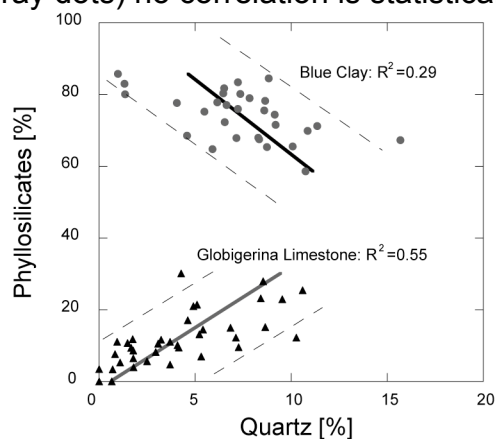

Figure 8: Phyllosilicates [%] vs. Quartz [%]. Black triangles represent samples in the Globigerina Limestone, dark gray dots samples in the Blue Clay formation. A positive correlation of phyllosilicate and quartz contents exists in the Globigerina Limestone. This correlation is negative or statistically insignificant in the Blue Clay Formation.

2.6.3 Longer versus shorter-term variability in continental runoff and carbonate production

Continental runoff, or the rate at which particulate and dissolved matter are transported from the continent into the basin, plays an important role in the ocean-continent geochemical coupling. Quartz and phyllosilicates content can be used as continental runoff proxies in the Maltese sections since 1) quartz is highly crystallized, indicating a continental origin as opposed to poorly crystallized marine opal and 2) clay have been considered to result mainly from continental weathering. As a consequence, the variability of the non-carbonate fraction, mainly composed of quartz and phyllosilicates (see Fig. 4B and C), is an indicator of input of terrigenous material. In order to reconstruct fluxes of terrigenous sediment and carbonate production, Mass Accumulation Rates (MAR) were calculated. MAR of carbonate averaged over 1 Ma time intervals (Fig. 9) are more or less constant through time (around 1 g/cm^2/k.y.), but MAR of non-carbonate phases show high fluctuations. Thus, MAR of non-carbonate, reflecting continental runoff, show a threefold increase between 13-14 Ma (onset of the Blue Clay) and reach a maxima between 12-13 Ma ("Mi 4", coolest event recorded). This indicates that carbonate content is mainly a function of changing flux in terrigenous material: when this flux is high, carbonate content diminishes through a dilution effect, even if primary carbonate production remains constant.
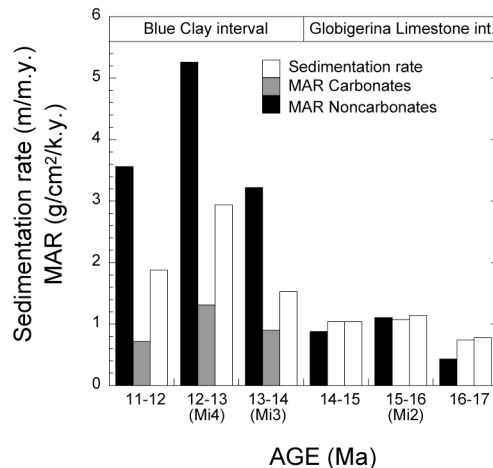
Figure 9: Bulk sedimentation rate [m/m.y.] and Mass Accumulation Rates (MAR) of carbonate and non-carbonate phases [g/cm^2/ky.]. Values are averaged over 1 m.y. MAR of carbonates are relatively constant while MAR of non-carbonate phases greatly increase around 13-14 Ma. The various Mi events (Miller et al, 1991) are indicated below the time interval where they appear. Int. = interval.

As was suggested from the clay fraction and bulk rock mineralogy, the long-term global climate cooling resulted in a change from warm arid to warm humid (Fig. 10). However, the Miocene also experienced shorter-term climatic events generally interpreted as reflecting periods of cooler climate when ice accumulated on Antarctica ("Mi" events (Miller et al., 1991a). Four of these Mi events (Mi 2, 3a, 3b and 4) were identified in the δ^{18}O record (Fig. 7 C). Each of these periods is associated with a decrease in carbonate content (compare Fig. 7 A with Fig. 7 B), and thus by extension to an increase in terrigenous flux (see paragraph above). For instance, the Mi2 event corresponds to the decrease in carbonate content observed in the CRI, and the drop in carbonate content at the OBC corresponds to the onset of the major cooling phase of the Mi3 event. A carbonate content vs. δ^{18}O plot (Fig. 11) further stresses this relationship. These two parameters are strongly negatively correlated for samples located above Phosphatic Layer 2 (diamond shape), with a squared correlation coefficient of 0.65.

If local tectonic processes can control carbonate dilution and terrigenous fluxes through variation in topography, this mechanism is unable to explain the strong correlation between δ^{18}O values, reflecting global climatic trends, and carbonate content. We thus believe, in agreement with earlier investigators (Visser, 1991; Jabobs et al., 1996) that climate, not tectonic, played the major role in determining these parameters. Hence, shorter-term global climate cooling events were regionally characterized by increased terrigenous input. The larger fluxes of terrigenous material reflect increased continental runoff, which is ultimately driven by increased precipitation on land. Moreover, cooler periods when ice cover over Antarctica was important were probably characterized by rapid (100 k.y. scaled) and large amplitude changes in climate (as suggested for the Pliocene by Peizhen et al., 2001).

30
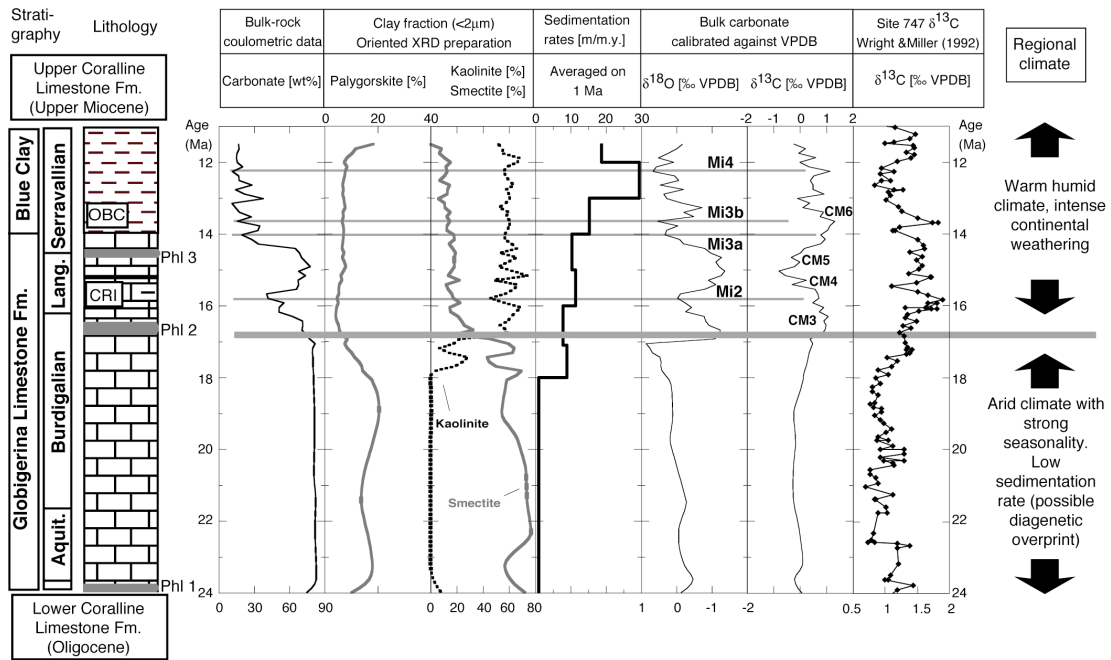
Figure 10: *Summary of the various proxies and climatic interpretation. A lithology key can be found on FIGURE 3. Carbonate [wt%, coulometric], $\delta^{18}O$ [‰ VPDB] and $\delta^{13}C$ [‰ VPDB] curves are interpolated. Palygorskite, kaolinite and smectite (% of the clay fraction) curves are smoothed. Sedimentation rates [m/m.y.] are averaged over 1 Ma when time resolution permits (i.e. for ages younger than 18 Ma). Prominent Mi events and CM events recognized in this study are featured on the oxygen isotopes and carbon isotopes curves respectively. Deep sea $\delta^{13}C$ for ODP site 747 (Kerguelen Plateau, Wright and miller, 1992) is shown as a comparison. Regional climate interpretation is featured on the right.*

Changes in ice volume such as the ones inferred to happen at the Mi3 events imply major eustatic readjustments. Superimposed to these longer-term eustatic changes, rapid shorter-term eustatic changes occurred and had as a consequence to frequently modify the equilibrium of the sediment slope, and thus to favor resedimentation. Both of these rapid changes in climate and eustasy would have prevented the landscape to approach equilibrium in the late Middle Miocene, hence the mass of sediment being eroded was greater.

Figure 11: Carbonate content [wt%] vs. $\delta^{18}O$ [‰ VPDB]. Black triangles are samples below Phosphatic Layer 2, gray 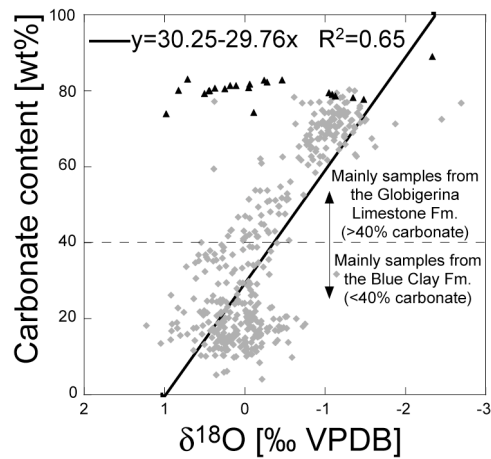diamonds samples above Phosphatic Layer 2. A relationship between high carbonate content and low $\delta^{18}O$ exists above this Phosphatic Layer.

2.6.4 Possible mechanism for increased rainfall during Miocene pulses in glaciation

Part of the answer to why global climate cooling would be recorded on the North African continental margin as an increase in terrigenous input probably lies in the Miocene continental ice distribution. One major difference when comparing the early Middle Miocene world with the modern one is that the North Pole was ice-free at that time. Thus, waxing and waning of Antarctic ice sheets was probably playing a predominant role in determining the oceanic and atmospheric current patterns. Jansen et al. (1996) have shown that in the Quaternary the Angola-Benguela front latitudinal movement was controlled by eccentricity-driven waxing and waning of the southern hemisphere ice fields In the Miocene, pulses in glaciation ("Mi" events) were periods when the thermal gradients between the northern and the southern poles were the largest. Consequently, it is reasonable to assume that atmospheric and oceanic circulation sensitive to pressure gradients should haven been affected by Mi events with amplitude in changes greater than during the Quaternary. We propose that a major consequence of Mi events was that northward winds coming from the southern hemisphere were stronger than southward winds coming from the northern hemisphere. Atmospheric fronts, such as the Intertropical Convergence Zone (ITCZ) would thus have been shifted farther north of the equator than today (Fig. 12). This shift would imply that most of the water being evaporated in the tropical belt was carried further northward, and thus that regional precipitation increased on the Northern African continent. This mechanism, linked to regional drainage of North Africa towards the Mediterranean, is likely to impact weathering rates and sediment budget.
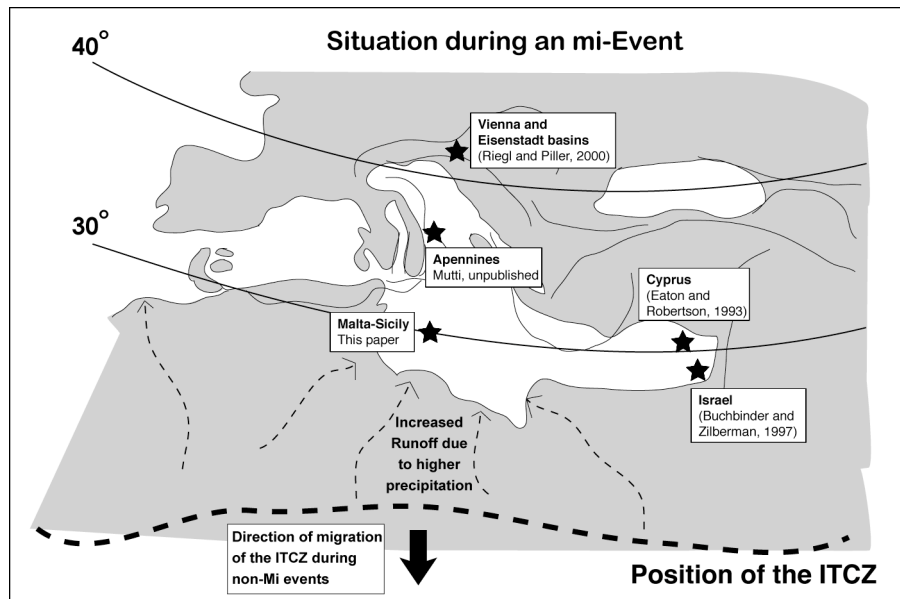
Figure 12: *ITCZ model with regional examples. Black stars indicate locations where terrigenous flux might have increased from the early to the late Miocene. The figure shows the situation during an Mi-event. Due to the cooling of the South Pole with respect to the North Pole, southern winds are stronger and the ITCZ is pushed northward, bringing more moisture and rainfall to the Northern African continent. This results in increased rainfall and runoff (small dashed arrows). The exact positions of the ITCZ is not realistic, but is only meant as a model. During a non-Mi event time, the ITCZ would lie more to the south (direction of the big arrow), and the region would be relatively arid. Paleomap is based on Dercourt et al. (1993).*

If this model is correct, then increased terrigenous fluxes should be recorded throughout the Mediterranean region, at least for basins having influx of African runoff waters. Although we have no data on quantified terrigenous fluxes, some outcrops indicate that sedimentation in the Mediterranean switched from carbonate-dominated in the Burdigalian to widely siliciclastic-dominated in the Late Burdigalian- Serravalian (Esteban, 1996). Regional examples (Fig. 12) include the Apennines (Mutti, unpublished data), Israel (Buchbinder and Zilberman, 1997), Cyprus (Eaton and Robertson, 1993) and even epicontinental basins such as the Vienna and Eisenstadt basins (Riegl and Piller, 2000). For sections located on the northern rim of the Mediterranean, the Alpine orogeny must also be taken into account: local alpine glaciers as well as a rapidly changing topography might overprint the sediment budget linked to climatic changes.

(Raymo and Ruddiman, 1992), based on strontium isotope data, suggested that the uplift of the Tibetan Plateau increased siliciclastic weathering and that this mechanism was responsible for the rapid cooling step observed in the Middle Miocene (Mi 3 event). Although more recent studies of Miocene geochemical budget have questioned this hypothesis (Goddéris and François, 1996), siliciclastic weathering remains a potential factor in controlling pCO_2. What the Maltese rock record suggests is that the Mediterranean continental weathering increase in the Middle Miocene was linked to changes in the position of atmospheric fronts rather than regional uplift.

33

2.7 CONCLUSIONS

(1) Beginning with the onset of the Mi2 phase of cooling, continental derived kaolinite was the main clay mineral produced on and exported from the African continent, suggesting long-term change in weathering from warm arid to warm humid conditions.

(2) The abrupt transition from limestone to marl observed between the Globigerina Limestone Formation and the Blue Clay Formation coincides with a global climate event (Mi 3 event). The increased water depth of the Blue Clay cannot in itself explain this change since the rate of carbonate accumulation remained constant, and the environment remained hemipelagic.

(3) During shorter-term periods of globally cooler climate (single "Mi" events), fluxes of terrigenous material were higher while carbonates fluxes remained constant. Since the carbonate and terrigenous contents are paralleling global events as recorded by $\delta^{18}O$, we infer, in agreement with all previous studies (Visser, 1991; Jacobs et al., 1996), that this relationship was mainly driven by climate, not tectonic. We furthermore suggest that increased fluxes in terrigenous material were linked to increased continental runoff.

(4) Episodes of Antarctic cooling probably resulted in stronger thermal gradient between the South and North poles, which would have induced a northward shift of the ITCZ. Hence, the tropical rain belt zone would have moved further north over Northern Africa. In addition, climate during Mi events was probably characterized by larger amplitude 100 k.y. changes which would have prevented landscape to approach equilibrium, therefore contributing to increased input of sediment in the Mediterranean.

2.8 APPENDIX: description of XRD methods

Bulk-rock analysis: Random powder of the bulk sample is used for characterization of the whole rock mineralogy. Nearly 20 gr. of each rock sample was ground with a "jaw" crusher to obtain small chips (1 to 5 mm) of rock. Approximately 5 grams were dried at 60 °C and then ground again to a homogenous powder with particle sizes <40μm. 800 mg of this powder were pressed (20 bars) in a powder holder covered with a blotting paper, and then analyzed by XRD. Whole rock composition was determined by XRD (SCINTAG XRD 2000 Diffractometer) based on methods described by Ferrero (1965, 1966), Klug and Alexander (1974) and Kübler (1983). This method for semi-quantitative analysis of the bulk rock mineralogy uses external standards. Clay content in the bulk-rock fraction was estimated using the intensity of the ~19.8 ° 2θ peak and a mixed phyllosilicates standard. Estimate of the relative percent of the various phyllosilicates species in the fine-silt and clay-sized oriented fraction (see below) remained however independent from this result.

Clay mineral analysis: Clay minerals analyses were done on the same sample set as for bulk-rock mineralogy. Analytical procedure was based on methods developed by Kübler (1987). Ground chips were mixed with de-ionized water (pH 7-8) and agitated. The carbonate fraction was removed with the addition of HCl 10% (1.25 N) at room temperature for 20 minutes or more, until all the carbonate was dissolved. Good desegregation of the sample was assured by plunging it for 3 minutes in an ultrasonic bath. The insoluble residue was washed and centrifuged (5-6 times) until a neutral suspension was obtained (pH 7-8). Separation of different grain size fractions (clay-sized <2μm, and fine-silt 2-16 μm) was obtained by the timed settling method based

34

on Stokes law. Each fraction was then pipetted onto a separate glass plate and air-dried at room temperature. XRD analysis of each oriented fractions were made after air-drying at room temperature ("normal sample"), and a second analysis was made for the clay-sized fraction after keeping the samples overnight in ethylen-glycol solvated conditions (in order to estimate the content in swelling, "glycolated sample"). Zeolite was determined to be of the heulandites-clinoptilolite series on the XRD diffractograms of the fine-silt fraction (Fig. DR1 A). Typical clay-sized fraction diffractograms for the Globigerina Limestone ("B") and the Blue Clay formation ("C") are also shown in this figure.

Quantification of clay minerals: The files generated with SCINTAG were raw data (.RD), subsequently converted by the software (DMS program, v. 2.63, graphic-normal display) into calculated (.NI) files. The calculations are the following: Fast Fourier noise filter, background subtraction and Kα2 stripping. Measurements are made on calculated files. The intensities of selected XRD peaks characterizing each clay mineral present in both the fine-silt and clay-sized fraction (e.g. chlorite, mica, kaolinite, palygorskite, zeolite and smectite) were measured for a semi-quantitative estimate of the proportion of clay minerals present. Therefore, clay minerals are given in relative percent abundance without correction factors. Where clay mineral peaks overlapped (typical for the K002/C003 peaks at ~24.5-25.2^{o} 2θ, or the palygorskite-smectite peaks), a mathematical profile fitting was applied using the DMS 2000 software. Content in swelling (% smectite) was estimated by using the method of Moore and Reynolds (1989).

- CHAPTER 3 -

History Of The African Monsoon Inferred By Middle Miocene Sapropels-Like Deposits In The Mediterranean

3.0 ABSTRACT

We present new organic geochemical data (TOC, N_{org}/C_{org}, $\delta^{13}C$, $\delta^{15}N$) from Middle Miocene mixed carbonate-siliciclastic deposits outcropping on the Maltese Islands (central Mediterranean). These results suggest that sapropel-like deposits already existed in the Middle Miocene. Since Pleistocene sapropels reflect periods of stronger African monsoon, we infer that our record contains a history of the monsoon during the Miocene. By tuning carbonate content to orbital parameters we obtain an age model that suggests that the African monsoon probably initiated around 16.7 Ma and underwent a major strengthening around 13.8 Ma. We argue based on recent seismic studies that the teleconnection existing nowadays between the Asian and African monsoon was already established in the Miocene.

3.1 INTRODUCTION

The monsoonal circulation, a dominant feature of tropics of Southeast Asia and Africa, is characterized by seasonal shift in wind direction. In the winter, the continents are colder than the ocean and induce northeasterly dry winds toward the Arabian Sea (Asian Monsoon) and the Gulf of Guinea (African Monsoon, Hastenrath, 1985). In the summer the continent heats up and the resulting low-pressure cell creates advection of humid air from the ocean in a southwesterly direction, enhancing precipitation on land. The strength of the African monsoon is known to have played a major role in determining sedimentation pattern in the Mediterranean during the Plio-Pleistocene (Rossignol-Strick, 1985). Stronger monsoons resulted in increased rainfall over Ethiopia, thus triggering larger Nile river floods (Rossignol-Strick, 1985). The input of a large quantity of fresh water in the Mediterranean weakened the existing anti-estuarine circulation (Stratford et al., 2000), and triggered the formation of an oxygen minimum zone and the deposition throughout the Mediterranean of organic-rich layers called "sapropels" (Rossignol-Strick, 1985).

Dating the onset or strengthening of the monsoon is usually based on Asian records. Recent studies suggest that the Monsoon intensified prior to 8 Ma (Blisniuk et al., 2001; Clift and Gaedicke, 2002; Guo et al., 2002). Work on the Maltese Islands in the Central Mediterranean (Xatt-L'Ahmar section, Fig.1) has shown that these mixed carbonate-siliciclastic shelf sequences record a history of African rainfall during the Miocene (Visser, 1991; Jacobs et al., 1996; John et al., 2003). In this paper we aim to show that 1) the Xatt-L'Ahmar section contains evidence of sapropel-like deposits already in the Middle Miocene, and thus by extension is a record of the strength of the African monsoon 2) that, as expected for a record of monsoonal strength, cyclicity associated with orbital parameters are present in the proxies studied, and 3) that this record, in contrast with its Asian equivalents, can be precisely dated by using orbital tuning techniques.
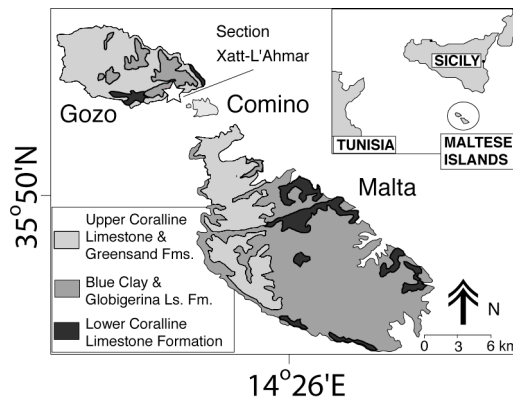
Figure 1: General map of the Maltese Islands showing the location of Malta, Gozo and Comino. Stars show the location of the Xatt-L'Ahmar outcrop on Gozo. Modified after John et al (2003).

3.2 SETTING AND PREVIOUS STUDIES OF THE MALTESE ISLANDS

The Maltese Islands, now in the central Mediterranean, were located on the northern African Plate during the Miocene (Dercourt et al., 1993). The section studied (Fig. 1 and Fig.2) consists of two distinct lithological units (Felix, 1973): the carbonate-rich Globigerina Limestone Formation (Early to Middle Miocene in Age) and the clay-rich Blue Clay Formation (Middle Miocene in age). Additionally, a significant clay-rich interval (CRI) was found in the Globigerina Limestone formation. Clay mineral data at the onset of the CRI (Fig. 2) suggest that North African climate switched from warm arid to warm humid around 16.5 Ma (Visser, 1991; John et al., 2003), during a phase of Antarctica glaciation known as Mi2 (Miller et al., 1991a; Zachos et al., 2001). Moreover, a link between each phase of Antarctic glaciation ("Mi" events) and increased mass accumulation rates (MAR) of terrigenous material due to increased rainfall on the North African continent was established and interpreted as possible northward shifts of the Inter Tropical Convergence Zone (ITCZ, John et al., 2003). The position of the ITCZ over Africa is directly linked to the strength of the monsoon since it determines how far north the rain brought by the low level westerly winds will fall (Rossignol-Strick, 1985).
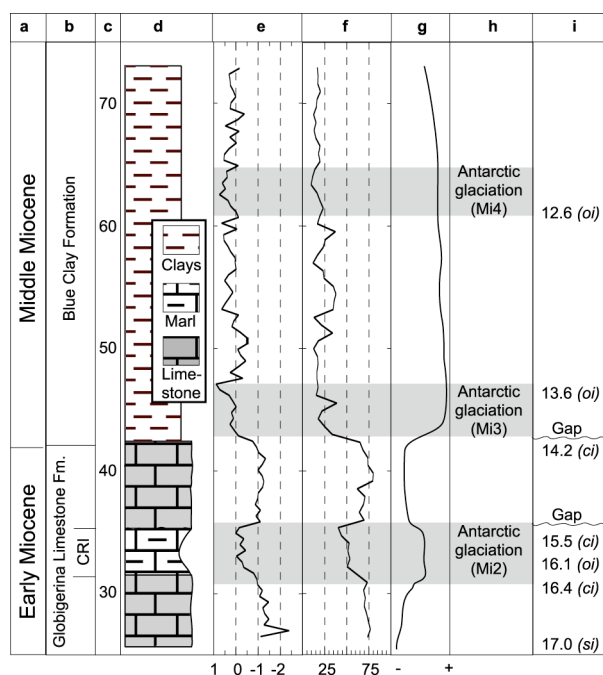
Figure 2: *Summary of the climate history inferred from the Xatt-L'Ahmar section by previous studies. a) Epoch. b) Lithostratigraphic formation. c) Height (in meters) of the section. d) Lithology. e) $\delta^{18}O$ values of bulk carbonate [‰]. f) Carbonate content [wt%]. g) Inferred strength of continental runoff based on Mass Accumulation Rates and clay minerals assemblages. h) Timing of Antarctic glaciation. i) Tie points for the age model and sedimentation gaps recognized on the field. Acronyms in parenthesis designate the type of time point: "oi" are Mi events recorded on oxygen isotopes, "ci" are CM events recorded on carbon isotopes, "si" are strontium isotopes ages measured on carbonates (Jacobs et al., 1996). Columns e, f and g are after John et al., 2003.*

3.3 ANALYTICAL METHODS

A total of 466 samples were collected for this study in the Xatt-L'Ahmar section (Maltese Island of Gozo), with a sampling density of 1 sample per 10 cm. Samples were hand grinded at the University of Stuttgart using an agate mortar, and the resulting powders were used for geochemical analysis.

Total carbon (TC) and total nitrogen (TN) content were measured at the University of Southern California (USC) using a Carlo Erba elemental analyzer. Total inorganic carbon (TIC) was measured at the University of Stuttgart using a coulometric method. Carbonate content was obtained by multiplying TIC by 8.33. Total organic carbon (TOC) was obtained by subtracting TIC to TC. Bound (inorganic) nitrogen content was estimated by averaging TN values of samples with 0 wt% TOC. Organic nitrogen (N_{org}) was calculated by subtracting the averaged value for bound nitrogen to TN. C_{org}/N_{org} ratios were calculated for samples with TOC > 0.1 wt%. Each term was divided by its atomic mass to obtain moles, and than the molar ratio was calculated.

Stable isotopes measurements on organic matter were made at the University of British Columbia, Canada. Nitrogen isotope ratios of the samples were measured on a Fisons NA1500 elemental analyzer coupled to a VG prism mass spectrometer in a continuous flow of helium. Analytical precision is ± 0.2 " (1s) and the values are reported relative to air N_2. The carbon isotopic composition of organic matter was measured on decalcified (10% HCl followed by oven drying without washing) samples using a Fisons NA 1500 elemental analyzer coupled to a VG prism mass spectrometer with an analytical precision of ± 0.1 ‰.
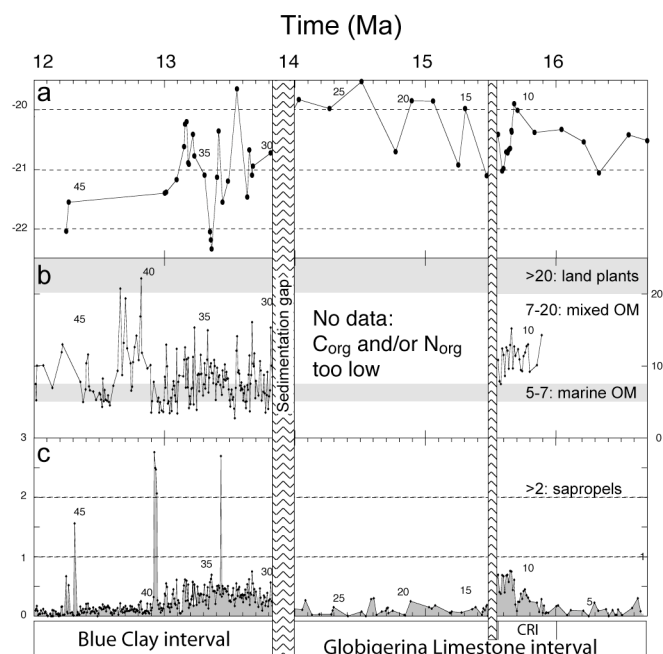
Figure 3: *Analysis of the organic matter. a) $\delta^{13}C$ values [‰] of the organic matter. b) C_{org}:N_{org} molar ratio [no unit]. No data could be obtained for this proxy in the Globigerina Limestone interval outside of the CRI due to low TOC and/or N_{org} values. c) Total Organic Carbon values [wt%]. The small numbering (1-45) refers to the eccentricity maxima recognized in the age model. OM: organic matter. CRI: Clay-rich interval. All data presented on this figure are available in table DR1.*

3.4 RESULTS AND DISCUSSION
3.4.1 Organic geochemical results

Results obtained for stable isotopes analysis of the organic matter (Fig. 3a, Table DR1) show that $\delta^{13}C$ values in the Globigerina Limestone interval are around ~ -20.5‰, and slightly lower in the CRI (~ -21‰). Values in the Blue Clay interval are significantly lower, with $\delta^{13}C$ minima around –22.5‰ (-21.3‰ in average). C_{org}:N_{org} results (Fig. 3b, Table DR1) show that values in the CRI and Blue Clay interval range from 22 to ~3, with base values centered around 5-7. No C_{org}:N_{org} values could be obtained for the Globigerina limestone. Total organic carbon content (TOC, Fig. 3c, Table DR1) in the Globigerina Limestone interval is in average below 0.5 wt%, while values in the Blue Clay and CRI intervals are generally higher (0.6wt% in average). Finally, $\delta^{15}N$ values of the organic matter measured for this study are ranging from 3 to 5‰ (Table DR1).

3.4.2 Signature of Miocene sapropels-like deposits

Pleistocene sapropels are distinguished by high TOC (>2 wt% TOC, Kidd et al., 1978) due to dysaerobic conditions, mixing between terrigenous and marine organic matter and low carbonate content (Rossignol-Strick, 1985; Schenau et al., 1999). If the CRI and Blue Clay intervals represent proto-sapropels, we expect them to display similar characteristics. Carbonate content in the Blue Clay interval is low (~20wt% base value, John et al., 2003), and TOC content exceeds 2wt% in two discreet layers (Fig .3c). Though TOC values otherwise rarely exceed 0.6 wt%, we argue that primary organic matter content might have been high but not preserved by geological processes, a phenomenon commonly observed in ancient sapropels (Schenau et al., 1999). C_{org}:N_{org} ratio and $\delta^{13}C$ value of the organic matter can

be used to determined the degree of organic matter mixing. A higher content of terrigenous organic matter would reflect input by increased rivers runoff linked to higher precipitation (monsoon), and would thus mean that the interval is compatible with a sapropels-like mechanism of deposition. Land plants commonly have $C_{org}:N_{org}$ values above 20 and very low $d^{13}C$ values (<21‰, Sackett and Thomson, 1963; Hecky et al., 1993), whereas the $C_{org}:N_{org}$ ratio for purely marine organic matter ranges from 5 to 7 and its average $d^{13}C$ value is ~ –20.6 ‰. $C_{org}:N_{org}$ ratio values in our section (Fig.3b) suggest that the organic matter has a mixed marine and continental origin. This is also supported by $\delta^{13}C$ values: $\delta^{13}C$ values in sapropels have been shown to be more negative due to mixing with ^{12}C –rich land plants (Schenau et al., 1999), and thus the low values in the Blue Clay (and to some extend in the CRI) are reflecting a greater input of terrestrial organic material (Fig. 3c). Additionally, $d^{15}N$ values between 3 and 5 ‰ are in good agreement with values found in regions with large river inflow (Schubert and Calvert, 2001). This last result suggests increased fresh water input, consistent with higher runoff during deposition of the Blue Clay Formation.

Ancient sapropels currently recognized in the Mediterranean date back to 10 Ma and have been shown to reflect the same mechanism of formation as their Plio-Pleistocene counterparts (Schenau et al., 1999). The CRI and Blue Clay intervals represent time of high runoff, with increased mixing of terrigenous organic matter and higher TOC content linked. We thus propose that they reflect a mechanism of deposition similar to sapropels, and by extension that they contain a record of the strength of the African monsoon.

3.4.3 Spectral analysis of the Blue Clay deposits and orbitally tuned age model

Since the strength of the monsoonal circulation is directly linked to the quantity of solar energy reaching the surface of the continent (Rossignol-Strick, 1985; Prell and Kutzbach, 1992), it is dependant on orbital parameters regulating insolation such as the shape of Earth's orbit around the sun (eccentricity), the tilt of its axis (obliquity) and the wobbles of this axis (precession). Spectral analysis of carbonate content data from the Blue Clay interval (Fig.4) reveals the presence of cycles with frequencies compatible with the eccentricity signal (~100-110 ky). An ambiguous 54-59 ky cycle could reflect the rather weak 54 ky obliquity cycle, or might be a precession or obliquity cycle shifted by a combination of sampling aliasing and nonlinearity of the response to insolation forcing (our sampling resolution is ~6 ky). The sampling resolution also prevented the unbiased identification of precession cycles, and the ~33ky and 22 ky cycles are here tentatively interpreted as reflecting precession. Spectral analysis thus suggests that eccentricity and, to some extent, precession and obliquity parameters were instrumental in pacing the sedimentation of the Blue Clay. These Milankovitch frequencies are often found in areas dominated by the monsoon (Prell and Kutzbach, 1992). Here, it is thought that the eccentricity modulates the precession cycles of the monsoon, and thus that these frequencies are present.
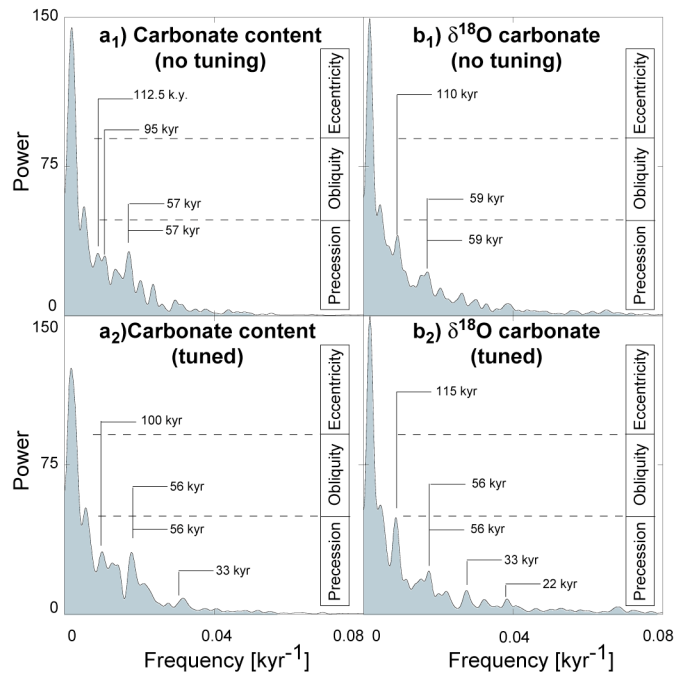
Figure 3: Spectral analysis of the Carbonate content (a) and of the $\delta^{18}O$ values for bulk carbonate (b) in the Blue Clay interval. Results are shown on the interval before orbital tuning (a_1 and b_1) and after tuning (a_2 and b_2). The orbital parameter associated with the frequency of each marked peak is indicated on the right. Periodograms were obtained using the Blackman-Tuckey method with 1/3 lag and Barlett window.

This also means that we can use carbonate content to "tune" our sedimentary record with a calculated curve of the eccentricity of the Earth's orbit and thus obtain a precise dating of the section. Orbital tuning and spectral analysis were performed combining the use of "TRIP", an internal time series analysis program developed at the "Observatoire de Paris", and Analyseries 1.2 (Paillard et al., 1996). The carbonate content curve was first linearly de-trended and re-sampled with a constant step of 1 ky. Two different tuning methods were then applied depending on the interval. In the Blue clay interval the time resolution is higher and the age model was obtained following three steps. **1)** 400 ky-filtered curves were obtained by applying a Gaussian filter to the eccentricity (Laskar, 2001) and carbonate content curves. The two tie points for the carbonate content (Mi3 = 13.7±0.5 Ma and Mi4 = 12.9±0.5 Ma) were iteratively changed within their time uncertainties until the overlapping of both 400 ky-filtered curves was maximal (optimum age for the tie points: Mi3=13.6, Mi4=12.8). **2)** The 400 ky-filtered carbonate content curve obtained was manually adjusted to perfectly fit the 400 ky eccentricity curve. **3)** 100 ky-filtered curves for the eccentricity and for the carbonate content (adjusted as in step 2) were calculated and manually adjusted to fit the 100 ky-filtered eccentricity curve. Precision for the ages obtained in the Blue Clays by this method is considered to be ±0.1 Ma.

Time resolution in the other intervals did not permit such a fine adjustment. The carbonate content signal was directly compared to the eccentricity curve and manually adjusted until a satisfying mathematical fit between the two curves was obtained. The 100 ky-filtered curves of the eccentricity and the carbonate content (same settings as above) were then compared to ensure a good result. Precision with this method is estimated to be of ±0.2 Ma or better, especially since the density of tie points in this interval is high.
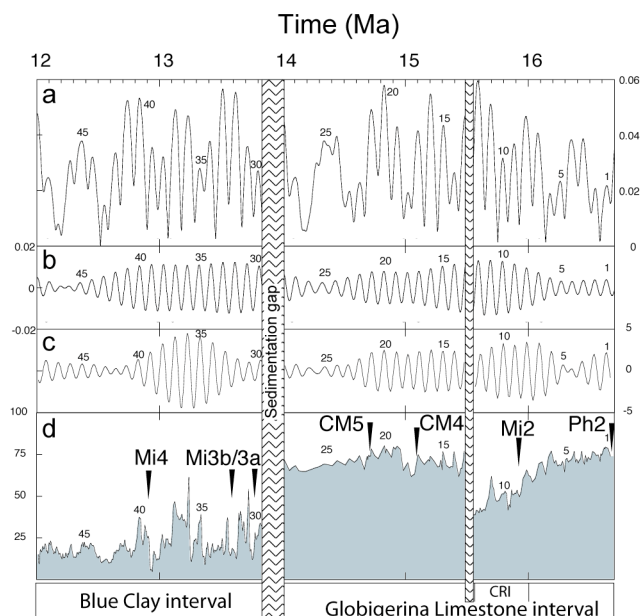
Figure 5: Orbitally tuned age model obtained for the Xatt-L'Ahmar section. a) Eccentricity of the earth orbit (Laskar, 2001). b) 100 ky-filtered curve of the eccentricity (bandwidth of the filter is 10^{-3}). c) 100 ky-filtered curve of the carbonate content (bandwidth of the filter is 10^{-3}). d) Carbonate content [wt%]. The small numbering (1-45) refers to the eccentricity maxima and can also be traced in Fig. 2. The black arrows and larger numbering refer to the isotopes tie points identified in the section (see John et al.,2003, for a complete description) and used for orbital tuning. Oxygen isotopes events (described in Miller et al., 1991): Mi2 (16.2±0.5 Ma), Mi3a (14.1±0.5 Ma), Mi3b (13.7±0.5 Ma), Mi4 (12.9±0.5 Ma). Carbon isotopes events: CM4 (15.1±0.5 Ma), CM5 (14.6±0.5 Ma). Strontium isotopes measured in phosphatic layers (Jacobs et al., 1996): Phl2 (17±0.8 Ma). CRI: Clay-rich interval. Data for the age model is available in table DR2.

Results of the orbital tuning (Fig.5, Table DR2) provide timing for sapropels-like deposition, and by extension for the history of the African monsoon. Consequently, we infer an onset of the African monsoon around 16.7 Ma (CRI), it weakening around 15.55 Ma, its subsequent strengthening around 13.8 Ma (Blue Clay) and finally its demise around 12 Ma when shallow-water carbonate ramps are re-established on the Maltese shelf.

3.5 CONCLUSIONS

Since they reflect times of higher continental runoff, with increased TOC content and mixing of organic matter, and since orbital parameters forced their deposition, the CRI and Blue Clay intervals can be regarded as proto-sapropel deposits. Furthermore, the timing of events discussed implies that the history of the African monsoon is intimately linked to the history of global climate since its onset corresponds to the Mi2 glaciation, its weakening to the Middle Miocene warm period and its establishment in strength to the major cooling and Antarctic ice build-up phase of the Mi3 glaciation (Zachos et al., 2001). Our data for the onset of the African monsoon are also in good agreement with recent seismic stratigraphy studies on the Oman margin (Clift and Gaedicke, 2002) which suggest an onset of the Asian monsoon around 16.5 Ma. The coherence of these two dates indicates that the teleconnection existing nowadays between the African and Asian monsoonal circulation was already established at that time. Computer modeling of the history of the monsoons (Fluteau et al., 1999) has shown that the shrinkage of the Parathetys and the closure of the Tethys seaway played a major role in

43

enhancing and coupling the Asian and African monsoons. Thus, our results might help to constrain the timing of the closure of the Tethys seaway, and also suggest the existence of a link between this event and global climate.

- CHAPTER 4 -

Relative Controls Over Slope Sedimentation In A Miocene Subtropical Heterozoan Carbonate System (Marion Plateau, ODP Leg 194)

4.0 ABSTRACT

Several carbonate platforms initiated in the Early Miocene on the Marion Plateau (Northeastern Australia), and although they occurred in low-latitude subtropical waters, these edifices were composed mainly of heterozoan organisms. Here we address the question of the relative control of paleoceanography, eustatic sea-level and water temperature over the deposition of slope carbonate sediments on this plateau. We investigated an upper to distal slope transect located close to the Northern Marion Platform, the sediments analyzed coming from sites drilled during ODP Leg 194. We reconstructed mass accumulation rates of carbonate as well as oxygen, carbon and strontium stable isotopes. Using chemostratography, we significantly improved time correlation between distal and proximal slope sites. We furthermore confirmed the existence of an as yet inferred hiatus/condensed horizon occurring in the upper slope site 1194, and we were able to date its onset and duration. Subtracting the effect of long-term global carbon reservoir changes to our $\delta^{13}C$ record suggests the existence of 6 productivity cycles, each likely tied to sea-level changes. We conclude that sedimentation over the plateau was mainly controlled by strength and direction of oceanic currents, and further modulated by sea-level and eustatic changes.

4.1 INTRODUCTION

For the last several decades, works on Cenozoic paleoceanography and paleoclimatology have mainly focused on deciphering the deep-sea record. Deep-sea sediments are far from the direct influence of land masses and less sensitive to salinity changes. Paleo-temperature and paleo-circulation can thus be more easily reconstructed using geochemical methods. On the other hand, shallow-water systems record the influence and feedback of continents and shallow-water seas, and there is an increasing awareness that archives complementary to the deep-sea record have to be exploited in order to reach a more comprehensive understanding of global climate change. Carbonate systems have a particular importance in the context of shallow-water ocean margin's environments. First, precipitated calcareous shells of marine organisms record changes in the physico-chemical parameters of their environment, and biological assemblages present in carbonate rocks are indicative of past environments. Then, carbonate rocks constitute an important carbon reservoir which might directly control the quantity of greenhouse gases present in the atmosphere (Berger, 1982). Carbonate systems consequently represent a sensitive archive of climate and sea-level changes (e.g. Schlanger and Premoli-Silva, 1986; Fairbanks, 1989; Pigram et al., 1992a; Eberli et al., 2002; Isern, Anselmetti, and Blum, 2002). Deciphering paleoceanography from carbonate system has

proved a valuable tool (Mutti et al., 1999). Factors other than water-temperature, in particular nutrients level and water turbidity can influence the type of organisms present (Hallock, 1988; James, 1997; Mutti et al., 1999; Hallock, 2001; Mutti and Hallock, In press).
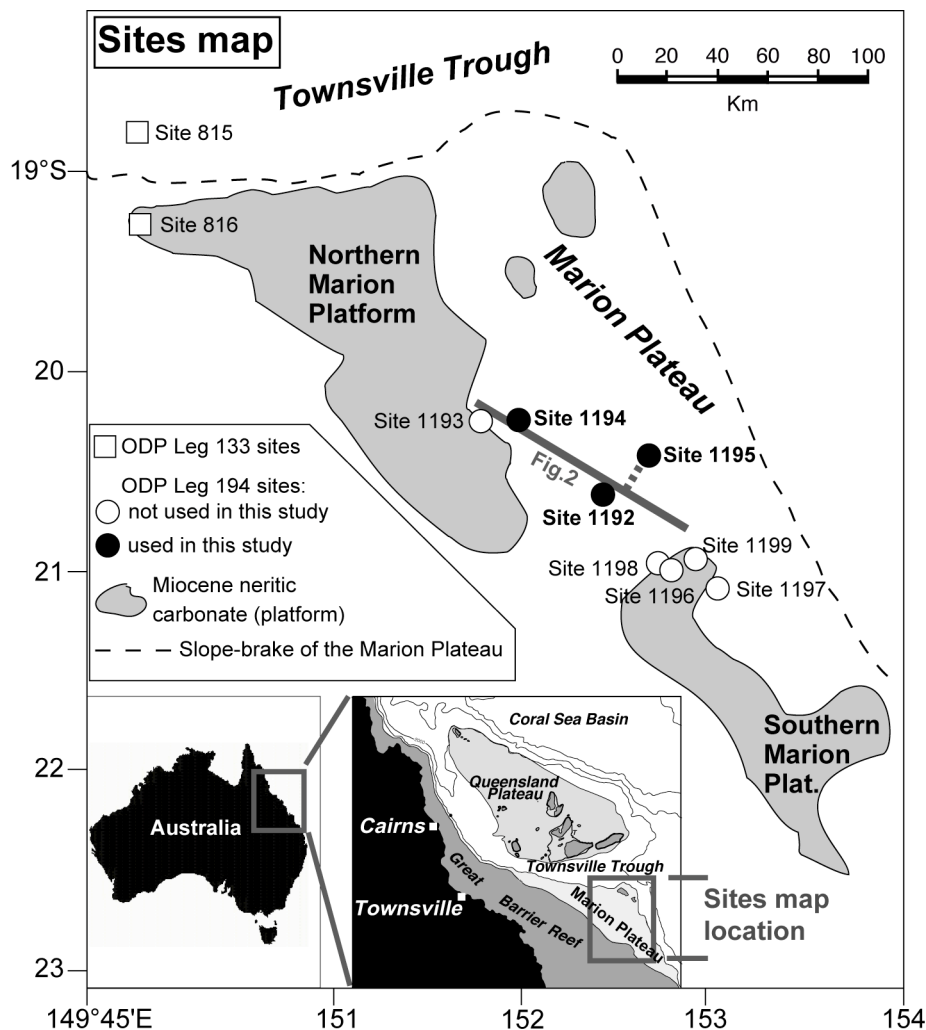

Figure 1: *Location of the sites investigates in this study, and of other regional sites drilled by ODP. Locations of the three sites discussed in this paper (sites 1194, 1192 and 1195) are indicated by black points. Note the thick gray line indicating the direction of projection for Fig.2.*

Carbonate sediments deposited on the Marion Plateau (offshore Townsville, Northeastern Australia, Fig.1), offer a unique opportunity to study the response of a heterozoan carbonate system to global climate, sea-level and paleoceanographic changes. Facies recovered on the northern rim of the Northern Marion Platform (Fig.2, ODP Site 816, McKenzie and Davies, 1993) were described as subtropical photozoan associations, while time equivalent facies recovered on the southern rim of the same platform were rich in bryozoans, red algae and mollusks but yielded almost no green algae or corals (Isern, Anselmetti and Blum 2002). These low-latitudes mixed heterozoan-photozoan carbonates suggest that oceanographic factors were important over the occurrence and evolution of these two widely different biotic assemblages present on the same platform. Sea-level variations over the Marion Plateau being relatively well constrained (N12-N14 event, Isern,

46

Anselmetti, and Blum, 2002; John et al., under review), this setting offers a rare chance to investigate the role of paleoceanographic background and climate over the evolution of such carbonate systems.
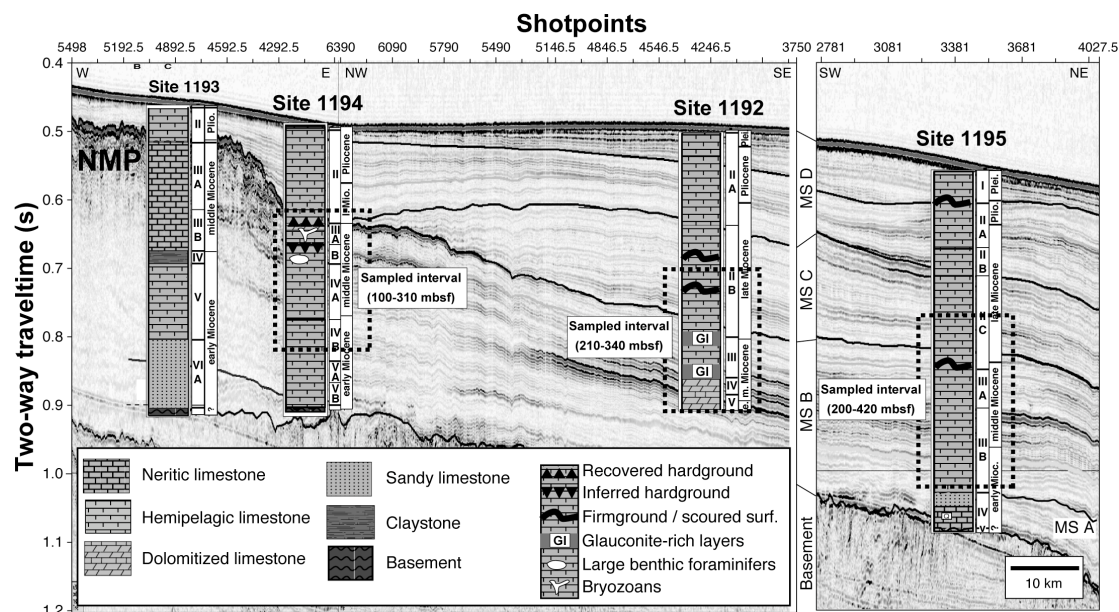

Figure2: *Relative position along a projected seismic profile of the various sites investigated by this study, as well as platform site 1193. The dashed boxes indicate the approximate interval sampled. NMP: Northern Marion Plateau. MSA: Megasequence A. MSB: Megasequence B. MSC: Megasequence C. MSD: Megasequence D.*

The main question addressed by the present study is whether heterozoan carbonates of the Marion Plateau were affected by mid Miocene cooling, and if yes by which mechanisms and with what impact. Our approach is to study sediments recovered along a Northern Marion Platform ("NMP") to slope transect (from ODP Site 1194, to sites 1192 and 1195, see Figs.1 and 2). Carbonate slope sediments offer the advantage that they reflect changes in the type of sediments produced on the platform, but also that they record sea-level and climatic fluctuations at a higher-resolution than the platform (John et al., 2003). In this paper we 1) tune the age model of the sites along the transect in order to better constrain the timing of events along the slope, 2) determine changes in carbonate accumulation in the slope sites, 3) attempt to reconstruct the changes in productivity and water temperature on the plateau using stable isotopes and finally 4) tie these parameters to mid-Miocene global eustasy and climatic changes.

4.2 GEOLOGICAL SETTINGS AND STRATIGRAPHY

The oldest recovered sediments deposited over the Jurassic basement of the Marion Plateau are Oligocene in age (Shipboard Scientific Party, 2002a). However, neritic carbonate sedimentation started in the Early Miocene and resulted in the formation of several Miocene carbonate platforms (see Fig.1, Shipboard Scientific Party, 2002a). The two largest platforms were designated as Northern Marion Platform (hereafter "NMP") and Southern Marion Platform (hereafter "SMP") during Leg 194 (Isern, Anselmetti, and Blum, 2002, see Fig.1). Five seismic megasequences, corresponding to different phases of evolution on the plateau, were recognized (Isern,

Anselmetti, and Blum, 2002): 1) pre-Oligocene basement, 2) initial flooding of the plateau during the Oligocene (megasequence A, "MSA"), 3) establishment of both the NMP and the SMP during the Early Miocene (megasequence B, "MSB"), 4) N12-N14 sea-level fall followed by drowning of the NMP (megasequence C, "MSC"), and 5) final drowning of the SMP and deposition of drift deposits (megasequence D, "MSD"). Sites used in this study (sites 1194, 1192 and 1195) are located on a NMP to slope transect (see Figs.1 and 2). Site 1194 is the most proximal site, being located at the foot of the NMP (Fig.2). Sites 1192 and 1195 are distal sites, Site 1192 being closer from the SMP than Site 1195 (Fig.1 and 2). Since the timeframe of interest for this study is the late Early to early Late Miocene (from 18-10 Ma), Site 1194 was sampled from 100-310 mbsf (meters below sea-floor), Site 1192 from 210-340 mbsf, and Site 1195 from 200-420 mbsf. Sampling intervals for each site were determined using the shipboard age-models (Isern, Anselmetti, and Blum 2002). The stratigraphy of these sites, summarized here, was also defined during Leg 194 (Isern, Anselmetti and Blum, 2002).

Site 1194 comprises five lithological units and subunits (Fig.2). Unit II, composed of Miocene to Pliocene hemipelagic mudstone/wackestone drift deposits, is the only unit comprised within MSD sampled for this study. Subsequent units sampled for this study are comprised within MSB (Fig.2) and record sedimentation during the deposition of the carbonate platforms. The packstones and floatstones of Unit III are divided into two subunits, Subunit IIIA dominated by bryozoans and Subunit IIIB dominated by benthic foraminifers. Unit III was considered to record the N12-N14 sea-level fall and subsequent flooding of the Plateau. At the top of Unit IIIA, a lowstand ramp composed of ~1 meter of dolomitized limestone is topped by a 1 cm-thick irregular surface coated by reddish laminae. This interval was interpreted as the hardground formed during the flooding phase that followed the N12-N14 sea-level fall (Shipboard Scientific Party, 2002a). A second interval with physical proprieties similar to this hardground was identified by downhole logging around 160 mbsf (Shipboard Scientific Party, 2002d), marking the boundary between Subunit IIIA and Subunit IIIB. However, this second hiatus/condensation interval was never recovered by drilling, which is not surprising considering that the average recovery for this interval was 7.6%. Unit IV, consisting of highly abraded carbonate particles, indicate a more distal carbonate source or a higher energy environment, and was deposited prior to the N12-N14 sea-level fall. Subunit IVA was distinguished from Subunit IVB by higher dolomite content and absence of quartz grains.

Site 1192 is located on the distal slope of the NMP (Fig.2).The sampled interval at this site consists of four lithostratigraphic units and subunits. Subunit IIB, comprised within MSC, consists of heavily bioturbated planktonic foraminifer mudstones to packstones with clay. All subsequent units sampled are comprised within MSB and reflect the deposition of a distal carbonate platform. Unit III consists of foraminiferal packstones and mudstones with clay and abundant quartz and glauconite grains, whereas Unit IV is similar to Unit III but additionally contains dolomite rhombs. Unit V, the last interval drilled at this site, consists of silt-sized dolomitic grainstones with clay. Site 1195 is the most distal of the sites sampled for this study, and yielded the most complete record (Figs.1 and 2). Subunit IIC, comprised within MSC, consists of skeletal wackestones to packstones/grainstones with clay and common occurrences

of planktonic foraminifers. All the subsequent units and subunits are comprised within MSB. Subunit IIIA is similar to Subunit IIC, but contains only rare planktonic foraminifers, with common benthic foraminifers and neritic carbonate particles, and Subunit IIIB additionally contains quartz grains.

4.3 ANALYTICAL METHODS

493 samples (74 samples from ODP Site 1194, 140 samples from Site 1192 B, and 277 samples from ODP Site 1195 B, Fig.1 and 2) were collected with a sampling resolution of 1 sample/50 cm wherever possible. One aliquot (10 cc) of the sampled material was dried overnight in an oven (60^0C), soaked for 10-12 hours in 10% oxygenated water and subsequently sonicated for 10 minutes to ensure good desegregation. Desegregated samples were washed over a 63μm sieve, dried in an oven (60^0C) and finally dry-sieved in three size fractions (140-280 μm, 280-500 μm and >500 μm). Around 6 pristine specimens of the epi-benthic foraminifera genus *Cibicidoides spp* were hand picked under a microscope in the 280-500 μm fraction to avoid sampling juveniles. 342 picked samples were found suitable for stable isotopes analysis (site 1194A+B: 39; site1192B: 108 samples; site 1195B: 197 samples), and were dissolved in phosphoric acid at the University of Bremen (Germany). The resulting CO_2 gaz was measured with a FINNIGAN MAT 251 mass-spectrometer. An internal standard calibrated against the international NBS 19 standard was used. Standard deviation was 0,07‰. Oxygen and carbon isotopes results ($\delta^{18}O_{benthic}$) are expressed with the standard δ notation. A correction factor (+0.64‰) was systematically applied to the oxygen isotopes result to take into account specie specific fractionation due to biological processes (Shackleton et al., 1984). Additionally, 39 bulk isotopes were measured on powdered samples (see below) for Hole 1194B since this hole yielded only four intervals containing *Cibicidoides spp* specimen.

A second aliquot of sample (10 cc) was hand grind using an agate mortar, and the resulting powder used for geochemical analysis. Carbonate content of the 493 samples was measured at the University of Stuttgart (Germany). The powders were dried overnight in an oven set at $60\,^{\circ}$C. Between 40 and 60 mg of sample material were analyzed using a Coulometer 5020 from UIC Inc. attached to a CM TIC Auto sampler from Orbis bv. Results were converted to calcite values by multiplying the TIC (Total Inorganic Carbon) results by the appropriate factor (8.33). Reproducibility based on triplicates from samples was ± 2wt% carbonate. Sr-isotope composition was measured for 4 bulk samples coming from hole 1194B with the Re-double filament technique on a Finnigan MAT 262 RPQ$^+$ in static mode at the University of Kiel (Germany). Usually 100 to 200 ^{87}Sr/^{86}Sr ratios were collected for each measurement, which resulted in a internal precision of better than 10 ppm (2 SE) of the ^{87}Sr/^{86}Sr value for most of the samples. The whole procedure Sr blank is less than 500 pg. However, sample sizes are sufficiently large (approx. 1 µg of Sr) that blank corrections are negligible. A mean ^{87}Sr/^{86}Sr value of 0.710236 ± 34 (2 standard deviation) for the NIST 987 standard solution was calculated from 12 analyzes, covering the whole measurement period of the data set. It represents the minimum uncertainty assigned to any individual sample measurement.
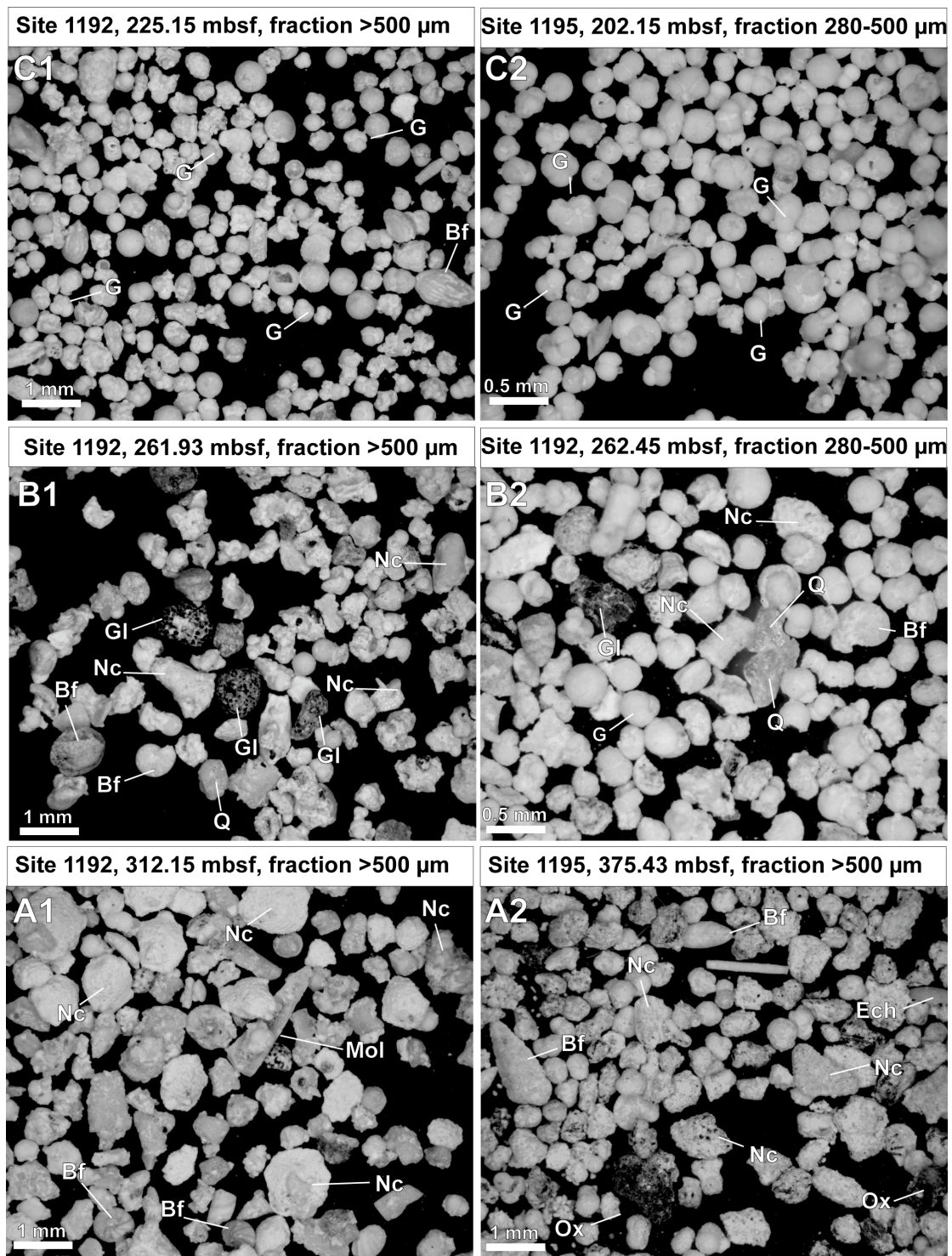
Figure 3: *Sediments characteristics before, during and after the glauconite and quartz-rich interval. Sediments before the glauconite-rich interval (A1 and A2) are characterized by dominant neritic carbonate, with occurances of iron oxides for the deeper sediments (A2). Note that this interval has the highest cementation level. Sediments occurring during the quartz-rich interval (B1 and B2) are characterized by glauconite grains as well as quartz grains, and common occurrences of neritic carbonate particles as well as benthic foraminifers. Sediments occurring after this interval (C1 and C2) are characterized by the strong dominance of planktonic foraminifers, and good preservation. G: planktonic foraminifer of the Globigerinoides family. Bf: benthic foraminifer. Nc: undifferentiated neritic carbonate. Mol: mollusk shell fragments. Ech: echinoid fragments. Gl: glauconite grains. Q: quartz grains. Ox: iron oxides.*

50

4.4 ANALYTICAL RESULTS

Analytical results presented here are available for download as a data report item in the scientific results of Leg 194 (John et al., in prep, http://www-odp.tamu.edu/publications). Results obtained are the following:

Sedimentology: All sediments analyzed at the studied sites are composed of hemipelagic carbonates mixed in various amounts with heterozoan bioclasts fragments reworked from shallow sites (i.e. mainly composed of heterotroph organisms fragments such as mollusks and echinoids, James, 1997). Visual observation of the sieved samples during picking revealed that sediments from sites 1192 and 1195 could be divided into three distinct intervals. **A)** The deepest (oldest) interval starts below 295 mbsf at Site 1192 and below 287 mbsf at Site 1195. This interval is characterized by a hemipelagic sediment rich in large (>500 μm) neritic carbonate fragments and benthic foraminifers (Fig.3A). Incipient cementation is important, and well preserved carbonate particles rare. Iron oxides can be observed in the deeper sections of Site 1195 (Fig.3A2). **B)** The second interval spans from 260 to 295 mbsf at Site 1192 and from 250 to 287 mbsf at Site 1195. It is characterized by relatively abundant glauconite grains, and the presence of quartz grains (Fig.3B). Quartz grains were not observed in any other intervals along the transect for the studied interval. Glauconite grains present in this level are millimetric in size, abraded and well rounded. These features are indicative of transported glauconite as opposed to authigenic glauconite. Neritic carbonates are present, but in minor amounts as compared with interval A, and foraminifers are becoming more abundant. **C)** The last interval starts above 260 mbsf at Site 1192 and above 250 mbsf at Site 1195, and spans the rest of the studied interval. The assemblage for this interval is characterized by the predominance of planktonic foraminifera, and the absence of glauconite, quarz and bioclastic debris derived from neritic areas.
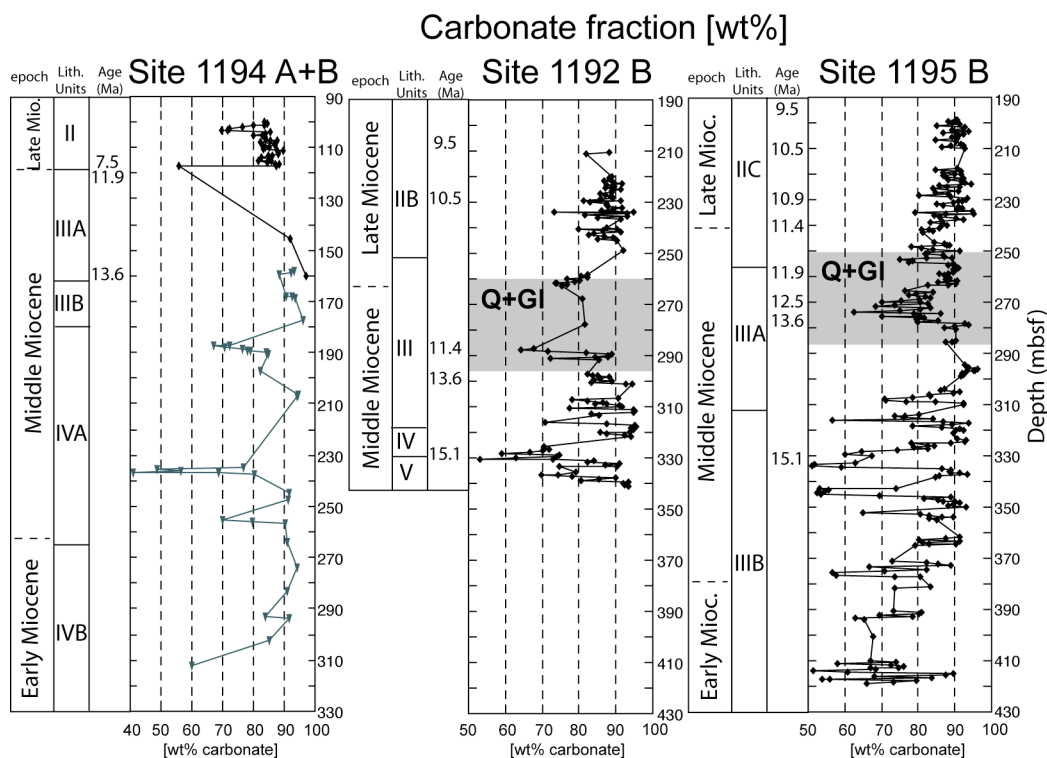

Carbonate fraction [wt%]

Figure 4: Carbonate content results measured with a coulometric method. Values are in wt%. The gray areas indicate occurrences of transported glauconite and quartz (see text for explanation).

Carbonate content: Carbonate content at Site 1194 varies from 40wt% to 100wt% (Fig.4), with a mean value around 85wt%. A minima in carbonate content (40 wt%) occurs at 233 mbsf, but most of the values for this site are close to 85wt%. At sites 1192 and 1195, minimum in carbonate content are around 50wt% and maxima around 90wt%. In average these sites have a carbonate content of around 80wt%. Carbonate content evolution at sites 1192 and 1195 can be divided into three main phases (Fig.4): **A)** an intreval when carbonate content varies often with low values close to 50wt% (Site 1192: below 320 mbsf, Site 1195: below 310 mbsf), **B)** a plateau phase with few variations in carbonate content and values around 90wt% (Site 1192: 290-320 mbsf, Site 1195: 280-310 mbsf), and **C)** a drop in carbonate content followed by a gentle recovery trend, with little variation in the amplitude of the carbonate content (Site 1192: above 290 mbsf, Site 1195: above 280 mbsf).
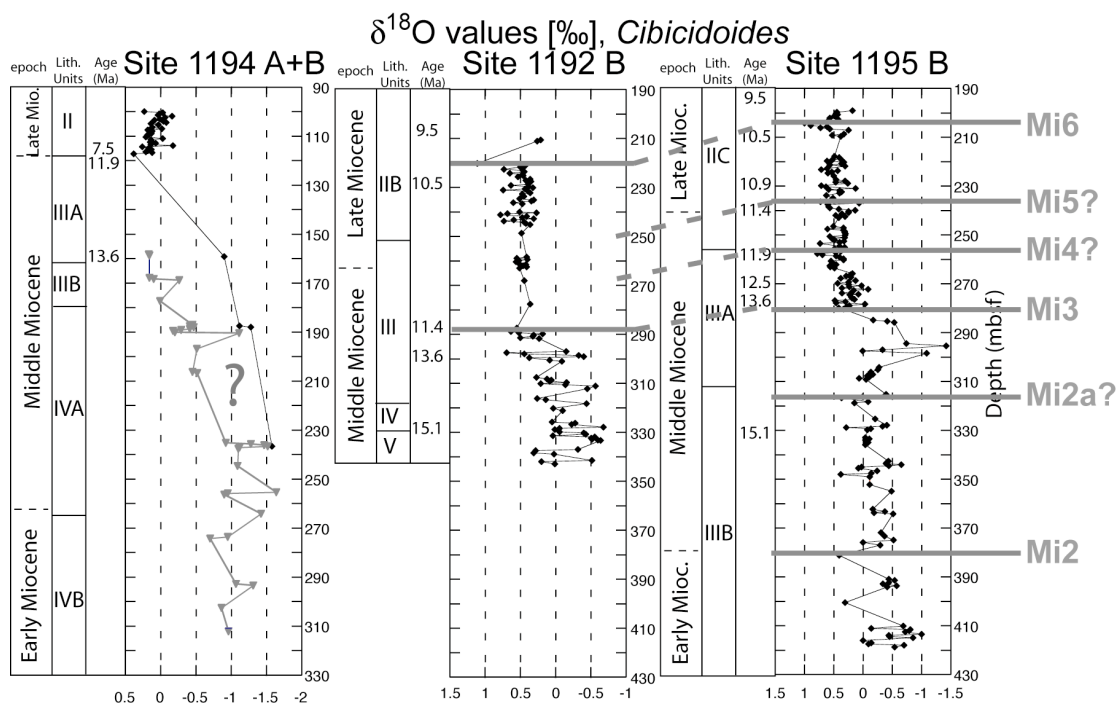

Figure 5: Oxygen isotopes results measured on Cibicidoides spp *(black curve) and bulk rock (gray curve at Site 1194). Values are in per mil [‰], and the location of the various Miocene oxygen isotopic events (Miller et al., 1991b, see text) are indicated.*

Oxygen and carbon stable isotopes: Oxygen isotopes results for *Cibicidoides spp* ($\delta^{18}O_{benthic}$, Fig.5) ranged from −1.5‰ to 0‰ at Site 1194, -0.5‰ to 0.5‰ at Site 1192 and −1‰ to 0.5‰ at Site 1195. The bulk results at Hole 1194B (Fig.4) ranged from −1.5‰ to 0.25‰. The major feature of these curves is a pronounced drop in $\delta^{18}O_{benthic}$ (165 mbsf at Site 1194, 290 mbsf at Site 1192 and 280 mbsf at Site 1195). Other positive $\delta^{18}O_{benthic}$ peaks were observed at Site 1194 (272 mbsf), 1192 (330 mbsf) and 1195 (232 mbsf, 262 mbsf, 312 mbsf, and 378 mbsf). Carbon isotopes results for *Cibicidoides spp* ($\delta^{13}C_{benthic}$, Fig.6) ranged from 2.5‰ to 0.5‰ for Site 1194 and from 2.5‰ to 1‰ for sites 1192 and 1195. Bulk-rock results for Hole 1194A ranged from 2.5‰ to 1‰. Several positive excursions in $\delta^{13}C_{benthic}$ were observed at Site 1194 (173 mbsf, 240 mbsf, 290 mbsf), Site 1192 (255 mbsf, 310 mbsf) and Site 1195 (240 mbsf, 300 mbsf, 312 mbsf, 333 mbsf, 361 mbsf and 390 mbsf).
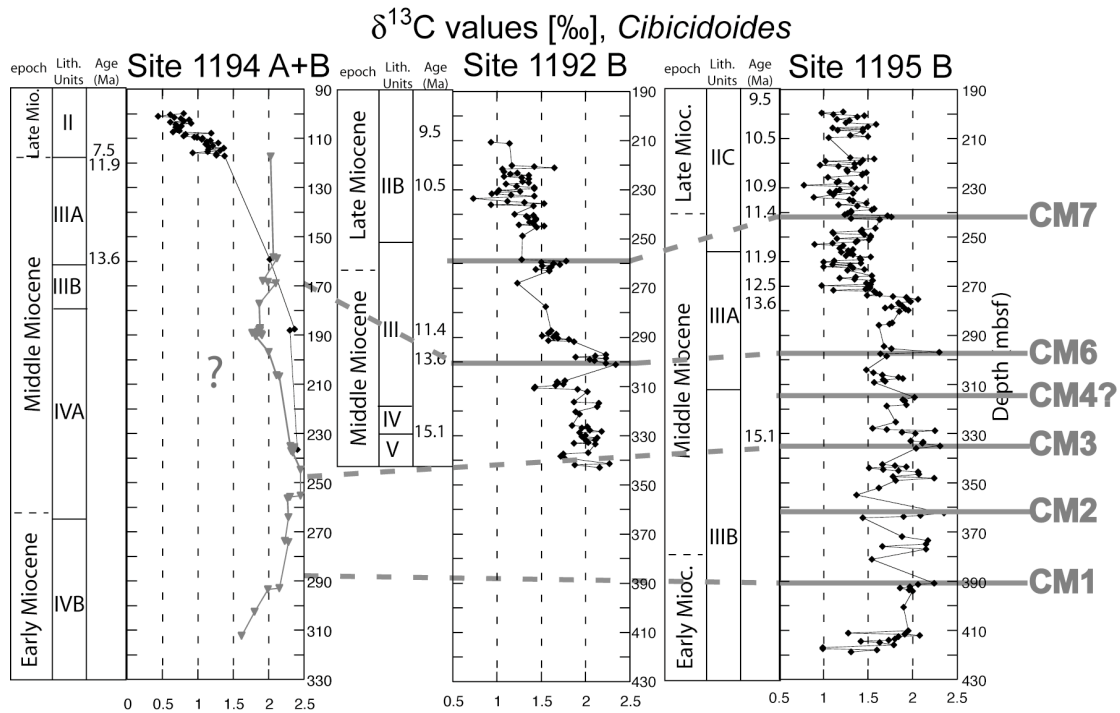
Figure 6: Carbon isotopes results measured on Cibicidoides spp *(black curve) and bulk rock (gray curve at Site 1194). Values are in per mil [‰], and the location of the various Miocene carbon isotopic events (Woodruff and Savin, 1991, see text) are indicated.*

Strontium isotopes: $^{86}Sr/^{87}Sr$ isotopes results for the four samples of hole 1194B (Table 1) yielded results between 0.7088 and 0.7086. The first value was converted into an age using the orbitally-tuned strontium curve of Martin et al. (1999). This curve does not extent sufficiently in time to be applied to the other three samples, and thus the conversion was made using the Oslick et al. (1994) curve. Ages obtained by these conversions (Table 1) are 11.4±0.7 Ma, 15.6±0.7 Ma, 16.6±0.7 Ma and 17.4±0.7 Ma, respectively.

Sample	Depth (mbsf)	87Sr/86Sr	Analytical Error	Age*
D15825	158.25	0.70881536	0.000003	11.4±0.7 Ma
D19047	190.47	0.7087515	0.000003	15.6±0.7 Ma
D23615	236.15	0.70869887	0.000003	16.6±0.7 Ma
D31221	312.21	0.70863837	0.000003	17.4±0.7 Ma

Table 1: *Strontium isotopes results. Column one contains the sample name, column two its depth (in mbsf). $^{87}Sr/^{86}Sr$ results are indicated in column three and the analytical error in column four. The fifth column contains the age obtained after conversion of the $^{87}Sr/^{86}Sr$. Sample D15825 was converted using the scale of Martin et al. (1999). Conversion for the three other samples was made using the Oslick et al. (1994) calibration. See text for explanation.*

4.5 DATA INTERPRETATION
4.5.1 Interpretation of Longer-Term Patterns in Oxygen and Carbon Isotopes

Oxygen isotopes measured on foraminiferal calcite ($\delta^{18}O_{foraminifer}$) are influenced by changes in water temperature (kinetic effect), input of fresh-water (salinity effect: fresh water has low $\delta^{18}O$) and global ice volume (16O-enriched ice is stored on land, Shackleton and Kennett, 1975). On the timescale of 100 000 years to million years, glacioeustasy is the dominant

mechanisms regulating global ocean isotopic ratios, though the kinetic effects of regional water-temperature are susceptible to overshadow the ice-volume effect. When looking at the average ocean composition, periods of Antarctic glaciation during the Miocene are reflected by increases in $\delta^{18}O_{foraminifer}$ (Vincent and Berger, 1985; Miller et al., 1987; Miller et al., 1991a; Miller et al., 1996a). These peaks can be traced in ocean basins around the world and used as chemostratigraphic markers, and Miller et al. (1991b) recognized 6 intervals of increased $\delta^{18}O_{foraminifer}$ for the Miocene that were named "Mi" events 1 to 6. Other works have shown that this correlation technique could be successfully applied to shallow-water environments (see e.g. Miller et al., 1998; John et al., 2003). By comparing the 5 positive shifts in oxygen isotopes identified at Site 1195 with the global oxygen isotope curve (Miller et al., 1991a; Miller et al., 1996a; Miller et al., 1998), we interpret these increases as events Mi2, 2a, 3, 4 and 6, respectively (see Fig.5 and table 2). Events Mi3 Mi6 could be traced to site 1192.

Event	Age assigned (Ma)	Site 1194 (mbsf)	Site 1192 (mbsf)	Site 1195 (mbsf)
Mi6	10.3	-	220	205
Strontium	11.4	158.25	-	-
Mi5	11.4	-	-	232 ?
CM7	11.49	-	255	240
Mi4	12.9	-	-	262 ?
Mi3	13.6	-	288	275
CM6	14.2	-	310	300
Mi2a	14.8	-	330 ?	312 ?
CM4	15.09	-	-	312 ?
CM3	15.52	-	-	333
Strontium	15.6	190.47	-	-
CM2	15.8	-	-	361
Mi2	16.1	-	-	378
CM1	16.4	-	-	390
Strontium	16.6	236.15	-	-
Strontium	17.4	312.21	-	-

Table2: Summary of the new chemostratographic datum obtained in this study. Column one yields the event name and column two its assigned age. Column three to five record the depth (in mbsf) where the given event occurs for each site. Strontium: $^{87}Sr/^{86}Sr$ ages. Mi: oxygen isotopes events (after Miller et. al 1991). CM: carbon isotopes events (after Woodruff and Savin 1991).

Fluctuation in carbon isotopes have been shown to reflect primarily changes in the rate of organic carbon versus carbonate carbon burial (Woodruff and Savin, 1991; Weissert et al., 1998). Since organic matter has a very low $\delta^{13}C$ ratio as compared to carbonate carbon, the relative burial of one versus the other influences the marine carbon reservoir. Since the Miocene has abundant organic-rich deposits, positive shifts in $\delta^{13}C$ occurring during this period are traditionally associated with increased productivity and burial of organic carbon (Vincent and Berger, 1985; Isaacs et al., 1987; Föllmi et al., 1991; John et al., 2002). Woodruff and Savin (1991) identified 7 positive $\delta^{13}C$ excursions during the Miocene, and they named these shifts events CM 1 to CM 7. Like the oxygen isotope events, the carbon isotopes excursions can be

traced in oceanic basin worldwide, thus providing a chemostratographic framework. Other work on Miocene slope sections have validated the use of this technique for this time frame (see e.g Jacobs et al., 1996). Moreover, work on Cretaceous sections have shown that global carbon excursions observed in basin settings could be traced on carbonate platforms (Weissert et al., 1998). It has also convincingly been demonstrated that shallow-water diagenesis on the platform produced an amplification of the original $\delta^{13}C$ signal, but that the pattern of the excursions could nonetheless be recognized (Grötsch et al., 1998). We interpret therefore the 6 positive shifts in carbon isotopes identified at Site 1195 as events CM1, 2, 3, 4, 6 and 7, respectively (see Fig.6 and table 2). Events CM6 and CM7 to both sites 1192, and no events could be traced to Site 1194.
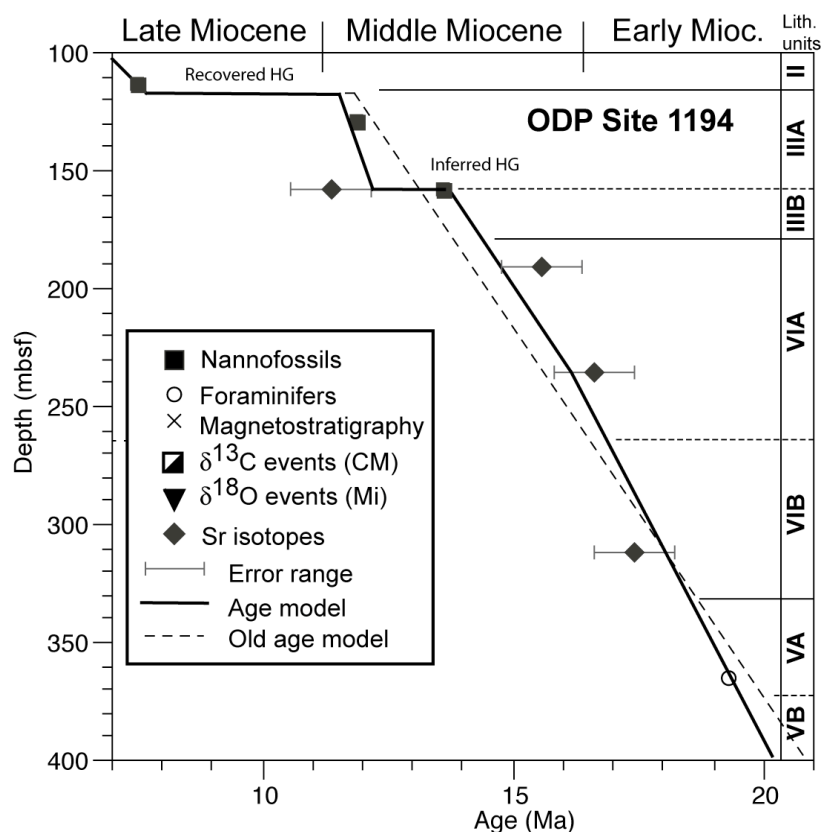

Figure 7: *Age model for Site 1194, including new oxygen, carbon and strontium isotope datum (this study). Age model developed during Leg 194 is indicated as a dashed line where it diverges from the age model developed in this paper. Note the hiatus/condensed interval around 155 mbsf.*

4.5.2 Modifications To The Age Models

Carbon, oxygen and strontium isotope results from this study provide new age points (Table 2) that can be plotted into the age models developed for each sites during Leg 194 (Isern, Anselmetti, and Blum, 2002), thus improving them. This approach is especially important for Site 1194 Hole B below 117 mbsf since the age model for this 300 m-thick interval was established using only 4 age points (Fig.7), and for Site 1192 where nannofossil events are scattered (Fig.8a). The modified age models (Fig.7 and Fig.8) are plotted as solid lines, and where the shipboard age model diverges from the new model it is represented as a dashed line. The modifications applied to the existing age models are as follow:

55

Site 1194: 4 [86]Sr/[87]Sr ages have been added (see Table 2, and Fig.7) to the existing 4 age points for the sampled interval. Carbon and oxygen isotopic events were considered too unreliable for this site. A constant sedimentation rate of 3.9 cm/k.y. from the base of the sampled interval to 236 mbsf is here inferred, with a change of sedimentation rate from 236-160 mbsf to 2.8 cm/k.y. A more complex manual fit, linking the center of each event, could have been established but this solution was considered unrealistic in view of the error range of each event and the resulting frequent changes in accumulation rates. Sedimentation rate between 160 and 158 mbsf was inferred to be ~0 cm/k.y. This is constrained by the presence of one one nannofossil datum at 160 mbsf (indicating an age of 13.6 Ma), and one strontium datum at 158 mbsf (age of 11.5±0.7 Ma). The depth below sea-floor of this condensed interval corresponds well to the condensation signature identified by downhole physical propreties around 160 mbsf (Shipboard Scientific Party, 2002d). This is also in good agreement with sedimentological data since the interval between 159.4–167.6 mbsf was never recovered, and that this transition corresponds to a change in consolidation of the sediment (Shipboard Scientific Party, 2002d). We thus argue that our new age model confirms that a hiatus/condensed interval exists between 168 and 158 mbsf, and furthermore that its duration can be estimated to span the interval from 13.9 to 12.2 Ma. Between this inferred condensed interval and the recovered hardground at 117.4 mbsf the sedimentation rate is 5.9 cm/k.y. The timing and duration of this later hardground are not significantly modified by the new age model.
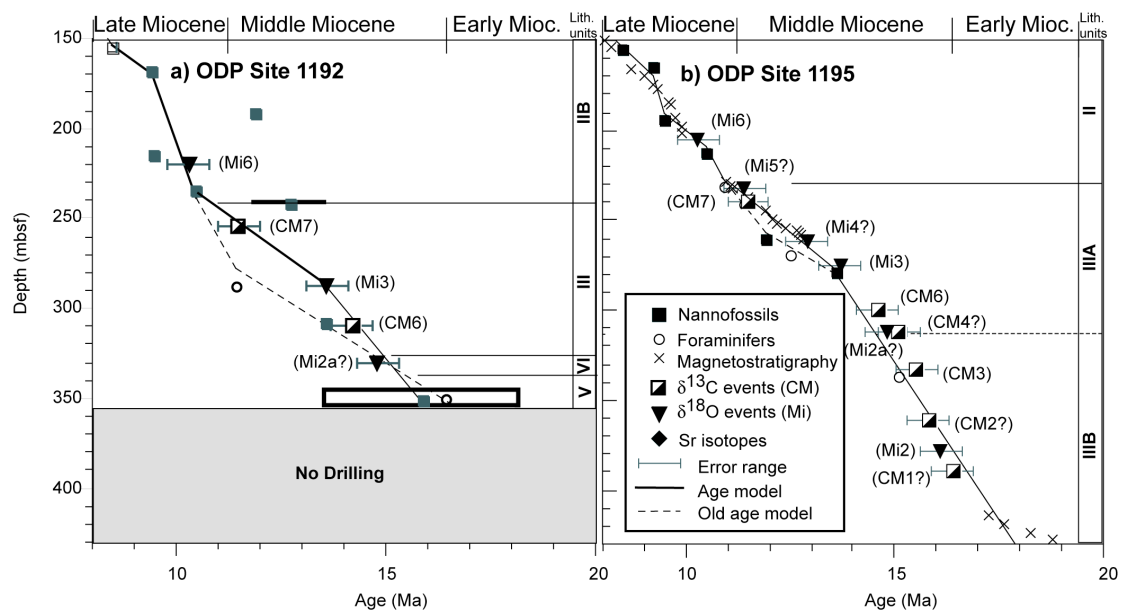

Figure 8: Age model for Site 1192 (a) and Site 1195 (b), including new oxygen and carbon isotope datum (this study). Age model developed during Leg 194 is indicated as a dashed line where it diverges from the age model developed in this paper. Note that new sedimentation rates for the two distal slope sites are similar.

Site 1192: 5 new age points (2 Mi and 3 CM events, table 2) were identified at Site 1192 (Table 2, Fig 8a). In contrary to foraminifer and nannofossils datum, isotopic events between 290 and 320 mbsf are consistent and not widely scattered (Fig. 8a). They thus provide a better age constraint for this interval, and the age model was modified accordingly. The new age model is very similar to the age model of site 1195, and suggests an

56

accumulation rate of 2.7 m/m.y. below 290 mbsf, 1.6 m/m.y. between 290 and 245 mbsf, and 4.2 m/m.y. between 245 and 170 mbsf.

Site 1195: Site 1195 was the site with the best recovery and the most complete and accurate age model (Shipboard Scientific Party, 2002e), and the 12 new age points (6 Mi and 6 CM events, Table 2, Fig.8b) plot well within the existing age model. However, between 240 and 280 mbsf the isotopic events are in perfect agreement with Leg 194 magnetostratigraphic data, whereas biostratigraphic data are scarce and in disagreement with these data sets. Consequently, we suggest to slightly modifying the age model by changing the sedimentation rate to a constant 2.0 m/m.y. between 240 and 280 mbsf (Fig.8b).
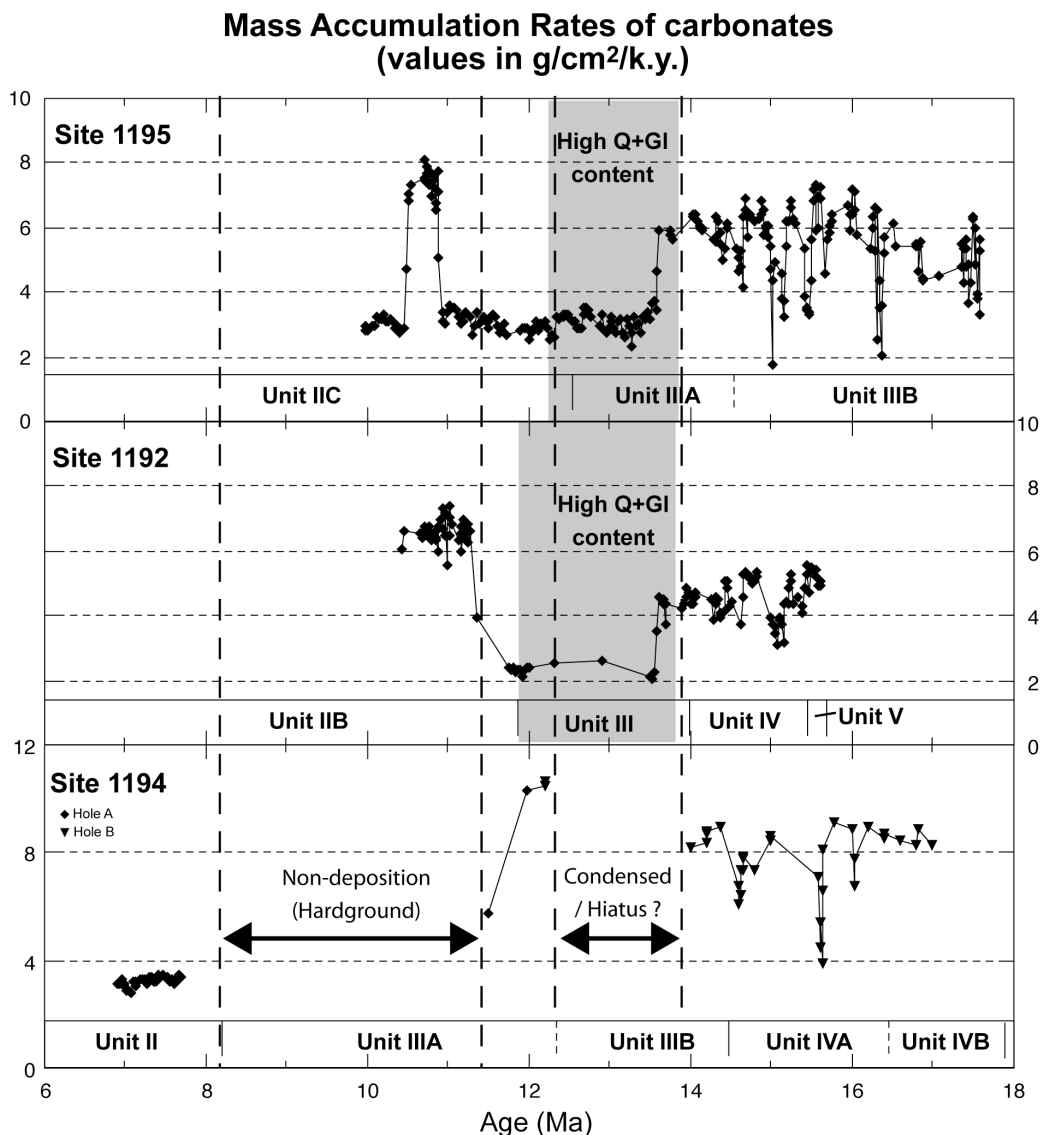

Figure 9: *Mass accumulation rates (MAR) of carbonate versus time for the three sites investigated. These MAR's were obtained by combining carbonate content and age model from this study with density measurements made during Leg 194 (Isern, Anselmetti, Blum 2002). The gray areas indicate occurrences of transported glauconite and quartz. Dashed lines indicate the limits of hardground and hiatus/condensed intervals at Site 1194.*

4.5.3 Carbonate Accumulation

To decipher fluxes and accumulation history of carbonate, one has to build accumulation rates of carbonates where the amount (in grams) of

carbonate per unit of time (1 thousand years) and surface (cm^2) is quantified. This was done here by combining carbonate content from this study, accumulation rates as determined using the modified age models presented earlier, and density measurements made on board the ship (Isern, Anselmetti, and Blum, 2002). Mass accumulations rates of carbonate ($MAR_{carbonate}$) are then calculated by this formula:

$$MAR_{carbonates} = Density\ [g/cm^3] * ARate\ [cm/k.y.] * CarbCont\ [wt\%]$$

Where "Density" is bulk sediment density, "ARate" the sediment accumulation rate and "CarbCont" the percent of carbonate. Resulting $MAR_{carbonate}$ are expressed in $g/cm^2/k.y.$, and reflect fluxes of carbonate at the given sites. Carbonate $MAR_{carbonate}$ at slope sites are affected by the primary production and export of neritic carbonate from the platform, by production of benthic carbonates on the slope, by planktonic foraminifers production in the water column, as well as by carbonate dissolution factors. Results show that $MAR_{carbonate}$ of carbonate for the three intervals studied are similar (Fig.9), suggesting that a single set of parameters controlled accumulation of carbonate at every site. From 18 to 13.9 Ma, the accumulation rates of carbonate are high (in average 6 $g/cm^2/k.y.$ for Site 1195, 5 $g/cm^2/k.y.$ for Site 1192, and 8 $g/cm^2/k.y.$ for Site 1194). This interval is also characterized by big fluctuations in $MAR_{carbonate}$ that affect the whole slope transect (Fig. 9). The most important drop in carbonate accumulation occurs at 13.5 Ma at sites 1192 and 1195 (values falls to 2-3 $g/cm^2/k.y.$). This interval, which lasts until 12.2 Ma, corresponds to the accumulation of glauconite and quartz in the distal slope sites, and to the inferred hardground at Site 1194. $MAR_{carbonate}$ remained low at the distal sites until 11.3 Ma, though another change in sedimentation occurs around 12.2 Ma when quartz and glauconite cease to be accumulated and planktonic foraminifers dominate the assemblage. 12.2 Ma is also the time when carbonate accumulation at Site 1194 increases to 10 $g/cm^2/k.y.$, reflecting the establishment of a shallow water ramp (Unit IIIA). Finally, at 11.3 Ma carbonate accumulation at Site 1194 drops to 0 $g/cm^2/k.y.$ (recovered hardground), but peaks at sites 1192 (7 $g/cm^2/k.y.$) and 1195 (8 $g/cm^2/k.y.$).

4.6 DISCUSSION
4.6.1 Changes In Productivity And Water-Temperature
Since $\delta^{13}C$ results for sites 1194, 1192 and 1195 are similar in trend and magnitude, they were combined in a single curve expressing the carbon isotopes evolution on the Marion plateau (Fig.10, dark line). This regional $\delta^{13}C$ curve was compared to a global $\delta^{13}C$ curve established from deep-sea cores (Fig.10, dashed line, after Zachos et al., 2001). The evolution of both curves is similar, but regional differences are visible: some minima in the global curve correspond to maxima on the Marion Plateau curve (to highlight this, the difference between to two curves is filled in light gray in Fig.10). Conversely, 6 minima in the difference between the two curves occur (showed by a black arrow in Fig.10). These are local events and are referred here as Marion Plateau "Carbon Minima Events" CE1 to CE6. In order to highlight the difference between the two curves, the deep-sea curve of Zachos et al. (2001) was re-sampled using the scale of the Marion Plateau curve, and $\delta^{13}C$ values from the deep-sea were subtracted to time-equivalent points of the Marion Plateau. Since the global $\delta^{13}C$ curve reflect changes of the marine carbon

reservoir, the difference between this curve and the Marion Plateau curve reflects regional changes on the Marion Plateau. Events CE1-CE6 are visible on the resulting $\Delta\delta^{13}C$ curve (Fig.11c). Several factors can affect regional $\delta^{13}C$ at this time-scale. One of the prominent mechanism is changes in productivity: photosynthesis favors the use of the lighter isotopes and thus sea-water is depleted in ^{12}C (Shackleton, 1985; Vincent and Berger, 1985).
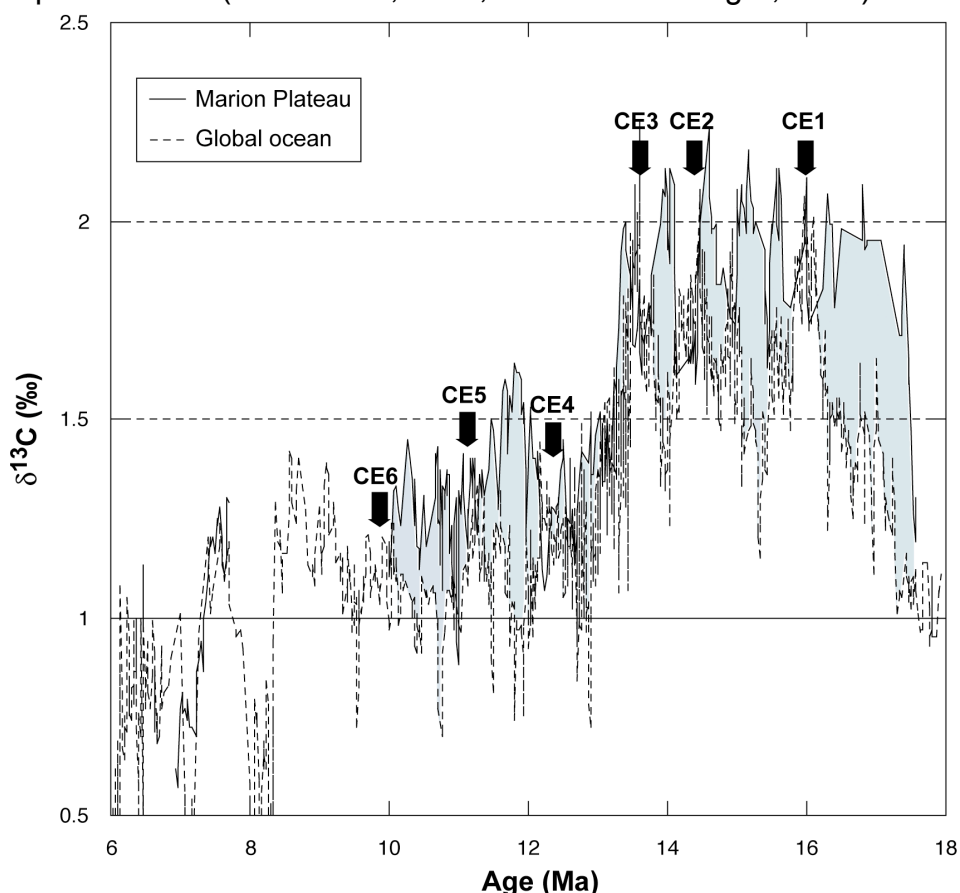

Figure 10: Comparison between a global $\delta^{13}C$ curve from the deep sea (dashed line, Zachos et al., 2001) and the regional $\delta^{13}C$ curve for the Marion Plateau obtained by combining values from sites 1194, 1192 and 1195 (solide line). The difference between the two curves is filled in gray. Note the presence of 6 minima in the difference between the two curves designated in this paper as events CE1 to CE6.

Inversely, carbonate dissolution would increase $\delta^{13}C$ (Shackleton, 1985; Corfield and Cartlidge, 1992). For shallow-water system, it has also been demonstrated that organism respiration on top of carbonate platforms as well as input of ^{13}C-depleted dissolved organic matter from land resulted in low $\delta^{13}C$ waters (Patterson and Walter, 1994). As the sediments we analyzed are not directly coming from the platform (ruling out the respiration mechanism), we tentatively interpret the $\Delta\delta^{13}C$ curve (Fig.11c) as a record of marine productivity on the Marion Plateau. We do not completely rule out that periodic input of dissolved organic matter from land could have affected $\Delta\delta^{13}C$ during low-stands, but we regard these as unlikely since 1) terrigenous material is only present in small amounts in the slope sediments and 2) oxygen isotopes do not indicate periodic input of river water. Thus, we conclude that 6 productivity cycles of in average 1.5 m.y. duration each can

59

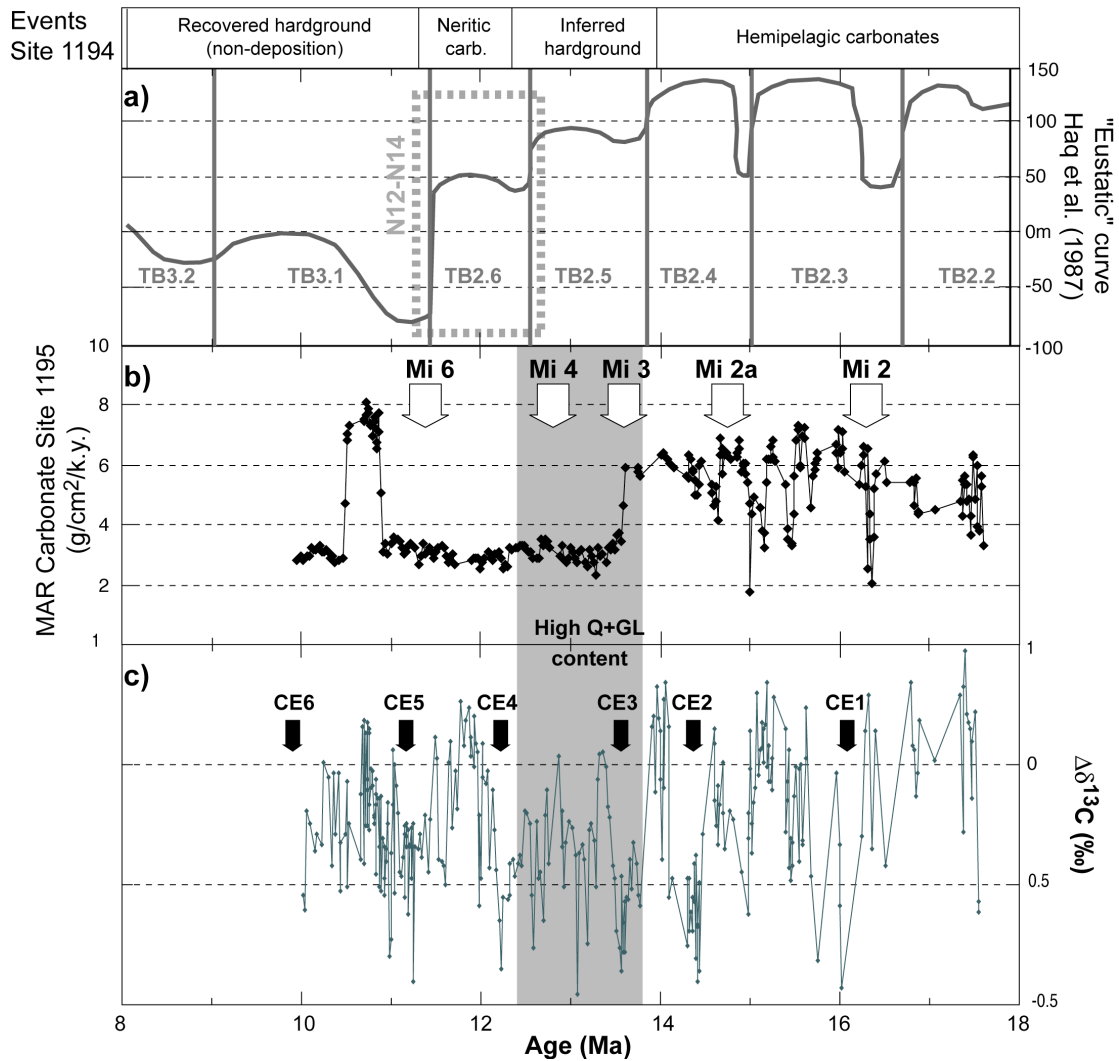be observed between 18 to 10 Ma (Fig.11c), and we regard CE events as recording minima in productivity.

Figure 11: a) *Eustatic curve established by Haq et. Al (1987). Sequence boundaries are indicated by a vertical gray line. Time span of the N12-N14 sea level fall is marked by a gray dashed box. **b)** Mass accumulation rates of carbonates at Site 1195. Note that sequences TB2.2 and TB2.3 correspond each to a decrease in MAR's. The gray area indicates the presence of transported glauconite and quartz. The white arrows point to the position of Mi events (Miller et al., 1991) identified in the oxygen isotope record. Note the coherence between decrease in MAR$_{carbonates}$ and the major Mi3 event. **c)** difference between Marion Plateau $\delta^{13}C$ and global ocean $\delta^{13}C$ (Zachos et al., 2001). This $\Delta\delta^{13}C$ curve is interpreted as reflecting productivity on the Marion Plateau (see text for explanation). Note that CE events (black arrows) are always bounded by two sequence boundaries (gray lines, after Haq et al., 1987).*

$\delta^{18}O$ results can be used to reconstruct water-temperature changes and result for all sites (Fig.12) clearly show that –as expected- water temperature was higher (lower $\delta^{18}O$ values) than in the deep sea. Though reconstructing absolute water-temperature in the Miocene is rendered difficult by the fact that $\delta^{18}O$ is sensitive to salinity and global ice volume changes, we can attempt to estimate the difference in temperature with the deep-sea curve using the linear equation of Bemis et al. (1998). Results show that compared to the deep-sea Site 1194 was 13°C warmer at ~15 Ma and 14°C warmer at 7 Ma. Compiled $\delta^{18}O$ curves for Sites 1192 and 1195 (Fig.12) show that water

temperature for the distal slope was intermediate between Site 1194 and the deep sea, namely 7°C warmer at 15 Ma and 7.5°C warmer at ~11.5 Ma. If we accept deep-sea temperature estimates of Billups et al. (2002, 4°C before 13.8 Ma, 2°C after), we can estimate water temperatures before 13.8 Ma to be ~17°C at Site 1194 and 10 °C at sites 1192 and 1195. After 13.8 Ma, water temperatures would fall by ~1°C at all sites.
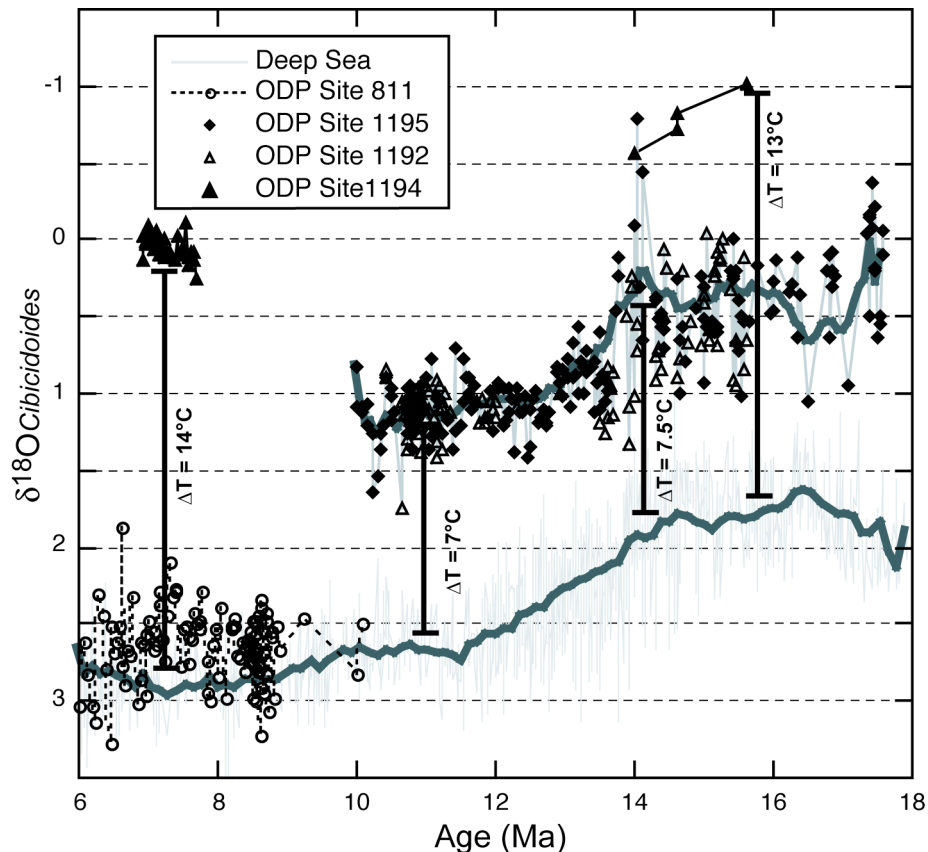

Figure 12: *Comparison between* Cibicidoides $\delta^{18}O$ *values from the Marion Plateau (this study), the Townville through (open circles, Isern et al., 1996) and a global deep-sea curve (light gray, Zachos et al., 2001). The differences in temperature between the various sites were calculated using the linear equation of Bemis et al. (1998).*

Regional changes in water-temperature was proposed as the control for the Late Miocene drowning of the Queensland reefs (Isern et al., 1996). However, results on the Marion Plateau indicate that this mechanism is more complex. Water temperatures obtained are relatively cold but consistent with paleo- water depths estimates for the different sites (Isern, Anselmetti, and Blum 2002). If water temperature on the southern edge of the NMP could potentially explain the absence of photozoan associations, the small difference in temperature after the N12-N14 fall is unlikely to explain the drowning of the NMP platform. This observation is strengthened by the fact that heterozoan organisms (producing carbonate at Site 1193) are tolerant to wider water-temperatures, water-depth and turbidity spectrums (James, 1997; Hallock, 2001).

4.6.2 Relative Controls On The Evolution Of The Marion Plateau Carbonate System

The principle motivation behind the choice of the Marion Plateau as the target for Leg 194 was that the area was considered to have experience a

constant and uniform thermal subsidence during the Miocene (Isern, Anselmetti, and Blum 2002). Thus, the difference in sea-level at two different locations must only be caused by eustatic changes during the N12-N14 event.

However, a surprising result of our study is that such a major event as the N12-N14 fall does not impact accumulation rates of slope carbonates (Fig.11, a and b). Even in heterozoan systems, a drop of this magnitude (between 70-90 meters, John et al., under review) should affect production of carbonate, especially since the dominant producers on the NMP platform -red algae and larger benthic foraminifers- are light dependant (Bosence, 1983; Hallock, 2001). Also, the basinward shifting of the carbonate factory during sea-level low stand should increased export of neritic carbonates to the deepest sites. Conversely, a dramatic reduction in $MAR_{carbonates}$ (Fig.11 a and b) occurs around 13.8 Ma, a time when no major eustatic fall takes place (Haq et al., 1987) and when carbonate production on the platforms is still active (Isern, Anselmetti and Blum 2002). Moreover, this transition corresponds to a marked change in the type of sediment accumulated (see Fig 3), as already sustained by shipboard data (Shipboard Scientific Party, 2002e, b). Before the drop in $MAR_{carbonate,}$ planktonic foraminifers are rare and the assemblages are generally dominated by unidentified large (neritic?) fragments, with abundant benthic foraminifers. After the drop however, quartz and glauconite accumulate, and large neritic carbonate fragments are less abundant. Planktonic foraminifers are progressively replacing larger benthic foraminifers and neritic fragments and finally dominate the assemblages around 12.3 Ma.
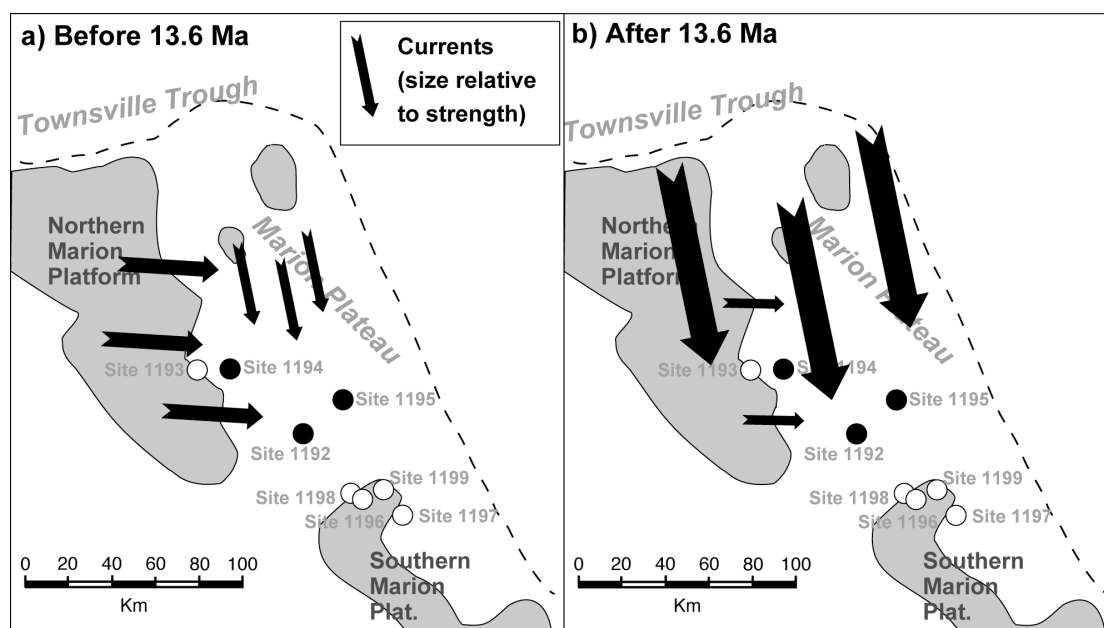

Figure 13: Summary of the model proposed to explain changes in carbonate mass accumulation rates around 13.6 Ma. A) Before 13.6 Ma, Antarctica is not glaciated and ocean currents are not strongly sweeping the plateau. As a consequence, carbonate derived from the Platform accumulate at slope sites 1192 and 1195. B) After 13.6 Ma, currents are stronger due to increased thermal gradient link to the permanent establishment of Antarctica. Less carbonate particles are being accumulated, and quart and glauconite are being transported and deposited at sites 1192 and 1195.

The discrepancy between eustasy and $MAR_{carbonates}$ as well as the sudden occurrence of terrigenous quartz and reworked glauconite leads us to discuss the role of strength and direction of oceanic currents over accumulation rates on the slope of the Marion Plateau. Oceanic currents have

been previously reported to impact slope sedimentation on the Great Bahama Bank (Anselmetti et al., 2000). The modern current-swept Marion Plateau is an ocean facing area with surface waters dominated by the southern edge of the westward-flowing South Equatorial Current (Pickard et al., 1977; Tomczak and Godfrey, 1994). This configuration and the influence of the Northwest Monsoon during austral summer implies that the plateau is sensitive to relatively small changes in climate and in the position and strength of the major current. During the Miocene, current patterns were probably controlled by Antarctic climate, as the permanent establishment of the East Antarctic ice sheet around 13.6 Ma implied major changes in worldwide oceanic circulation and climate (Kennett, 1985; Miller et al., 1991b; Flower and Kennett, 1994). The good coherence between the timing of this event and the age of the major drop in $MAR_{carbonates}$ suggest that current pattern on the plateau were shifted in response to global changes (Fig.13). Data from Leg 194 as well as from this study support this interpretation. The generally fine-grained and abraded sediments recovered during Leg 194, as well as the seismic geometries in the Marion Plateau sediment packages (Shipboard Scientific Party, 2002a) speak in favor of deposition under a strongly current-dominated regime. Moreover, hardgrounds occurring in temperate carbonate system have been documented as proxies for high productivity events linked to changes in current pattern (Glenn and Kronen, 1993; Mutti and Bernoulli, 2003). Hence, the recovered hardground at 117 mbsf and to some extent the non-recovered hiatus/condensed interval at 155 mbsf (Site 1194) suggest major changes in the strength of the current sweeping the Plateau. This in turn probably changed the depocenter of platform-derived material and triggered deposition of transported terrigenous quartz and glauconite on the distal slope.

If sea-level changes were not the main control over sedimentation on the plateau, they nevertheless played an important role. First, the mechanical effects of eustatic lowering were probably superimposed on the longer-term climatic control: eustatic fall induced shoaling of the slope sites, and thus likely resulted in increased current strength as well as change in wave base. This could explain some low accumulation rates events occurring in all slope sites before 13.6 Ma (Fig.9). Then, a relationship between $\Delta\delta^{13}C$ and third order sea-level cycles could be argued (Fig.11 a and c): CE events are always bounded by two third-order sequence boundaries. Hence, productivity seems to have been influenced by sea-level, and the $\Delta\delta^{13}C$ proxy could reflect third-order sea-level changes where CE events represent lowstands. Two main controls could be suggested to link these two processes. First, sea-level constrains the aerial extend of the shelf and thus the space available for organic matter or carbonate carbon deposition. Secondly, it can modify local topographical upwelling cells and regulate the proximity of river input, thus controlling nutrient availability on the shelf. Here, we favor a scenario where nutrient availability was controlled by ocean currents, since no strongly negative $\delta^{18}O$ signal was observed as would be expected if periodic fresh-water input took place.
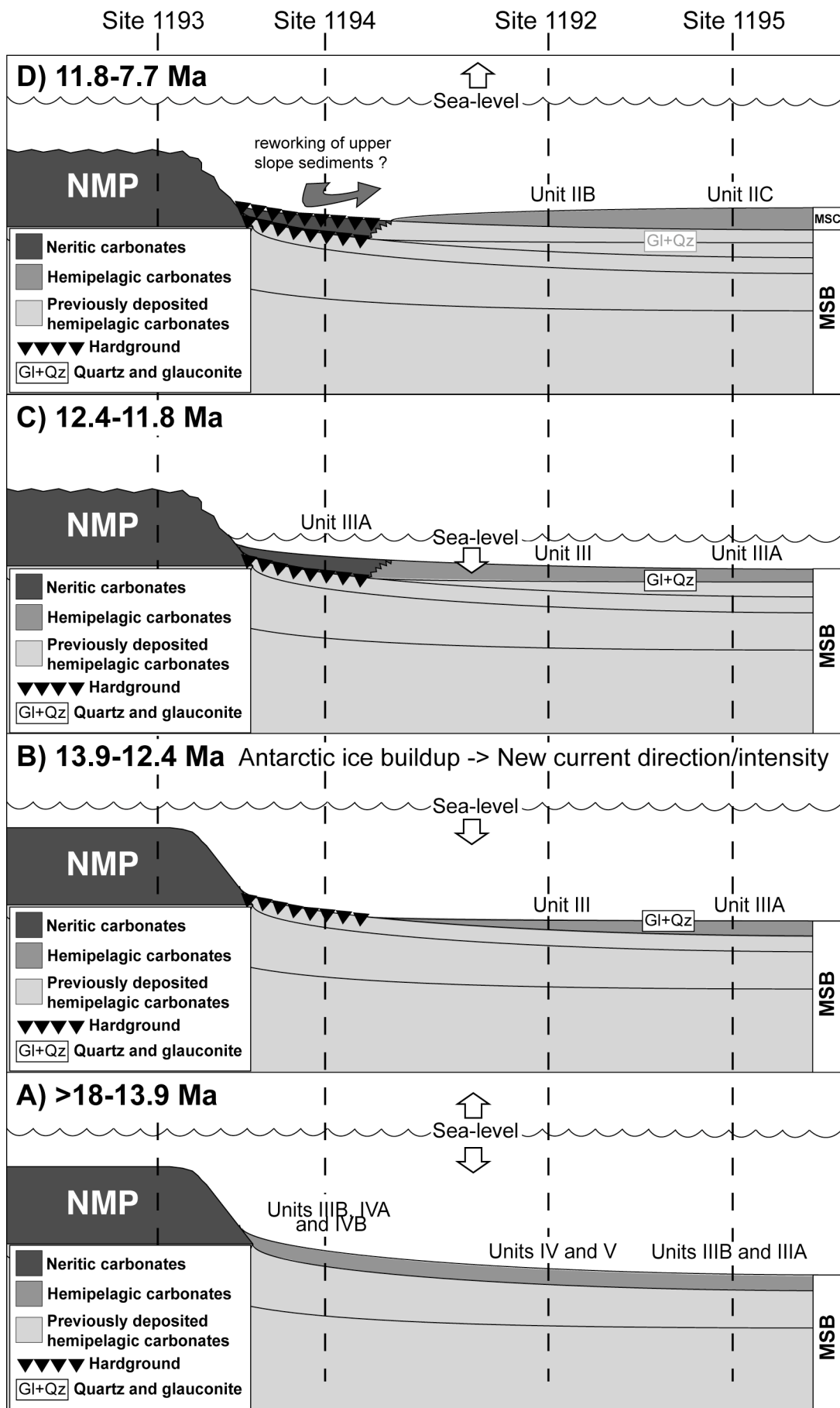
Site 1193　　Site 1194　　　Site 1192　　　Site 1195

D) 11.8-7.7 Ma

Sea-level

NMP

reworking of upper slope sediments ?

Unit IIB　　　Unit IIC

MSC

GI+Qz

MSB

- Neritic carbonates
- Hemipelagic carbonates
- Previously deposited hemipelagic carbonates
- ▼▼▼▼ Hardground
- GI+Qz Quartz and glauconite

C) 12.4-11.8 Ma

NMP

Unit IIIA

Sea-level

Unit III　　　Unit IIIA

GI+Qz

MSB

- Neritic carbonates
- Hemipelagic carbonates
- Previously deposited hemipelagic carbonates
- ▼▼▼▼ Hardground
- GI+Qz Quartz and glauconite

B) 13.9-12.4 Ma Antarctic ice buildup -> New current direction/intensity

Sea-level

NMP

Unit III　　　Unit IIIA

GI+Qz

MSB

- Neritic carbonates
- Hemipelagic carbonates
- Previously deposited hemipelagic carbonates
- ▼▼▼▼ Hardground
- GI+Qz Quartz and glauconite

A) >18-13.9 Ma

Sea-level

NMP

Units IIIB, IVA and IVB

Units IV and V　　　Units IIIB and IIIA

MSB

- Neritic carbonates
- Hemipelagic carbonates
- Previously deposited hemipelagic carbonates
- ▼▼▼▼ Hardground
- GI+Qz Quartz and glauconite

64

Based on these considerations, we propose to sum up the evolution of the Marion Plateau between 18-10 Ma in four phases (see Fig.14):

1) Beginning before the studied interval (~18 Ma) and lasting until 13.8 Ma, eustatic sea-level is in general high and hemipelagic carbonates accumulate at sites 1194, 1192 and 1195 (Fig.9, Fig.14A). These sediments are characterized by a mixing between carbonate produced in situ and neritic carbonates exported from the various platforms.

2) At 13.8 Ma (Fig.9 and 13B), the east Antarctic ice sheet is permanently established inducing major changes in the strength and direction of the world's ocean currents (Kennett, 1985). As a consequence of these changes, current patterns on the plateau are modified (Fig.13) and glauconite and quartz-rich sediment are being transported and deposited at sites 1192 and 1195. Neritic carbonates derived from the platforms are becoming less abundant. During this time interval, a hiatus/condensed interval (non-recovered) is formed at Site 1194. Leg 194 shipboard scientific party (2002c) has described three scoured surfaces on the NMP (Site 1193) that were overlain by glauconite and planktonic foraminifers. These features are suggestive of non-deposition surfaces followed by drowning and could be related to the glauconitic accumulation phase on the slope sites.

3) From 12.4 to 11.8 Ma (Fig.14C), sea-level is relatively stable for ~1 Ma and then falls abruptly (N12-N14 event, TB3,1 in Fig.11). This phase and the following sea-level lowstand corresponds to the establishment of the bryozoan-rich lowstand ramp at Site 1194 (Shipboard Scientific Party, 2002d). Sites 1192 and 1195 are still characterized by low-sedimentation rates, but glauconite and quartz are no longer being deposited. In the deeper slope sites, planktonic foraminifers dominated the assemblages and neritic carbonate particles are absent. Both the NMP and SMP platforms are being exposed.

4) After 11.8 Ma (Fig. 14D), sea-level rises and the NMP and SMP platforms are flooded again. Neritic sedimentation on the SMP resumes, but the NMP is drowned. As a consequence of this major drowning event, Site 1194 is characterized by a hardground whereas hemipelagic sediments dominated by planktonic foraminifers are deposited at sites 1192 and 1195. The intervals of high carbonate accumulation at sites 1192 and 1195 (see Fig.9) could indicate reworking of upper-slope sediments, these later being destabilized by water loading following sea-level rise, but could also simply result from a shift in the depocenter of current-transported sediments.

4.7 SUMMARY-CONCLUSIONS

Global climatic cooling during the mid Miocene did affect the sedimentation on the Marion Plateau by controlling the strength and direction of oceanic currents sweeping the area. Currents were dramatically modified after the Mi3 event, when East Antarctica was permanently glaciated, and were also probably strengthen by shoaling on the slope during each eustatic sea-level falls. Water-temperature on the other hand only played a limited role in controlling rates of carbonate production/export and productivity, although cool waters could possibly explain the predominance of heterozoan

organisms at Site 1193. Sea-level highstands were times of higher productivity on the plateau, and six productivity cycles were recognized in $\Delta\delta^{13}C$, each bounded by eustatic sequence boundaries. These cycles, identified by geochemical proxies in slope sediments, could be potentially traced on the platforms. The open question remaining is whether or not the platform responded to these climatic changes, and if this response correlates with the events that we observed on the slope, in particular the productivity events.

- CHAPTER 5 -

δ^{18}O and Marion Plateau backstripping: combining two approaches to constrain late Middle Miocene eustatic amplitude

5.0 ABSTRACT

$\delta^{18}O_{benthic}$ values from ODP sites 1192 and 1195 (Leg 194) were combined with deep-sea values to reconstruct the magnitude range of the mid-Miocene N14-N12 sea level fall. In parallel, an estimate for the N14-N12 sea level fall was calculated from the preserved stratigraphy sampled during Leg 194, and the structural geometry of the Marion Plateau. The effects of thermal subsidence induced by late Cretaceous rifting were taken into account for these estimates. By overlapping the sea level range of both the deep-sea isotopes and the results from the backstripping analysis, we demonstrate that the amplitude of the N14-N12 sea level fall was 79±11m. Including an estimate for sea level variation using the $\delta^{18}O_{benthic}$ results from the Marion Plateau, the range is narrowed to 73±4m. Our result implies that the extent of ice buildup in the Miocene was larger than previously estimated.

5.1 INTRODUCTION

The establishment of a precise eustatic sea level curve for the Cenozoic is critical in order to understand the stratigraphic architecture of passive continental margins and the relationship between ice volume and climate change. Two principal methods are generally applied to determine the amplitude and timing of sea level variations. The first method involves mapping the sequence stratigraphic development of siliciclastic passive margins (Vail and Hardenbol, 1979; Haq et al., 1987; Miller et al., 1996a), and the depositional history of carbonate atolls and banks (Schlanger and Premoli-Silva, 1986; Eberli et al., 2002). The second method involves the calibration of oxygen isotope ratios since these ratios reflect the effects of water cooling and glacioeustatic changes (Fairbanks and Matthews, 1978; Miller et al., 1987). While there is general agreement between the timing of major sea level events, the amplitude of those events remains controversial (Pigram et al., 1992b). For example, estimates of the amplitude of the major late middle Miocene sea level fall (nannofossils zones N12-N14, 12.5 – 11.4 Ma, TB3.1 of Haq et al., 1987) range from 25m (Miller et al., 1998) to >180m (Pigram et al., 1992b).
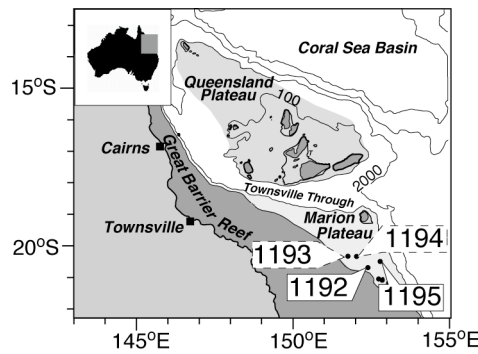
Figure 1: *Map of the Marion Plateau with location of the four ODP Leg 194 Sites discussed in this paper. Sites 1193 (Northern Marion Platform) and upper slope site 1194 were used for backstripping estimates (dashed text boxes). Distal slopes 1192 and 1195 were sampled and measured for oxygen isotopes data, this study (solid text boxes). Modified after (Isern, Anselmetti and Blum, 2002).*

The N14-N12 event is significant as it is associated with the permanent establishment of the East Antarctic Ice sheet (Zachos et al., 2001), and by extension, to important climatic and oceanographic changes in the Neogene (Kennett, 1985). Pigram et al (1992b) originally recognized that the carbonate platforms of the Marion Plateau (Northeastern Australia, Fig.1) might be used to reconstruct the magnitude of the N14-N12 mid-Miocene eustatic fall. They identified two carbonate platforms and using seismic stratigraphy, interpreted their development and modification as a consequence of a Middle Miocene highstand and a late Middle Miocene lowstand. Eustatic variations were estimated using the seismic geometry of these edifices (Pigram et al., 1992b), but subsequent drilling of the Plateau showed that the depositional and stratigraphic relationships underlining this model were much more complicated than assumed, thereby questioning the validity of the amplitude in eustatic change (ODP Leg 194, Isern, Anselmetti and Blum, 2002).

The Marion platform provides a unique setting where both stratigraphic and stable isotope approaches can be applied in parallel to mutually constrain the amplitude of sea-level variations. Carbonate platforms and their slopes are particularly sensitive indicators of sea-level changes, as they predominantly record growth during sea-level highstands and shut down during sea-level lowstands. Sampling these edifices records sea-level in a "dipstick" fashion (Isern, Anselmetti and Blum, 2002). Furthermore, in contrary to purely siliciclastic systems, carbonate systems have a better preservation potential for the benthic assemblages and thus increase the reliability of paleobathymetric estimates. This paper summarizes the most recent estimates for the amplitude of the N12-N14 eustatic change based on backstripping of the Marion Plateau stratigraphic sequences, and compares the results with the fall in sea level estimated using oxygen isotope proxies. Oxygen isotope methods comprise: 1) new glacioeustatic estimates based on existing $\delta^{18}O_{benthic}$ values from deep-sea sediments (Zachos et al., 2001), and 2) estimates based on new $\delta^{18}O_{benthic}$ values for the Marion Plateau sequences.

5.2 ANALYTICAL METHODS

417 samples (140 samples from ODP Site 1192 B, and 277 samples from ODP Site 1195 B, Fig.1) were collected with a sampling resolution of 1 sample/50 cm. An aliquot (10 cc) of the sampled material was soaked for 10-12 hours in 10% oxygenated water and subsequently sonicated for 10 minutes to ensure good desegregation. Desegregated samples were washed over a 63μm sieve, dried in an oven (60^0C) and finally dry-sieved in three size fractions (140-280 μm, 280-500 μm and >500 μm). Around 6 pristine specimens of the epi-benthic foraminifera genus *Cibicidoides spp* were hand picked under a microscope in the 280-500 μm fraction to avoid sampling juveniles.

305 samples were found suitable for stable isotopes analysis (site1192B: 108 samples; site 1195B: 197 samples). Samples were dissolved in phosphoric acid at the University of Bremen (Germany), and the resulting CO_2 measured with a FINNIGAN MAT 251 mass-spectrometer. An internal standard calibrated against the international NBS 19 standard was used. Standard deviation was 0,07‰. Oxygen isotopes results ($\delta^{18}O_{benthic}$) are expressed with the standard δ notation:

$$\delta^{18}O_{sample} = [(^{18}O/^{16}O)_{Sample}/ (^{18}O/^{16}O)_{Standard}-1] \times 1000$$

A correction factor (+0.64‰) was systematically applied to take into account specie specific fractionation due to biological processes (Shackleton et al., 1984).

5.3 OXYGEN ISOTOPES RESULTS

Stable isotopes results from site 1192 and 1195 were integrated into a composite section using shipboard age models (Isern, Anselmetti and Blum, 2002). $\delta^{18}O_{benthic}$ results for the Marion Plateau (Fig.2b) and for the deep-sea (Zachos et al., 2001) are plotted together, as well as smoothed curves of the data (in gray, Fig.2). First, a Stineman function was applied to the data. To arrive at the smoothed curve, the output of this function had a geometric weight applied to the current point and ±10% of the data range. The general pattern of both deep-sea and Marion Plateau curves is similar and reflects the major glacioeustatic events recognized in oxygen isotopes for the Cenozoic ("Mi" events from Miller et al., 1991b). A small offset exists between the age of the two datasets, reflecting imprecision in the age model for both curves. Events Mi3 and Mi4 are clearly visible (Fig.2). Marion Plateau $\delta^{18}O_{benthic}$ values are lighter than their deep-sea counterpart, reflecting deposition in warmer, shallow waters. The amplitude of the $\delta^{18}O$ drop between the beginning of the Mi3 and the end of the Mi4 events is an essential parameter used in estimating the magnitude of sea level variations (Miller et al., 1991b; Billups and Schrag, 2002). In order to minimize errors introduced by short-term variations in $\delta^{18}O$ (due mainly to temperature effects), $\Delta\delta^{18}O$ was measured from the smoothed curves. Thus, the maximum range in $\delta^{18}O$, measured from the deep-sea curve (Δds) and from the Leg 194 Marion Plateau curve (ΔLeg194) is 0.99‰ and 0.80‰, respectively (Fig. 2a, Fig 2b and Table 1).
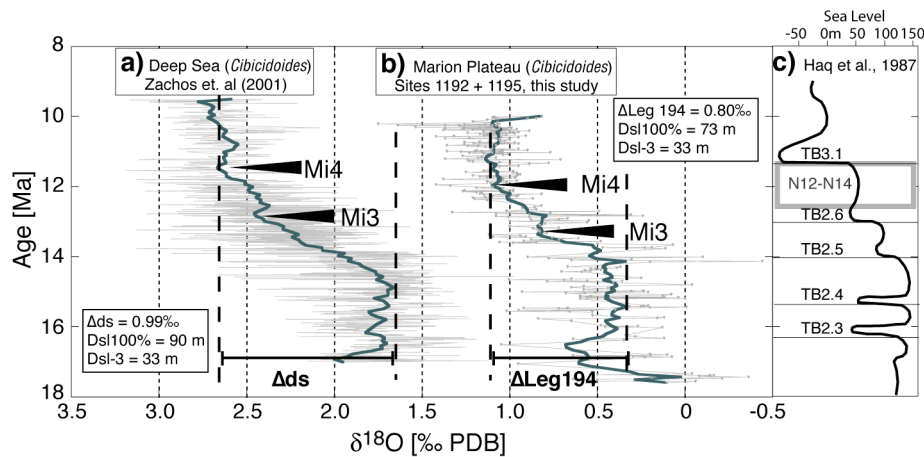
Figure 2: *Benthic foraminifers oxygen isotopes results. **a)** Compilation of deep-sea Cibicidoides data from Zachos et. al (2001). **b)** $\delta^{18}O_{benthic}$ measured for this study at sites 1192 and 1195. Both sites are compiled using the shipboard age model (Isern, Anselmetti and Blum, 2002). Mi3 and Mi4 events are described in Miller et al. (1991). Δds and ΔLeg194 are the difference (in ‰) between pre-Mi3 and Mi4 oxygen isotopes values for the deep-sea and for the Marion plateau sites, respectively. Dsl100% is the calculated sea level fall associated with 100% of the oxygen isotope fall (no cooling). Dsl-3 corresponds to the sea level calculated for the deep sea when considering a 3°C cooling (see text for details). **c)** "Eustasy" curve from Haq et al. (1987). The middle Miocene sea level fall estimated in this paper corresponds to the TB3.1 regression. Age range of the N12-N14 fall is indicated.*

5.4 SEA-LEVEL ESTIMATES USING BACKSTRIPPING

Leg 194 sea level estimates were based on the geometrical relationship between the highstand carbonate platform (Site 1193, Fig.1) and the late Middle Miocene carbonate ramp deposited during the lowstand on the proximal slope of this platform (Site 1194, Fig.1, Isern, Anselmetti and Blum, 2002). The relative small horizontal distance between Site 1193 and Site 1194 (~12 km, Fig.1), the undisturbed and consistently dipping pre-carbonate platform sediments, as well as the horizontal basement geometry between the sites as seen on seismic data suggested that no significant differential subsidence occurred between the sites (Isern, Anselmetti and Blum, 2002). Thus, it is reasonable to assume that the flexural response to sediment loading was associated with a flexurally strong basement. In order to determine the bathymetric relief of the platform and its slope, the effects of both sediment compaction and sediment and water loading must first be considered. Then, paleowater-depth estimates before the drop (Site 1193) and after the drop (Site 1194) were used to estimate the amplitude of the N12-N14 sea-level fall. Using this approach, the sea level fall was estimated to be 86±30m (Isern, Anselmetti and Blum, 2002). The rather large range is a direct consequence of uncertainties in the paleowater depth estimates based on benthic microfossil assemblages (water depth estimates at Site 1193: 10-50 m, at Site 1194: 30-50 m).

Next, post-rift thermal subsidence of the Marion Plateau during the 2 m.y. of the N14-N12 sea level fall also has to be taken into account. Backstripping the sediment assemblages for Sites 1193 and 1194 suggests that thermal subsidence during the sea-level fall can generated 12-20m of accommodation space (Karner et al., In prep). Using these values implies a total sea level fall amplitude of 102±34 m.

70

5.5 SEA-LEVEL ESTIMATES USING STABLE ISOTOPES
5.5.1 Principle of $\delta^{18}O$ glacioeustatic reconstructions

The isotopic composition of seawater (dw) is a function of ice volume, water temperature, and salinity. Therefore, provided that salinity and water temperature are known, ice volume fluctuations can be reconstructed by measuring the $\delta^{18}O$ composition of foraminifer calcite that precipitates in equilibrium with (or with an known offset to) seawater. However, water temperature is rarely well constrained and has a significant impact on Miocene bottom waters (Kennett, 1985; Wright et al., 1992; Zachos et al., 2001), thus potentially masking the glacioeustatic signals. Hence, in order to calculate the glacioeustatic component of the drop, a reasonable estimate of the amount of water cooling has to be made first (Fairbanks, 1989; Miller et al., 1991b). Direct calibrations of the amount of $\delta^{18}O$ associated with sea level lowering for the Pleistocene were obtained by measuring coral $\delta^{18}O$ and by assuming that water temperature did not change during Isotope Stage 2 (Fairbanks and Matthews, 1978). The Pleistocene gradient is 0.11‰ for a 10m change in sea level.

5.5.2 Sea level estimates based on oxygen isotopes

In order to avoid making unreasonable estimates of water cooling and possible salinity changes, we propose to construct a range of sea-level fall estimates based on minimal assumptions and then compare these with the backstripping results. As with earlier workers (e.g. Miller et al., 1998), we will assume that the Pleistocene rate of $\delta^{18}O$/sea level change is applicable for the Miocene after correcting for the effect of water temperature changes. The upper limit of the sea level range is then obtained by considering that no water-cooling occurred, i.e. by applying the Pleistocene calibration directly to the Δds and ΔLeg194 values. Results (Table 1) are 90m for Δds and 73m for ΔLeg194.

	Backstripping	Oxygen isotopes (deep sea)	Oxygen isotopes (Sites 1192+1195)
Pre Mi3 $\delta^{18}O$ cibicidoides	-	1.68 ‰	0.34 ‰
Post Mi4 $\delta^{18}O$ cibicidoides	-	2.67 ‰	1.14 ‰
$\Delta \delta^{18}O$	-	0.99 ‰	0.80 ‰
Lowest value Backstripping	68 m	-	-
Highest value Backstripping	136 m	-	-
Stable isotopes (no cooling)	-	90 m	73 m
Stable isotopes (3°C cooling)	-	33 m	33 m (deep sea)
Range of sea-level fall	**102±34 m**	**62 ± 29 m**	**53 ± 20 m**

Table 1: Summary of the various parameters and results discussed in the text. Relevant data are presented for (in column) the backstripping, the deep sea isotopes and the Marion Plateau isotopes. Parameters are (in row): $\delta^{18}O_{benthic}$ before the Mi3 event, $\delta^{18}O_{benthic}$ after the Mi4 event, the difference between these two values ($\Delta\delta^{18}O$, corresponding to Δds and ΔLeg194 of Fig. 2). Lowest and highest values for backstripping results are constrained by water-depth estimates. "Stable isotopes (no cooling)" is the sea level fall estimate obtained when considering 100% of the $\delta^{18}O_{benthic}$ signal, "Stable isotopes (3°C cooling)" is an estimates based on a cooling of 3°C for the deep sea (see text for details). The last row sums up the range of the sea level fall estimated by the three approaches.

To obtain the lower limit of the sea level range, we have chosen to take into consideration the 3°C of cooling inferred for deep waters by (Billups and Schrag, 2002). Though somewhat arbitrary, this approach gives a smaller minimum value than calibrations used in previous Miocene studies (e.g. Miller et al., 1996a). To convert the 3°C into ‰ changes, we use the simple linear equation from Bemis et al. (1998):

$$T [°C] = 16.5 – 4.8 (dc-dw)$$

where dc and dw are the isotopic composition of the foraminifer calcite and of the surrounding seawater, respectively. Considering $\Delta T=3°C$, and dw to be constant (we only deal with a temperature change), we calculate a Δdc of 0.63‰. Minimum sea level fall values are obtained by subtracting Δdc to Δds and then applying the Pleistocene calibration. The result is 33m (Table 1). Since no direct temperature estimates exist for the Marion Plateau, and that this subtropical shallow-water site is likely to have experienced less cooling than the deep-sea, we consider this value as a conservative minimum for the ΔLeg194 sea level range (Table 1).
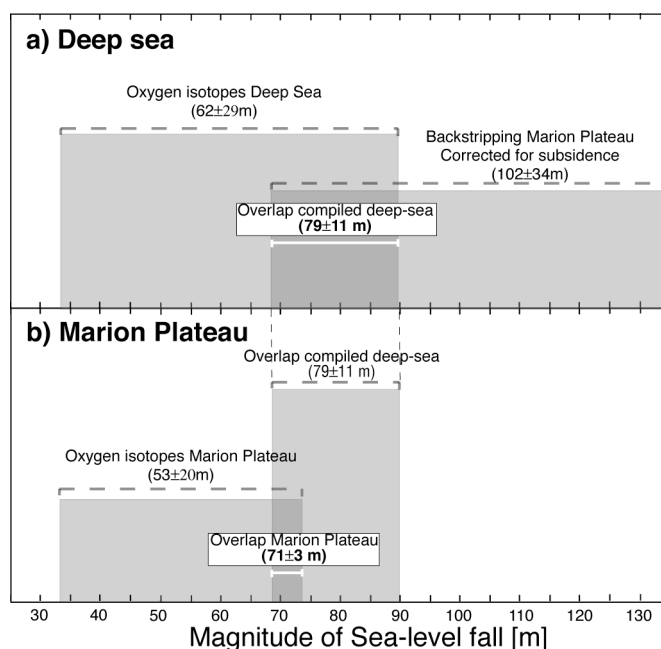
Figure 15: Sea level estimates resulting from this study. a) Sea level range obtained from backstripping of the Marion Plateau (right) are plotted with glacioeustatic estimates coming from oxygen isotopes measured in the deep sea (isotope data compiled by Zachos et. al, 2001). The overlap is 79±11m. b) The overlap obtained in a) is plotted against estimates coming from shallow water sequences from the Marion Plateau. The overlap represents a range of 71±3m, but is less well established since it relies on only two sites.

5.6 DISCUSSION
5.6.1 Constraining late Middle Miocene eustasy

The overlap field between the backstripping and the deep-sea oxygen isotope results (Fig.3a) represents the estimate for which both approaches concur. Although both the backstripping and the deep-sea oxygen isotope estimates have large ranges, the overlap is small, thus constraining the magnitude of the sea-level fall between 68 and 90 m. Results also show that our approach for determining a minimum boundary for the isotope estimates was conservative since the backstripping minimum is higher. Therefore, provided that the backstripping for the Marion Plateau and our assumption of an applicable Pleistocene rate of sea level change are reasonable, the late Middle Miocene Sea level fall can be estimated to be 79±11m.

The particular setting of the Marion Plateau provides the opportunity to attempt further constraining of the sea-level change. Since these shallow waters were located in a sub-tropical setting, they were less prone to extensive cooling linked to Antarctic glaciations. Thus, their $d^{18}O$ signal should approximate a purely compositional signal and would therefore more closely reflect ice volume. The thermal decoupling between deep-sea and Marion Plateau waters is underlined by the fact that the Marion Plateau waters were significantly warmer and that their $\delta^{18}O$ drop is smaller (Fig. 2b). On the other hand, Marion Plateau waters did record glacioeustatic events since every major Mi event (Miller et al., 1991b) appears in the isotopic curve. Furthermore, the open ocean, none-secluded location of the Marion Plateau (Isern, Anselmetti and Blum, 2002) suggest minimal effects of salinity changes. The overlap between the Marion Plateau estimate and the overlap previously obtained using deep-sea results is small (Fig. 3b). The magnitude of the sea level fall as compatible with backstripping, deep-sea and Marion Plateau results ranges from 68 to 74m, or 71±3m. This result relies on

$\delta^{18}O_{benthic}$ data coming from two sites located in the same area, and a compiled curve for shallow water sites located in non-upwelling, low-latitudes areas is with no doubts needed to confirm it.

5.6.2 Comparison with other estimates

Studies of siliciclastic sequences (New Jersey margin transect, ODP Leg 154 and 154X) also reconstructed Cenozoic sea level variations by combining oxygen isotopes with backstripping (Miller et al., 1998; Steckler et al., 1999; Pekar et al., 2002). However, the amplitude of the late Middle Miocene fall determined on the New Jersey margin was 25-50m (Miller et al., 1996a). As previously discussed, $\delta^{18}O$ values alone are difficult to use as a sea-level proxy since temperatures have to be estimated. Even though some independent estimates of deep-water cooling based on Mg/Ca ratios have been reported for the Miocene (Billups and Schrag, 2002), their interpretation is controversial since the chemical intake of Mg into carbonate and subsequent diagenetic overprint effects are still poorly understood (Zachos, pers. Comun. 2002). As a consequence, the sea level range based on $\Delta\delta^{18}O$ obtained in this study (33-90m) overlaps both the New Jersey margin (25-50m) and the Marion plateau (68-134m) backstripping results.

The critical difference between the New Jersey and the Marion Plateau estimates resides in the backstripping technique employed. New Jersey Margin estimates were made assuming local isostasy, while infinite flexural strength was assumed for the Marion Plateau. Sea-level estimates made using local isostasy during Leg 194 are similar to New Jersey margin results (Isern, Anselmetti and Blum, 2002) , but this result was considered unreasonable in view of the relatively small distance separating the drilling sites used in this analysis (~12 km). We regard the Marion Plateau backstripping result as superior to the New Jersey margin result for the N12-N14 fall because: **a)** our analysis is focused on a single eustatic fall instead of the entire Cenozoic, **b)** the control on the geometry between the sites is excellent and **c)** because of the use of a more realistic model for the response of the lithosphere to loads, consistent with the lack of differential subsidence between the sites, the presence of undisturbed and constant-dipping sediments, and the absence of major faults. Additionally, carbonate sediments recovered during Leg 194 provided better constraints on the uncertainty of the water-depth of the recovered facies.

Our results suggest that ice accumulation over Antarctica during the N12-N14 fall was less important than suggested by preliminary seismic interpretation of the Marion Plateau architecture (>180 m), but greater than suggested by siliciclastic sequences (25-50 m). If we consider that the oxygen isotopes estimates from the Marion Plateau are correct (73±4 m), we can convert the thermal component of Δds into temperature using the equation of Bemis et al. (1998):

$$\Delta\text{ds} - \text{ice volume} = 0.99\text{‰} - (73\ [m]\ x\ 0.011\ [\text{‰/m}]) = 0.22\text{‰}$$

Applying this equation suggests ~1°C of bottom-water cooling, which is in good agreement with the amplitude of thermal changes suggest for Antarctic glaciations prior to the Mi3 event, but is less than the ~3°C interpreted from Mg/Ca ratio for the Mi3 event (Billups and Schrag, 2002). We thus propose that the Mi3 event might have been characterized from previous events by more extensive ice buildup and not by higher rates of cooling.

5.7 CONCLUSIONS

(1) Estimates of the N12-N14 late mid-Miocene sea level fall obtained by combining backstripping results of the Marion Plateau with oxygen isotope analyses of the deep-sea gives a value of 79±11m.

(2) When considering estimates based on Marion Plateau $\delta^{18}O_{benthic}$ results, this range is narrowed down to 73±4m.

(3) Assuming a sea level fall of ~73m implies deep-water cooling of ~1°C during the Mi3 event. This is in agreement with the range of bottom-water cooling estimates for older glaciations but is less than the ~3°C estimated from other studies.

- CHAPTER 6 -

General Conclusions, Acknowledgement and Cited References

6.1 General Conclusions

The first order question of this work was to know whether carbonate systems on continental margins responded to the mid Miocene cooling step at two different locations on the globe. From chapters 2 and 3, it is apparent that the mid Miocene cooling events impacted the Maltese section by drastically changing the amount of terrigenous material accumulated on the slope. We inferred that this resulted from increased African Monsoon linked to Northward migration of the ITCZ. Chapter 4 and 5 show that on the Marion Plateau, the mid Miocene cooling step impacted accumulation rates of carbonate instead. We argued that this could be explained by increased strength of oceanic currents, as well as changes in the oceanic current patterns. Thus, it appears clearly that both the Maltese and Marion Plateau systems were sensitive to the establishment of the East Antarctic ice sheet around 13.5 Ma. Hence, these shallow-water sedimentary systems are great recorded of global events and give the opportunity to extend the deep-sea record, and provide additional information on the influence of continental weathering.

As a second order question, we wanted to know whether the nature of this impact was similar from one location to the other. As was described in chapter 2 and chapter 3, the response of the Maltese system was largely linked to the continent: clay input dramatically increased after the Mi3 event. On the other hand, as shown by mass accumulations of carbonates, carbonate production did not decrease. When looking at the ocean facing Marion Plateau, it appears that its sedimentary record contains only small amounts of terrigenous material, even after the Mi3 event. Hence, continental weathering and runoff played at most a minor role in controlling sedimentation rates at this location. In contrary, the absence of a protecting barrier exposed the slope sediments to the effects of oceanic currents, and this system was consequently sensitive to changes in oceanographic parameters. Therefore, an interesting result of this study is to demonstrate that carbonate slope sediments are important archives of climate change, but also that the nature of this change can be complex as it is dependant on many regional factors. This has to be taken into consideration when interpreting shallow-marine records as an archive of global climate change.

6.2 Acknowledgements

6.3 Cited References

Anselmetti, F., Eberli, G., and Ding, Z.-D., 2000, From the Great Bahama Bank into the Straits of Florida: A margin architecture controlled by sea-level fluctuations and oceans currents: GSA Bulletin, v. 112, p. 829-844.

Bemis, B.E., Spero, H.J., Bijma, J., and Lea, D.W., 1998, Reevaluation of the oxygen isotopic composition of planktonic foraminifera; experimental results and revised paleotemperature equations: Paleoceanography, v. 13, p. 150-160.

Berger, W.H., 1982, Increase of carbon dioxide in the atmosphere during deglaciation: The coral reef hypothesis: Naturwissenschaften, v. 69, p. 87-88.

Billups, K., and Schrag, D.P., 2002, Paleotemperatures and ice volume of the past 27 Myr revisited with paired Mg/Ca and $^{18}O/^{16}O$ measurements on benthic foraminifera: Paleoceanography, v. 17, p. 3-1, 3-11.

Blisniuk, P.M., Hacker, B.R., Glodny, J., Ratschbacher, L., Bi, S., Wu, Z., McWilliam, M.O., and Calvert, A., 2001, Normal faulting in central Tibet since 13.5 Myr ago: NATURE, v. 412, p. 628-632.

Bosence, D.W.G., 1983, The occurence and ecology of recent rodoliths - a review, in Paryt, T.M., ed., Coated grains: Berlin, Springer-Verlag, p. 225-241.

Buchbinder, B., and Zilberman, E., 1997, Sequence stratigraphy of Miocene-Pliocene carbonate-siliciclastic shelf deposits in the eastern Mediterranean margin (Israel): effects of eustasy and tectonics: Sedimentary Geology, v. 112, p. 7-32.

Clift, P., and Gaedicke, C., 2002, Accelerated mass flux to the Arabian Sea during the middle to late Miocene: Geology, v. 30, p. 207-210.

Corfield, R.M., and Cartlidge, J.E., 1992, Oceanographic and climatic implications of the Paleaocene carbon isotope maximum: Terra Nova, v. 4, p. 443-455.

DePaolo, D.J., and Finger, K.L., 1991, High-resolution strontium-isotope stratigraphy and biostratigraphy of the Miocene Monterey Formation, central California: Geological Society of America Bulletin, v. 103, p. 112-124.

Dercourt, J., Bassoullet, J.-P., Baud, A., Butterlin, J., Camoin, G.F., Cavelier, C., Cecca, F., Enay, R., Fourcade, E., Guiraud, R., Lorenz, C., Marcoux, J., J.-P., M., Orszag, F., and Philip, J., 1992, Paleoenvironmental atlas of the Tethys from Permian to Recent, 29th international geological congress; abstracts.

Dercourt, J., Ricou, L.E., and Vrielynck, B., 1993, Atlas Tethys Palaeoenvironmental Maps.: Paris, Gauthier-Villars, p. 307.

Derry, L.A., and France-Lanord, C., 1996, Neogene Himalayan weathering history and river 87Sr/86Sr: impact on the marine Sr record: Earth and Planetary Science Letters, v. 142, p. 59-74.

Eaton, S., and Robertson, A., 1993, The Miocene Pakhna Formation, southern Cyprus and its relationship to the Neogene tectonic evolution of the Eastern Mediterranean: Sedimentary Geology, v. 86, p. 273-296.

Eberli, G.P., Anselmetti, F.S., Kroon, D., Sato, T., and Wright, J.D., 2002, The chronostratigraphic significance of seismic reflections along the Bahamas Transect: Marin Geology, v. 185, p. 1-17.

Esteban, M., 1996, An overview of Miocene reefs from the Mediterranean areas: general trends and facies models, in Franseen, E.K., Esteban,

M., Ward, W.C., and Rouchy, J.-M., eds., Models for carbonate stratigraphy from Miocene reef complexes of the Mediterranean region, Volume 5: Tulsa, Oklahoma, U.S.A., SEPM, p. 3-55.

Fairbanks, R.G., 1989, A 17'000-year glacio-eustatic sea level record: influence of glacial melting rates on the Younger Dryas event and deep-ocean circulation: Nature, v. 342, p. 637-642.

Fairbanks, R.G., and Matthews, R.K., 1978, The Marine Oxygen Isotope Record in Pleistocene Coral, Barbados, West Indies: Quaternary Research, v. 10, p. 181-196.

Felix, R., 1973, Oligo-Miocene stratigraphy of Malta and Gozo [Ph.D. thesis]: Utrecht, University of Utrecht.

Flower, B.P., and Kennett, J.P., 1993, Middle Miocene Ocean-Climate transition: High-resolution oxygen and carbon isotopic records from Deep Sea Drilling Project Site 588A, Southwest Pacific: Paleoceanography, v. 8, p. 811-843.

—, 1994, The middle Miocene climatic transition: East Antarctica ice sheet development, deep ocean circulation and global carbon cycling: Palaeogeography, Palaeoclimatology, Palaeoecology, v. 108, p. 537-555.

Fluteau, F., Ramstein, G., and Besse, J., 1999, Simulating the evolution of the Asian monsoons during the past 30 Myr using an atmospheric general circulation model: Journal of Geophysical Research, v. 104, p. 11995-12018.

Föllmi, K.B., 1995, 160 m.y. record of marine sedimentary phosphorus burial: Coupling of climate and continental weathering under greenhouse and icehouse conditions: Geology, v. 23, p. 859-862.

Föllmi, K.B., Garrison, R.E., and Grimm, K.A., 1991, Stratification in Phosphatic Sediments: Illustration from the Neogene of California, *in* al., E.e., ed., Cycles and Events in Stratigraphy, Springer-Verlag Berlin Heidelberg, p. 492-507.

Foresi, L.M., Caruso, A., Sprovieri, M., Sprovieri, R., Adriana, B., Neri, R., and Mazzola, S., 2001, Astrochronological Calibration of an Upper Langhian/Lower Serravallian Record from the Fomm Ir Rih Section (Malta Island, Central Mediterranean), *in* Geosciences, E.U.o., ed., EUG XI, Volume XI: Strasbourg, France, Cambridge Publications.

France-Lanord, C., and Derry, L.A., 1997, Organic carbon burial forcing of the carbon cycle from Himalayan erosion: Nature, v. 390, p. 65-67.

Gaaloul, N., Bobier, C., and Razgallah, S., 2001, The sedimentary evolution of Miocene series at east Tunisian margin: impact of eustatisme, tectonics and climate, *in* Wortmann, U.G., and Funk, H., eds., IAS 2001, 21st Meeting: Davos, Switzerland, International Association of Sedimentologists, p. 35-36.

Glenn, C.R., and Kronen, J.D.J., 1993, Origin and significance of late Pliocene phosphatic hardgrounds on the Queensland Plateau, Northeastern Australian margin, *in* Mackenzie, J.A., Davies, P.J., and Palmer-Julson, A., eds., Proceedings of the Ocean Drilling Program, Scientific results, Volume 133: College Station, Texas A&M.

Grötsch, J., Billing, I., and Vahrenkamp, V., 1998, Carbon-isotope stratigraphy in shallow-water carbonates: implications for Cretaceous black-shale deposition: Sedimentology, v. 45, p. 623-634.

Guo, Z.T., Ruddiman, W.F., Hao, Q.Z., Wu, H.B., Qlao, Y.S., Zhu, R.X., Peng, S.Z., Wei, J.J., Yuan, B.Y., and Liu, T.S., 2002, Onset of Asian

desertification by 22 Myr ago inferred from loess deposits in China: NATURE, v. 416, p. 159-163.

Hallock, P., 1987, Reefs and reef limestones in Earth history, International Thomson Publishing. New York, NY, United States. 1987., 13-42 p.

—, 1988, The role of nutrient availability in bioerosion; consequences to carbonate buildups: Palaeogeography, Palaeoclimatology, Palaeoecology, v. 63, p. 275-291.

—, 2001, Coral Reefs, Carbonate Sediments, Nutrients, and Global Change, *in* Stanley, G.D., ed., The History and Sedimentology of Ancient Reef Systems: New York, Kluwer Academic/Plenum Publishers.

Haq, B.U., Hardenbol, J., and Vail, P.R., 1987, Chronology of fluctuating sea-levels since the Triassic: Science, v. 235, p. 1156-1167.

Hastenrath, C., 1985, Climate and Circulation of the Tropics, D. Reidel, Norwell, Mass., 455 p.

Hecky, R.E., Campbell, P., and Hendzel, L.L., 1993, The stoichiometry of carbon, nitrogen, and phosphorus in particulate matter of lakes and oceans: Limnology and Oceanography, v. 38, p. 709-724.

Hodell, D.A., and Woodruff, F., 1994, Variations in the strontium isotopic ratio of seawater during the Miocene: Stratigraphic and geochemical implications: Paleoceonography, v. 9, p. 405-426.

Isaacs, C.M., Belfield, W.C., Ramirez, P.C., and Clarke, R.T., 1987, The Miocene Monterey formation- Depositional and Diagenetic fascies along the Santa Barbara, California coastal area, 1987 AAPG Annual convention: Los Angeles, CA.

Isern, A.R., Anselmetti, F.S., Blum, P., and et al., 2002, Proc. ODP, Init. Repts., [CD-ROM]. Available from: Ocean Drilling Program, Texas A&M University, College Station TX 77845-9547, USA.

Isern, A.R., McKenzie, J.A., and Feary, D.A., 1996, The role of sea-surface temperature as a control on carbonate platform development in the western Coral Sea: Palaeogeography, Palaeoclimatology, Palaeoecology, v. 124, p. 247-272.

Jacobs, E., 1996, The record of the Miocene Event in shallow shelf sediments of Malta (Central Mediterranean): stable isotopes and phosphogenesis as paleoclimatic indicators [Ph.D. thesis]: Zürich, ETHZ.

Jacobs, E., Weissert, H., Shields, G., and Stille, P., 1996, The Monterey event in the Mediterranean: A record from the shelf sediments of Malta: Paleoceanography, v. 11, p. 717-728.

James, N.P., 1997, The cool-water carbonate depositional realm, *in* James, N.P., and Clarke, J.A.D., eds., Cool-Water Carbonates: Tulsa, OK, SEPM Special publications, p. 1-20.

John, C.M., Föllmi, K.B., De Kaenel, E., Adatte, T., Steinmann, P., and Badertscher, C., 2002, Carbonaceous and Phosphate-rich sediments of the Miocene Monterey Formation at El Capitan State Beach (California): Journal of Sedimentary Research, v. 72, p. 282-296.

John, C.M., Karner, G.D., and Mutti, M., under review, d^{18}O and Marion Plateau backstripping: combining two approaches to constrain late Middle Miocene eustatic amplitude.

John, C.M., Mutti, M., and Adatte, T., 2003, Mixed carbonate-siliciclastic record on the North African margin (Malta) - coupling of weathering processes and mid Miocene climate: GSA Bulletin, v. 115, p. 217-229.

Karner, G., Anselmetti, F., Isern, A., Eberli, G., and John, C., In prep, Style and distribution of extension responsible for the development of the

Marion Plateau: constraints from sequence stratigraphy and ODP leg 194 drilling.

Kennett, J.P., 1985, The Miocene ocean, Geological Society of America, 337 p.

Kidd, R.B., Cita, M.B., and Ryan, W.B.F., 1978, Stratigraphy of eastern Mediteranean sapropel sequences recovered during Leg 42A and their paleoenvironmental significance, Init. Rep. DSDP, Volume 42A: College Station, Tx, Texas A&M, p. 412-413.

Kienel, U., Rehfeld, U., Bellas, S., and Kohring, R., 1995, The Miocene Blue Clay Formation of the Maltese Islands; sequence-stratigraphic and paleoceanographic implications based on calcareous nannofossil stratigraphy and calcareous dinoflagellate cysts, 6th International Nannoplankton Association conference; programme and abstracts.

Laskar, J., 2001, Astronomical Solutions for Paleoclimates Studies. Abstract U11A-01.: Eos Trans. AGU Fall Meet. Suppl. 82, and work in preparation by J.L. et al.

Martin, E.E., Shackleton, N.J., Zachos, J.C., and Flower, B.P., 1999, Orbitally-tuned Sr isotope chemostratigraphy for the late middle to late Miocene: Paleoceanography, v. 14, p. 74-83.

Matthews, R.K., and Poore, R.Z., 1980, Tertiary delta (super 18) O record and glacio-eustatic sea-level fluctuations: Geology (Boulder), v. 8, p. 501-504.

McKenzie, J.A., and Davies, P.J., 1993, Cenozoic evolution of carbonate platforms on the northeastern Australian margin; synthesis of Leg 133 drilling results.

Miller, K.G., and Fairbanks, R.G., 1985, Oligocene to Miocene carbon isotope cycles and abyssal circulation changes, The carbon cycle and atmospheric CO (sub 2) ; natural variations Archean to present.

Miller, K.G., Fairbanks, R.G., and Mountains, G.S., 1987, Tertiary oxygen isotope synthesis, sea level history, and continental margin erosion: Paleoceanography, v. 2, p. 1-19.

Miller, K.G., Feigenson, M.D., Wright, J.D., and Clement, B.M., 1991a, Miocene isotope reference section, Deep Sea Drilling Project Site 608; an evaluation of isotope and biostratigraphic resolution: Paleoceanography, v. 6, p. 33-52.

Miller, K.G., Mountain, G.S., Blum, P., Gartner, S., Alm, P.-G., Aubry, M.-P., Burckle, L.H., Guerin, G., Katz, M.E., Christensen, B.A., Compton, J., Damuth, J.E., Deconinck, J.F., de Verteuil, L., Fulthorpe, C.S., Hesselbo, S.P., Hoppie, B.W., Kotake, N., Lorenzo, J.M., McCracken, S., McHugh, C.M., Quayle, W.C., Saito, Y., Snyder, S.W., ten Kate, W.G., Urbat, M., Van Fossen, M.C., Vecsei, A., Sugarman, P.J., Mullikin, L., Pekar, S., Browning, J.V., Liu, C., Feigenson, M.D., Goss, M., Gwynn, D., Queen, D.G., Powars, D.S., Heibel, T.D., and Bukry, D., 1996a, Drilling and dating New Jersey Oligocene-Miocene sequences; ice volume, global sea level, and Exxon records: Science, v. 271, p. 1092-1095.

Miller, K.G., Mountain, G.S., Blum, P., Gartner, S., Alm Per, G., Aubry, M.P., Burckle, L.H., Guerin, G., Katz, M.E., Christensen, B.A., Compton, J., Damuth, J.E., Deconinck, J.F., de Verteuil, L., Fulthorpe, C.S., Hesselbo, S.P., Hoppie, B.W., Kotake, N., Lorenzo, J.M., McCracken, S., McHugh, C.M., Quayle, W.C., Saito, Y., Snyder, S.W., ten Kate, W.G., Urbat, M., Van Fossen, M.C., Vecsei, A., Sugarman, P.J.,

Mullikin, L., Pekar, S., Browning, J.V., Liu, C., Feigenson, M.D., Goss, M., Gwynn, D., Queen, D.G., Powars, D.S., Heibel, T.D., and Bukry, D., 1996b, Drilling and dating New Jersey Oligocene-Miocene sequences; ice volume, global sea level, and Exxon records: Science, v. 271, p. 1092-1095.

Miller, K.G., Mountain, G.S., Browning, J.V., Kominz, M., Sugarman, P.J., Christie-Blick, N., Katz, M.E., and Wright, J.D., 1998, Cenozoic global sea level, sequences, and the New Jersey transect; results from coastal plain and continental slope drilling: Reviews of Geophysics, v. 36, p. 569-601.

Miller, K.G., Wright, J.D., and Fairbanks, R.G., 1991b, Unlocking the ice house: Oligocene-Miocene oxygen isotopes, eustasy, and margin erosion: Journal of Geophysical Research, v. 69, p. 6829-6848.

Molnar, P., and England, P., 1990, Late Cenozoic uplift of mountain ranges and global climate change: chicken or egg?: Nature, v. 346, p. 29-34.

Mutti, M., and Bernoulli, D., 2003, Early Marine lithification and hardground development on a Miocene ramp (Maielle, Italy): key surfaces to track changes in trophic resources in nontropical carbonate settings: Journal of Sedimentary Research, v. 73, p. 296-308.

Mutti, M., Bernoulli, D., Spezzaferri, S., and Stille, P., 1999, Lower and Middle Miocene carbonate facies in the central Mediterranean: The impact of paleoceanography on sequence stratigraphy, SEPM (Society for Sedimentary Geology), 371-384 p.

Mutti, M., Bernoulli, D., and Stille, P., 1997, Temperate carbonate platform drowning linked to Miocene oceanographic events: Maiella platform-margin, Italy: Terra Nova, v. 9, p. 122-125.

Mutti, M., and Hallock, P., In press, Carbonate systems along nutrient and temperature gradients: some sedimentological and geochamical constrains.

Oslick, J.S., Miller, K.G., Feigenson, M.D., and Wright, J.D., 1994, Oligocene-Miocene strontium isotopes: Stratigraphic revisions and correlations to an inferred glacioeustatic record: Paleoceanography, v. 9, p. 427-444.

Paillard, D., Labeyrie, L., and Yiou, P., 1996, Macintosh program performs time-series analysis: Eos Trans. AGU, v. 77, p. 379.

Patterson, P., and Walter, L.M., 1994, Depletion of 13C in seawater C02 on modern carbonate platforms: Significance for the carbon isotopic record of carbonates.: Geology, v. 22, p. 885-888.

Pedley, H.M., and Bennett, S.M., 1985, Phosphorite, Hardgrounds and syndepositional solution subsidence: A palaeoenvironmental model from the Miocene of the Maltese Islands: Sedimentary geology, v. 45, p. 1-34.

Pekar, S.F., Christie-Blick, N., Kominz, M.A., and Miller, K.G., 2002, Calibration between eustatic estimates from backstripping and oxygen isotopic records from teh Oligocene: Geology, v. 30, p. 903-906.

Pickard, G.L., Donguy, J.R., Henin, C., and Rougerie, F., 1977, A review of the physical oceanography of the Great Barrier Reef and western Coral Sea.

Pigram, C.J., Davies, P.J., Feary, D.A., and Symonds, P.A., 1992a, Absolute magnitude of the second-order middle to late Miocene sea-level fall, Marion Plateau, northeast Australia: Geology, v. 20, p. 858-862.

Pigram, C.J., Davies, P.J., Feary David, A., and Symonds, P.A., 1992b, Absolute magnitude of the second-order middle to late Miocene sea-

level fall, Marion Plateau, Northeast Australia: Geology (Boulder), v. 20, p. 858-862.

Prell, W.L., and Kutzbach, J.E., 1992, Sensitivity of the Indian monsoon to forcing parameters and implications for its evolution: Nature, v. 360, p. 647-652.

Prentice, M.L., and Matthews, R.K., 1988, Cenozoic ice-volume history; development of a composite oxygen isotope record; with Suppl. Data 88-26: Geology (Boulder), v. 16, p. 963-966.

Raymo, M.E., 1991, Geochemical evidence supporting T.C. Chamberlin's theory of glaciation: Geology, v. 19, p. 344-347.

—, 1994, The Himalayas, organic carbon burial, and the climate in the Miocene: Paleoceanography, v. 9, p. 399-404.

Raymo, M.E., and Ruddiman, W.F., 1992, Tectonic forcing of late Cenozoic climate: Nature, v. 359, p. 117-122.

Raymo, M.E., Ruddiman, W.F., and Froelich, P.N., 1988, Influence of late Cenozoic mountain building on ocean geochemical cycles: Geology, v. 16, p. 649-653.

Riegl, B., and Piller, W.E., 2000, Biostromal Coral Facies - A Miocene Example from the Leitha Limestone (Austria) and its Actualistic Interpretation: Palaios, v. 15, p. 399-413.

Rossignol-Strick, M., 1985, Mediterranean Quaternary Sapropels, an immediate response of the African Monsoon to variation of insolation: Paleogeography, Paleoclimatology, Paleoecology, v. 49, p. 237-263.

Sackett, W.M., and Thomson, R.R., 1963, Isotopical organic carbon composition of recent continental derived clastic sediments of the eastern Gulf of Mexico: Am. Assoc. Pet. Geol. Bull., v. 47, p. 525-528.

Savin, S.M., and Woodruff, F., 1990, Isotopic evidence for temperature and productivity in the Tertiary oceans, Cambridge Univ. Press. New York, NY, United States. 1990., 241-259 p.

Schenau, S.J., Antonarakou, A., Hilgen, F.J., Lourens, L.J., Nijenhuis, I.A., van der Weijden, C.H., and Zachariasse, W.J., 1999, Organic-rich layers in the Metochia section (Gavdos, Greece); evidence for a single mechanism of sapropel formation during the past 10 My: Marine Geology, v. 153, p. 117-135.

Schlanger, S.O., and Premoli-Silva, I., 1986, Oligocene sea level falls recorded in the mid-Pacific atoll and archipelic apron settings: Geology, v. 14, p. 392-395.

Schubert, C.J., and Calvert, S.E., 2001, Nitrogen and carbon isotopic composition of marine and terrestrial organic matter in Arctic Ocean sediments: implications for nutrient utilization and organic matter composition: Deep-Sea Research, Part I, v. 48, p. 789-810.

Shackleton, N.J., 1985, Oceanic carbon isotope constraints on oxygen and carbon dioxide in the Cenozoic atmosphere, in Sundquist, E.T., and Broecker, W.S., eds., The Carbon Cycle and Atmospheric CO_2: Natural variations Archean to Present, Volume 32, American Geophysical Union, p. 455-468.

Shackleton, N.J., Blackman, J., Zimmerman, H., Kent, D.V., Hall, M.A., Roberts, D.G., Schnitker, D., Baldauf, J.G., Desprairies, A., Homrighausen, R., Huddlestun, P., Keene, J.B., Kaltenback, A.J., Krumsiek, K.A.O., Morton, A.C., Murray, J.W., and Westberg-Smith, J., 1984, Oxygen isotope calibration of the onset of ice-rafting and history of glaciation in the North Atlantic region: Nature, v. 307, p. 620-623.

Shackleton, N.J., and Kennett, J.P., 1975, Paleotemperature history of the Cenozoic and the initiation of Antarctic glaciation; oxygen and carbon isotope analyses in DSDP sites 277, 279, and 281: Initial Reports of the Deep Sea Drilling Project, v. 29, p. 743-755.

Shipboard Scientific Party, 2002a, Leg 194 summary, *in* Isern, A., Anselmetti, F.S., Blum, P., and et al., eds., Proc. ODP, Init. Repts., [CD-ROM]. Available from: Ocean Drilling Program, Texas A&M University, College Station TX 77845-9547, USA, p. 1-88.

—, 2002b, Site 1192, *in* Isern, A., Anselmetti, F.S., Blum, P., and et al., eds., Proc. ODP, Init. Repts., [CD-ROM]. Available from: Ocean Drilling Program, Texas A&M University, College Station TX 77845-9547, USA, p. 1-88.

—, 2002c, Site 1193, *in* Isern, A., Anselmetti, F.S., Blum, P., and et al., eds., Proc. ODP, Init. Repts., [CD-ROM]. Available from: Ocean Drilling Program, Texas A&M University, College Station TX 77845-9547, USA, p. 1-88.

—, 2002d, Site 1194, *in* Isern, A., Anselmetti, F.S., Blum, P., and et al., eds., Proc. ODP, Init. Repts., [CD-ROM]. Available from: Ocean Drilling Program, Texas A&M University, College Station TX 77845-9547, USA, p. 1-88.

—, 2002e, Site 1195, *in* Isern, A., Anselmetti, F.S., Blum, P., and et al., eds., Proc. ODP, Init. Repts., [CD-ROM]. Available from: Ocean Drilling Program, Texas A&M University, College Station TX 77845-9547, USA, p. 1-88.

Steckler, M.S., Mountain, G.S., Miller, K.G., and Christie-Blick, N., 1999, Reconstruction of Tertiary progradation and clinoform development on the New Jersey passive margin by 2-D backstripping

[Monograph] The formation of continental-margin strata: Marine Geology, v. 154, p. 399-420.

Stratford, K., Williams, R.G., and Myers, P.G., 2000, Impact of the circulation on sapropel formation in the eastern Mediterranean: Global Biogeochemical Cycles, v. 14, p. 683-695.

Tomczak, M., and Godfrey, S., 1994, Regional Oceanography: Oxford, Pergamon Press, 422 p.

Vail, P.R., and Hardenbol, J., 1979, Sea-level change during the Tertiary: Oceanus, v. 22, p. 71-79.

Vincent, E., and Berger, W.H., 1985, Carbon dioxide and polar cooling in the Miocene: The Monterey hypothesis, *in* Sundquist, E.t., and Broecker, W.S., ed., Natural variations Archean to present., American Geophysical Union, Geophysical Monographies.

Visser, J.P., 1991, Clay mineral stratigraphy of Miocene to Recent marine sediments in the central Mediterranean: Utrecht, University of Utrecht.

Weissert, H., Lini, A., Föllmi, K.B., and Kuhn, O., 1998, Correlation of Early Cretaceous carbon isotope stratigraphy and platform drowning events; a possible link?: Palaeogeography, Palaeoclimatology, Palaeoecology, v. 122, p. 189-203.

Weissert, H., and Mohr, H., 1996, Late Jurassic climate and its impact on carbon cycling: Palaeogeography, Palaeoclimatology, Palaeoecology, v. 122, p. 27-43.

Woodruff, F., and Savin, S.M., 1991, Mid-Miocene isotope stratigraphy in the deep sea; high-resolution correlations, paleoclimatic cycles, and sediment preservation: Paleoceanography, v. 6, p. 755-806.

Wright, J.D. and Miller, K.G., 1992, Miocene stable isotope stratigraphy, Site 747, Kerguelen Plateau, *in*: Wise, S.W., Jr., Schlich, R., et al, 1992, *Proc. ODP, Sci. Results*, 120: College Station, TX (Ocean Drilling Program), p.855-866.

Wright, J.D., Miller, K.G., and Fairbanks, R.G., 1992, Early and middle Miocene stable isotopes; implications for deepwater circulation and climate: Paleoceanography, v. 7, p. 357-389.

Zachos, J., Pagani, M., Sloan, L., Thomas, E., and Billups, K., 2001, Trends, rhythms, and aberrations in global climate 65 Ma to present: Science, v. 292, p. 686-693.

Zachos, J.C., Flower, B.P., and Paul, H., 1997, Orbitally paced climate oscillations across the Oligocene/Miocene boundary: Nature, v. 388, p. 567-570.

7 - Annexes

7.1 CURRICULUM VITAE
7.1.1General information

First names: <u>Cédric</u> Michaël
Last name: JOHN
Current Title: Swiss diploma , Geology
Nationality: Swiss

Current addresses:
Alte Stuttgarterstrasse 83
70195 Stuttgart
<u>Germany</u>

Home phone: 49-711-699-0204   e-mail: cjohn@geo.uni-potsdam.de

7.1.2 Education
November 2002-today: Finishing Ph.D. at the University of Potsdam
October 1999-oct. 2002: Ph.D. project at the Technical University of
              Stuttgart, Germany
July 1999: Graduated from the university of Neuchâtel, Diploma title
              (similar to an American M.S.), with distinction: "Bien".
1994-1998: Geology studies at the University of Neuchatel.
1990-1994: Cantonal Gymnasium of Neuchatel, graduated with a C-Type
              diploma (Scientific) in 1994.

7.1.3 Grants
1999- Jan. 2002: Stipend from the "Landesgraduirtes Förderung, Land
       Baden-Württemberg".
2001: Participation of C.John on Leg 194 paid by the DFG
        Schwerpunktprogram ODP.
2000: Grant for fieldwork on Malta, from the "Landesgraduirtes Förderung,
       Land Baden-Württemberg".
1999: Keck Fellowship, University of Southern California (declined by C.John)
1998: Grant from the "Fond Marguerite Wüthrich et Mattey-Dupraz" for Field
       Trip in California

7.1.4 Research experience
1999-today: PhD thesis at the University of Stuttgart and Potsdam. Theme:
       "Miocene climate as recorded in slope carbonates: examples from
       Malta (central Mediterranean) and the Marion Plateau (ODP Leg
       194)". Advisor: Prof. Dr. Maria Mutti
June 2001: Leg 194 first post cruise meeting (editorial), College Station, Tx
January-March 2001: Sedimentologist on ODP Leg 194
1997-1999: Diploma thesis at the University of Neuchatel, on the theme:
       "The Monterey formation at El
       Capitan State Beach (Santa Barbara Basin, California), an approach

combining mineralogy, sedimentology, stratigraphy and organic geochemistry". Advisor: Prof. Dr. Karl B. Föllmi

7.1.5 Field experience
January-March 2001: seagoing experience, sedimentologist on ODP Leg 194
October 1999: Field trip on Malta in the framework of the Ph.D. thesis
1997-1998:   2 months field work in the framework of the diploma thesis, including coastal mapping, stratigraphic log drawing, sedimentological structures studies and sampling at El Capitan, Santa Barbara Basin, California.
1996-1998: Several field trips in the framework of the undergraduate studies: Switzerland, France, Germany, Italy, Western USA..

7.1.6 Work experience
2001-2002: Assistant at the Geological Institute of the University of Stuttgart, in charge of the geochemical lab (maintenance, placing orders, running analysis, etc…).
1999-2001: Assistant at the Geological Institute of the University of Stuttgart, in charge of the Macintosh network, maintenance, software update and help to users.
1998-1999: Assistant at the Geological Institute of the University of Neuchâtel, in charge of the Macintosh network, maintenance, software update and   help to users.
1997: Editorial board for volume 2 (6th Conference on Limestone Hydrology and Fissured Media) of the   Proceedings of the 12th International Congress of Speleology. ISBN 2-88374-007-0 (Vol.2).
1996-1999: Assistant in the XRD lab of the university of Neuchatel.

7.2 LIST OF PUBLICATIONS
7.2.1 Published Papers
      John, C.M., Mutti, M., Adatte, T., 2003: Middle Miocene coupling of continental processes, atmospheric circulation and global climate - A North African margin record, GSA Bulletin, v.115, n 2, pp 217-229.
      John C.M., Föllmi K.B., De Kaenel, E., Adatte T., Steinmann P., and Badertscher C., 2002 : "Carbonaceous and phosphate-rich sediments of the Miocene Monterey formation at El Capitan state beach (california)", JSR, v.72, N.2, pp 282-296.
      John, **C**, 2001: "The Monterey formation at El Capitan State beach (Santa Barbara Basin, California)", diploma thesis, University of Neuchâtel, Switzerland.

7.2.2 ODP Related Publications

John, C.M., Andresen, N., and Leg 194 Shipboard Scientific Party, 2001: Estimating the Magnitude of Sea Level Fall by Drilling Carbonate Platforms: The case of ODP Leg 194, NE Australia, *in:* Reports of the German ODP Program, Year 2001.

Isern A., Anselmetti F., Blum, P. and Shipboard Scientific Party (including **C. John**), 2002. *Proc. ODP, Init. Repts*, 194: College Station, TX (Ocean Drilling Program).

Isern A., Anselmetti F.S., Blum, P. and Shipboard Scientific Party (including **C. John**), 2001: "Ocean Drilling Constrains Carbonate Platform Formation and Miocene Sea Level on the Australian Margin", EOS, Vol. 82, Number 41.

Shipboard Scientific Party (including **C.John**), 2001. Leg 194 Preliminary Report. ODP Prelim. Rpt., 94 [Online]. Available from World Wide Web: <http://www-odp.tamu.edu/publications/prelim/194_prel/194PREL.PDF>.

7.2.3 Publications in Preparation and Submitted

John, C.M., Mutti, M., in prep: "Relative controls over slope sedimentation in a Miocene subtropical heterozoan carbonate system (Marion Plateau, ODP leg 194)".

John, C.M., Mutti, M., Adatte, T., in prep: Reconstructing terrigenous import, climatic evolutions and paleoceanography: mineralogical data, Leg 194.

John, C.M., Mutti, M., Adatte, T., in prep: Stratigraphic correlations within the northern Marion Plateau slope sites: mineralogical and stable isotopes data.

John, C.M., Karner, G.D., Mutti, M., in review: $\delta^{18}O$ and Marion Plateau Backstripping: combining two approaches to constrain late Middle Miocene eustasy.

John, C.M., Mutti, M., Laskar, J., in prep: History of the African monsoon inferred by Middle Miocene sapropels-like deposits in the Mediterranean.